Model-Independent Extraction of Source Images in d+Au and Au+Au Collisions

P. Chung, A. Taranenko, N.N. Ajitanand, J. Alexander,
W. G. Holzmann, M. Harvey[2], M. Issah, Roy A. Lacey, A. Shevel[1]

[1] *Department of Chemistry, State University of New York at Stony Brook, Stony Brook, NY 11794*
[2] *Department of Physics, Brookhaven National Laboratory, Brookhaven NY*

(Dated: Draft-2 June, 2004)

In this note we report on the model-independent extraction of emission source images from Au+Au ($\sqrt{s_{NN}}$ = 200 GeV (run2)) and d+Au ($\sqrt{s_{NN}}$ = 200 GeV (run3)) collisions using the imaging method of D. A. Brown and P. Danielewicz. Source parameters extracted from these images indicate important contributions from long- and short-range emission sources in central Au+Au collisions. The m_T and centrality dependence of the source parameters for these emission sources are presented; they provide first insights on the character of the very large long-range source produced in central Au+Au collisions at RHIC.

Contents

1. Introduction 3
1.1. Imaging in Brief 3
1.2. Prior Application of the Technique 3

2. Analysis of Run-2 data: Run, event and track selections 4
2.1. Au+Au cuts 4
2.1.1. Run selection 4
2.1.2. Event selection 4
2.1.3. Track selection 4
2.1.4. PID selection in the EMC 4
2.1.5. PID selection in the TOF 5
2.2. d+Au cuts 5
2.2.1. Run selection 5
2.2.2. Event selection 6
2.2.3. Track selection 6
2.2.4. PID selection 6

3. Extracting correlation functions 7
3.1. Event Mixing 7
3.2. Determining Track-pair cuts 7
3.2.1. Inside-out Track Splitting Cuts 7
3.2.2. Inside-out Track merging cuts 9
3.3. Outside-in track-pair cuts for track splitting/merging 12
3.4. Summary of track merging and track splitting cuts 13
3.4.1. EMC 13
3.4.2. TOF 13

4. Consistency checks of the measured correlation functions 16
4.1. $\pi^+\pi^+$ and $\pi^-\pi^-$ pairs detected in EMC East 16
4.2. π^+ and π^- pairs detected in the TOF 16
4.3. Sensitivity to cut variations of σ PC3 association 21
4.3.1. EMC vs. TOF Correlations no PC3 association 21
4.3.2. EMC vs. TOF Correlations with PC3 association 21
4.4. Comparison of $\pi^-\pi^-$ pairs detected in EMC East and TOF 25
4.5. Comparison of $\pi^+\pi^+$ pairs detected in EMC East and TOF 28
4.6. EMC correlation functions: East vs. West 31
4.7. EMC-East correlation functions for $\pi^+\pi^+$: This work vs. PPG021 34
4.8. EMC-East correlation functions for $\pi^-\pi^-$: This work vs. PPG021 34
4.9. Comparison of Mixed-pair Correlation functions for $\pi^+\,\pi^-$ 39

5. Correlation functions from combined detections in EMC (E&W) and TOF 40
5.1. Correlation functions from EMC (E&W)+TOF 40
5.2. Consistency checks: EMC East vs EMC (E&W)+TOF 43
5.3. Consistency checks: TOF vs EMC (E&W)+TOF 43

6. Influence of cuts on the correlation functions 48
6.1. Sensitivity to cut variations of $\Delta\Phi_{DC}$ 48
6.1.1. $\Delta\Phi_{DC}$ variation for $\Delta zed > 5$cm 48
6.1.2. $\Delta\Phi_{DC}$ variation for $\Delta zed < 5$cm 51
6.1.3. Simultaneous variation of $\Delta\Phi_{DC}$ for $\Delta zed < 5$cm and $\Delta zed > 5$cm 54
6.2. Sensitivity to cut variations of ΔR 57
6.2.1. Cut variations of ΔR_{PC1} 57
6.2.2. Sensitivity to cut variations of $\Delta R_{EMC/TOF}$ 60
6.2.3. Summary of sensitivity cut variations of ΔR 60

7. Source image extraction 63
7.1. Extracting Source images 63
7.1.1. $\pi^-\pi^-$ images for $0 <$ centrality $< 30\,\%$ 63
7.1.2. $\pi^+\pi^+$ images for $0 <$ centrality $< 30\,\%$ 66
7.2. Extraction of source image parameters 69
7.2.1. Source image parameters for $\pi^+\pi^+$ 69
7.2.2. Source image parameters for $\pi^-\pi^-$ 72
7.3. m_T dependence of source image parameters for $\pi^-\pi^-$ and $\pi^+\pi^+$ 75

7.3.1. $0 < Centrality < 30\%$ 75
7.4. Centrality dependence of source image parameters for $\pi^-\pi^-$ and $\pi^+\pi^+$ 77
7.4.1. Centrality dependence of short-range source 77
7.4.2. Centrality dependence of Long-range source 77
7.5. m_T dependence of source image parameters for $\pi^-\pi^-$ and $\pi^+\pi^+$ 78
7.5.1. m_T dependence of the short-range source 78
7.5.2. m_T dependence of the Long-range source 78
7.6. Influence of pair-cuts on the source functions 79
7.6.1. $\Delta\Phi_{DC}$ variation for $\Delta zed > 5$cm 79
7.6.2. $\Delta\Phi_{DC}$ variation for $\Delta zed < 5$cm 83
7.6.3. $\Delta\Phi_{DC}$ variation for $\Delta zed < 1$cm 87
7.6.4. Simultaneous $\Delta\Phi_{DC}$ variations for $\Delta zed < 5$cm and $\Delta zed > 5$cm 91
7.7. A Quick Test of the Influence of Momentum Resolution 96
7.8. A Brief Note About Systematic Errors 100

1. INTRODUCTION

Two-particle relative momentum correlation studies (commonly referred to as HBT correlation studies) for various particle species, can provide an important probe of the space-time extent of the high energy density matter created at RHIC. Such correlations are usually obtained via the correlation function:

$$C(\vec{q}) = \frac{N_{cor}(q)}{N_{mix}(q)}, \quad (1)$$

where the numerator is the relative momentum distribution ($\vec{q}) = \vec{p}_1 - \vec{p}_2$) of particle pairs from the same event and the denominator is the relative momentum distribution of particle pairs obtained from mixed events. Here, $\vec{p}_1$ and $\vec{p}_2$ are the laboratory momenta of each particle in the pair. $C(\vec{q}) \equiv 1$ for large q-values where final-state interaction effects are negligible.

The correlation function is typically characterized by an enhancement at low q which reflects a combination of the Bose-Einstein (or Fermi-Dirac) statistics as well as the interactions between particle pairs. The analysis of the shape and magnitude of this enhancement serves as a basis for the extraction of the space-time extent of nucleus-nucleus collisions [1].

Traditional (HBT) correlation analysis rely on the assumption that Final-State Interactions (FSI) are weak and can be fully accounted for via one or more correction techniques. Following such a correction for FSI, one obtains a correlation function that is the Fourier Transform of the two-particle source function. This approximation is widely accepted as being valid for pions. However, for massive and/or strongly interacting particles such as protons or Λ hyperons, this approximation breaks down. Given the preponderance of different particle species (and their combinations) which can be employed toward the study of the space-time extent of RHIC collisions, it is worthwhile to investigate alternative approaches which are not hampered by the operational assumption of a weak FSI.

One such approach is the recent model-independent imaging technique proposed by Brown and Danielewicz [2]. Simply put, this technique *uses* the FSI encoded in the form of the particles' final state wave function, to extract the two-particle source function *directly* [2, 3, 5]. In earlier work, the technique has been used to address a few data sets; Panitkin et al.[8] have shown that this approach gives source radii similar to the conventional HBT approach (under the assumption of a Gaussian source) for $\pi^-\pi^-$ pairs emitted in central collisions for 2-8 AGeV Au+Au. By contrast, Verde et al.[9] have shown very different results for pp pairs from 75 AMeV ^{14}N+^{197}Au. Chung et al. [10] have used the method to extract and compare source images for pions, protons and Λ particles as discussed below. A key feature of the technique is that one can easily compare source functions across different species and assess the different space-time scales relevant for each particle pair – a feature that has been mentioned [2, 3, 4], but never seriously utilized at RHIC. In this note we introduce and apply the imaging technique to investigate emission source images for charged pions in d+Au and Au+Au collisions. Source images for a variety of particle species currently under investigation will be presented in future analysis notes.

1.1. Imaging in Brief

Theoretically, the correlation function can be calculated using the angle-averaged Koonin-Pratt equation [7]:

$$C(\vec{q}) = 4\pi \int dr r^2 K(q,r)\ S(r), \quad (2)$$

where the angle-averaged kernel $K(q,r)$ is calculated from the radial part of the anti-symmetrical two-pion relative wave-function. The source function $S(r)$, represents the probability distribution for emitting a pair of particles with relative distance r at the time the second particle is emitted. For identical spin-zero bosons with no final-state interactions (eg. pions), one can use the Coulomb force for the kernel:

$$K(q,r) = \frac{sin(2q\ r)}{2qr}.$$

For particles with final-state interactions:

$$K(q,r) = \sum_{l\ \ even} \frac{|g_l(r)|^2}{(2l+1)} - 1,$$

where, l is the orbital angular momentum quantum number and **g** is the relative final-state radial wave function. For protons **g** is the solution of the Schrödinger equation using the Coulomb potential and nucleon-nucleon potential [4, 5].

The main goal of an imaging analysis is the determination of the relative source function (S($\vec{r}$)) in Eq. [**?**] from the measured correlation function C($\vec{q}$). The success of this goal depends primarily on how well one is able to invert Eq. 2.

1.2. Prior Application of the Technique

We have successfully applied the imaging technique at lower energies [10] to extract source images for pions, protons and Λ particles. Fig. 1 shows an example of the source images so obtained. The left panels of Fig. 1 show the measured 1-D correlation functions for p-Λ, p-p and $\pi^-\pi^-$ pairs from Au+Au collisions at 6 GeV (shown in blue). The right panels show the corresponding source images and source parameters. It is important to note here that the imaging method allows one to obtain the restored correlation functions shown in red in the left

panel of the figure. The latter which is obtained by "unimaging" the data serves as an important cross check of the robustness of the extracted "source" parameters.

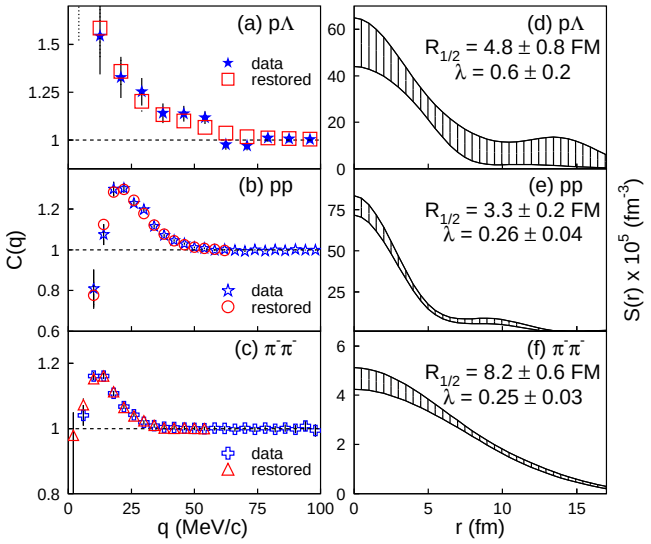

FIG. 1: *1D correlation functions, C(q), for pΛ (a), pp (b)and $\pi^-\pi^-$ (c) pairs from Au+Au collisions at 6 AGeV as measured by the E895 Collaboration [10]. The corresponding short-range source functions, S(r), are indicated in panels (d), (e) and (f) respectively. Restored correlation functions (open squares, circles and triangles) obtained from each source function are also shown. Hatched bands show the zone of one standard deviation. The figure is taken from [10].*

2. ANALYSIS OF RUN-2 DATA: RUN, EVENT AND TRACK SELECTIONS

In what follows, we discuss the run, event, and track selection cuts employed to obtain the correlation functions functions used in our imaging analysis.

2.1. Au+Au cuts

2.1.1. Run selection

The data analysis was performed with the "afterburner" version (v03) of the Central Track (CNT) nanoDST's for particles detected in the EMC (PbSc). For particles detected in the TOF, the Hadron Working Group (HWG) nanoDST's were used. Only full field runs (runs after run 27808) were used. In addition to the above selections, the following runs were also excluded:

- Photon converter runs and reverse field runs.
- Runs from the list MOM.txt [11]. For these runs the mean momentum of DC tracks are outside of the accepted range of 0.55 - 0.65 GeV/c).
- Runs from the list NDC.txt [11]. For these runs, the number of DC tracks are outside of the accepted range.
- Runs with known PC1 problems, ie. runs 32010-32441.
- Runs after number 32000. These runs show rather poor timing resolution for the PbSc.
- Runs in which number of segments are less than 10.

2.1.2. Event selection

Event selection fulfilled the following criteria:

- Events taken with the minimum bias trigger.
- Events satisfying the BBC vertex cut $|z_{BBC}| \leq 30\ cm$.
- Events satisfying the centrality range of $0 <$ centrality ≤ 92. Centrality was determined by the clock method.

The run and event selections itemized above, yielded a total of 22 M events for the analysis involving the EMC, and 20.2 M minimum bias events for the analysis involving the TOF [14].

2.1.3. Track selection

Tracks satisfying the following criteria were employed in the analysis:

- Tracks with quality 31 or 63.
- Tracks with abs(zed)<75 cm.
- Tracks which satisfied a 2σ "box" matching cut with hits in the EMC or TOF. For particles detected in the TOF we used a number of additional matching corrections as outlined in [13].

2.1.4. PID selection in the EMC

The charged pions used in this analysis were detected in sectors E1-E2 and W0-W4 of the EMC. The following cuts were applied to optimize clean PID separation and reduce background.

- A momentum cut of $0.25 < p < 1.0$ GeV/c.
- A timing cut of $0 <$ temc < 60 ns.
- PID selections satisfying the condition abs(isPip) $<$ 2 or abs(isPim) $<$ 2 [for pions], where isPip (π^+) and isPim (π^-) are probability functions which

define the number of sigmas by which the mass-squared of a track deviates from the assumption that it is a π^+ or π^-. It is noteworthy that these functions account for the different timing response of each calorimeter sector due to particle type, charge, deposited energy, and momentum (see [12] for details). For a 2σ momentum dependent PID cut it was possible to separate pions and kaons up to a momentum of 1.0 GeV/c. The rather good quality of this separation is illustrated in Fig. 5.

- Tracks which satisfied a 2.5σ "radial" association matching cut with PC3.

It is important to note here that matching cuts with PC3 are important for background suppression especially at low momentum. Our analysis shows that this background is due to random associations between reconstructed tracks and EMC/TOF clusters/hits. This is illustrated in Fig. 2 where we show the difference of the measured and the expected time for pions with $0.25 \leq p \leq 0.4$ GeV/c detected in a selected EMC sector. The blue curve shows the result for "true" pion tracks. The red curve shows the same distribution but for background tracks which make random associations between reconstructed tracks and clusters in the EMC. The latter was estimated by the Z-swap method. Fig. 2 clearly shows that background tracks can become significant for low momentum pions detected in the EMC. Accurate extraction of correlation functions require that these background tracks be removed.

Figs. 3 and 4 show the n-sigma distribution (isPion) for pions with and without an association requirement in PC3. Here again, an enhancement at negative values due to random background (blue curve) is clearly visible in Fig. 3. The green and red curves in Fig. 3 clearly indicates that this random background can be efficiently suppressed by requiring a relatively stringent association in PC3. A comparison of the same distributions with and without the PC3 association requirement for the TOF (cf. Fig. 4) indicates that the random background for the TOF is not as important.

2.1.5. PID selection in the TOF

For pions detected in the TOF the following cuts were employed:

- A momentum cut of $0.2 < p < 1.7$ GeV/c.
- A β dependent energy loss cut.
- A PID selection satisfying the condition abs(isPi)<2. For the latter cut we used the isPi-function from the utiHadPiD library.
- Tracks which satisfied a 3.0σ "radial" association matching cut with PC3.

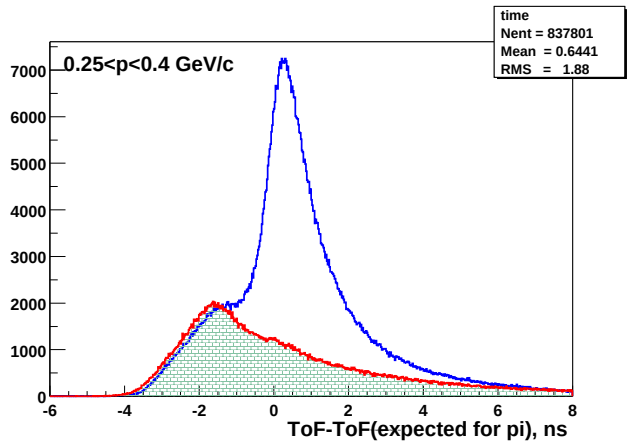

FIG. 2: *The difference of the measured and expected time for pions with momentum ($0.25 \leq p \leq 0.4$ GeV/c) for one of the EMC PbSc sector. The red curve shows the shape of background due to random associations between reconstructed tracks and clusters in the EMC. The latter is estimated by the Z-swap method .*

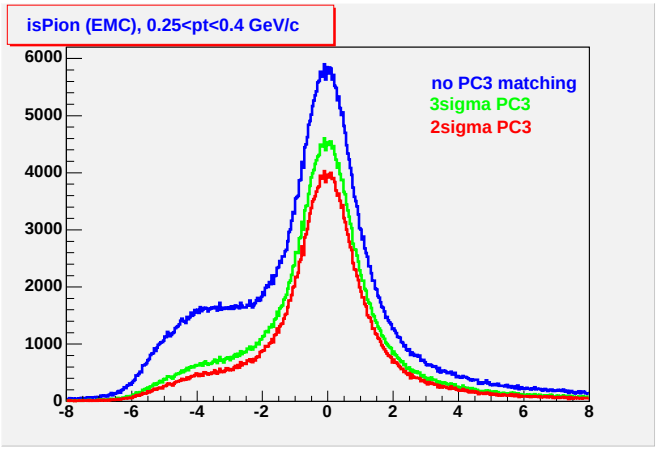

FIG. 3: *n-sigma PID distribution (isPion) for charged tracks of $0.25 \leq p_t \leq 0.4$ GeV/c) detected in sectors E2 and E3 of the EMC. The blue curve shows the result of a 2σ EMC matching cut. The green and red curves show results for a 2σ EMC matching cut in combination with a $2.5\,\sigma$ (green) and a $2.0\,\sigma$ (red) PC3 cut.*

2.2. d+Au cuts

2.2.1. Run selection

For analysis of d+Au data we used the minimum bias CentralTrack nanodst's (CNT) from the run3dAu_v03AG_pro48 production. Runs were selected following the PID and QA prescriptions detailed in Phenix Analysis Note AN 281 [16].

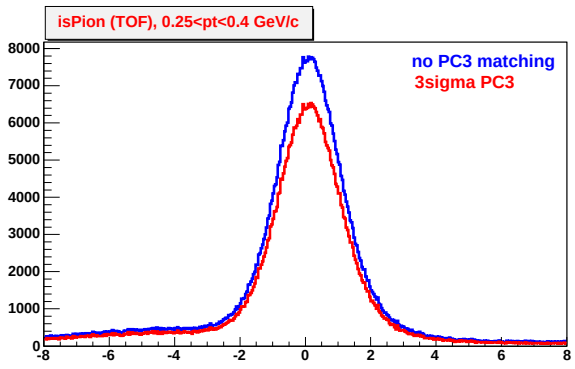

FIG. 4: *n-sigma PID distribution (isPion) for charged tracks of 0.25 ≤ p_t ≤ 0.4 GeV/c) detected in the TOF. The blue curve shows the result of for no PC3 matching. The red curves shows results for a 3σ PC3 matching cut.*

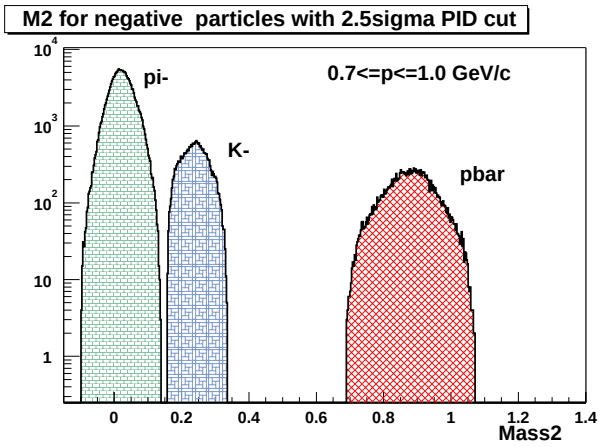

FIG. 5: *Mass-squared (mass^2) distributions for negative particles after a 2.5σ PID cut. Results are shown for the momentum range 0.7≤p≤1.0 GeV/c.*

2.2.2. Event selection

Our analysis was restricted to events fulfilling the following conditions:

- Events obtained with a Minimum bias trigger.
- Events satisfying the BBC vertex cut of $|z_{BBC}| \leq 30\ cm$.
- Events satisfying the centrality range 0 < centrality ≤ 88.5%.

The run and event selections indicated above, yielded ∼ 60 M minimum bias events.

2.2.3. Track selection

Our analysis was restricted to tracks fulfilling the following conditions:

- Tracks with quality 31 or 63.
- Tracks with abs(zed)<75 cm.
- Tracks satisfying a 2σ "box" matching cut with hits in the EMC.
- Tracks satisfying a 2.5σ "radial" matching cut with PC3.

2.2.4. PID selection

The pions used in the d+Au analysis were obtained primarily from sectors W0-W2 and E2-E3 of the EMC. The following PID cuts were applied to facilitate clean PID separation:

- A momentum cut of 0.25 < p < 1.0 GeV/c
- A timing cut of 0< temc < 60 ns.
- PID selections satisfying the condition abs(isPip) <2 for π^+ and abs(isPim) <2 for π^-, see [17].

In addition to the single particle cuts outlined above, pair cuts were applied prior to the construction of correlation functions for Au+Au and d+Au as discussed below.

3. EXTRACTING CORRELATION FUNCTIONS

The two-pion correlation function is obtained from a ratio of two distributions;

$$C(\mathbf{q}) = \frac{N_{cor}(q)}{N_{mix}(q)}, \quad (3)$$

where $N_{cor}(q)$ is the distribution of correlated track pairs with momentum difference $q = Q_{inv}/2$ and $N_{mix}(q)$ is the pair distribution obtained from mixed events.

$$Q_{inv} = \sqrt{|(E_1 - E_2)^2 - (\vec{p}_1 - \vec{p}_2)^2|}.$$

The mean transverse momentum k_T=($\mathbf{p}_{T,1}$+$\mathbf{p}_{T,2}$).

3.1. Event Mixing

Event mixing was done in 3cm bbc-vertex bins and in 5% centrality bins [for Au+Au collisions] to avoid multiplicity correlations and potential detector pathologies. For analysis of d+Au data, the lower multiplicities necessitated the the use of 5 cm bbc-vertex bins and 20% centrality bins. For both d+Au and Au+Au collisions, event mixing across runs was avoided in order to minimize distortions [to the correlation function] resulting from run-by-run efficiency changes.

3.2. Determining Track-pair cuts

Track splitting ("ghosts") and track merging can serve to distort the measured correlation functions especially at low q. In order to eliminate such distortions, we follow a procedure that is commonly exploited in correlation function studies. That is, we first carry out a careful study of the track-pair efficiency as a function of centrality and p_T to establish a robust set of track-pair cuts which removes track splitting, merging, inefficiencies of one sort or another, etc. Following this, we apply this set of track-pair cuts to both the distribution of correlated track pairs and the distribution of track-pairs obtained from the mixed-events prior to the construction of the correlation functions. This procedure ensures the same track-pair acceptance for correlated and uncorrelated or mixed events. Consequently, it ensures the elimination of any distortion to the correlation function which could result from track splitting, merging, inefficiencies, etc.

To assign track-pair cuts, we followed both an "inside-out" and an "outside-in" approach. That is, cuts were evaluated and applied in the order DCH→ PC1 → EMC/TOF (inside-out) and in the order EMC/TOF→ PC1 → DCH (outside-in). Subsequent to establishing track-pair cuts, we varied these cuts over "reasonable" ranges and studied the resulting effect on the extracted correlation functions and source images. As discussed below, these studies resulted in a robust set of cut values suitable for reliable extraction of the correlation functions.

3.2.1. *Inside-out Track Splitting Cuts*

The track reconstruction procedure can occasionally lead to the construction of a physical track multiple times. This results in a multiplet of tracks (commonly referred to as "ghosts") that have virtually every parameter in common. Particle pairs from a family of ghosts generally cluster tightly in phase space and can give rise to additional spurious near angle correlations. Figs. 6 and 7 show two dimensional correlation functions in Δzed - $\Delta\phi_{DC}$ space, which illustrates this effect. Δzed and $\Delta\phi_{DC}$ are the zed-difference, and the ϕ-difference at the Drift Chamber reference radius [for particle pairs] respectively. The rather prominent peak at relatively small values of $\Delta\phi_{DC}$ and Δzed is the characteristic signature attributed to "ghosts". Close inspection of Fig. 7 also reveals inefficiencies for small $\Delta\phi_{DC}$ and $\Delta zed \sim$ 1-5 cm. The latter is largely due to track merging as discussed below.

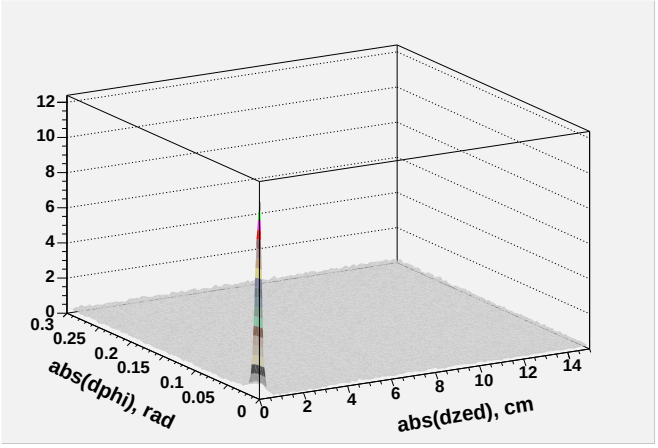

FIG. 6: *Two dimensional correlation function in Δzed - $\Delta\phi_{DC}$ for ++ pairs. No pair cuts are applied .*

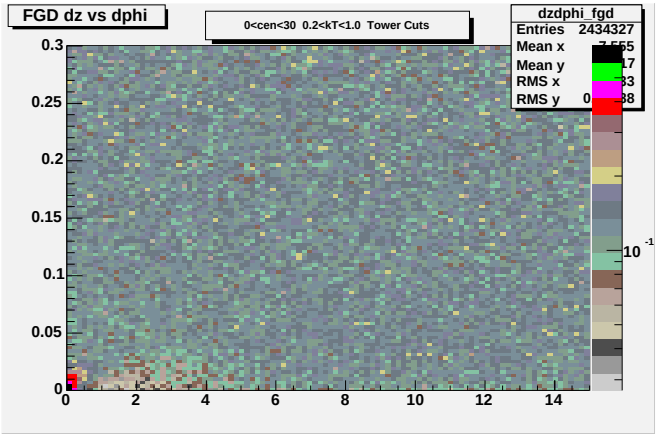

FIG. 7: *Two dimensional correlation function in Δzed - $\Delta\phi_{DC}$ for ++ pairs. No pair cuts are applied .*

Another tell-tale signature for ghosting is the charac-

teristic enhancement in the ΔR correlation functions for track projections to the EMC, PC1, PC3 and TOF;

- $\Delta R_{PC1} = \sqrt{(ppc1x_1 - ppc1x_2)^2 + (ppc1y_1 - ppc1y_2)^2 + (ppc1z_1 - ppc1z_2)^2}$
- $\Delta R_{EMC} = \sqrt{(pemcx_1 - pemcx_2)^2 + (pemcy_1 - pemcy_2)^2 + (pemcz_1 - pemcz_2)^2}$

Figures 8 and 9 show one dimensional correlation functions (ratio of correlated and mixed event distributions) of the distances between track projections in PC1 and the EMC respectively. Here again, one sees rather prominent peaks at small distances which result from "ghosting". By contrast, the inefficiencies due track merging, which are visible in Fig. 7 are clearly masked.

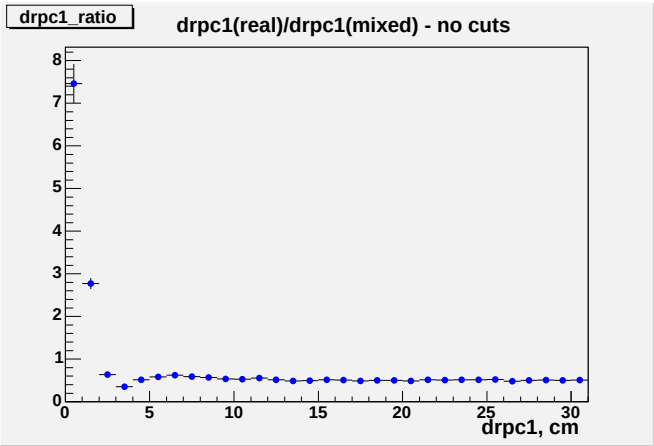

FIG. 8: *ΔR_{PC1} distance correlations ("true" events divided by mixed events) for positive pion pairs. No pair cuts are applied.*

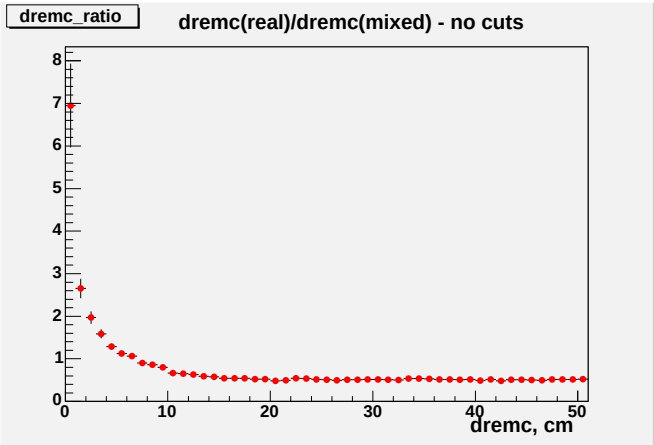

FIG. 9: *ΔR_{EMC} distance correlations ("true" events divided by mixed events) for positive pion pairs. No pair cuts are applied .*

If two particles hit the same TOF slat or the same EMC tower, then PID information is lost because the separate timing information for each particle is lost. Such pairs were removed from the data sample via so called tower/slat cuts. An important benefit of the removal of such track pairs is a substantial reduction in the number of "ghost" pairs. Figs. 10 and 11 show $\Delta\phi_{DC}$ correlation functions for the full p_T range and for the centrality selection 0-30%. Fig.10 shows correlation functions for Δzed cuts of 0-1, 1-2, 2-3, 3-4, 4-5 and 5-6 cm. Fig.11 shows the same correlation function for Δzed >8 cm with tower/slat cuts applied.

For the cut 0 < Δzed< 1 cm a clear ghosting peak can be seen (see top left panel). For all other Δzed selections, this prominent "ghost" peak is superseded by a rather clear track-pair inefficiency. We conclude that this inefficiency, which was partially visible in Fig. 7, is now made more apparent due to significant suppression of ghosts via the tower/slat cuts. As indicated earlier these inefficiencies are largely due to track merging.

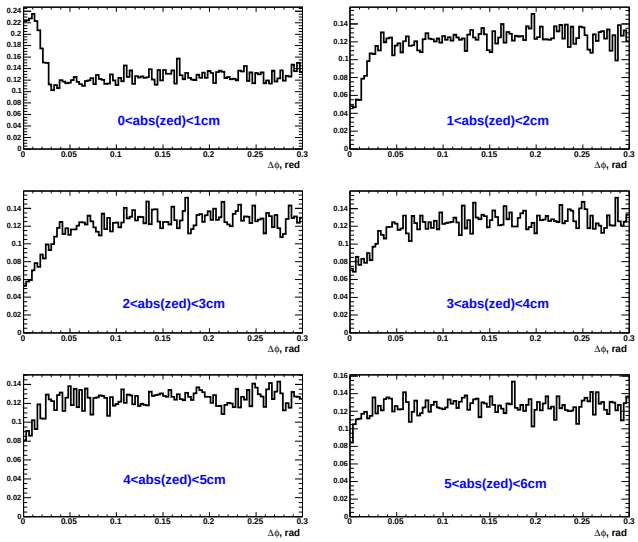

FIG. 10: *$\Delta\phi_{DC}$ correlations (ratio of correlated and mixed pair distributions) for Δzed cuts of 0-1, 1-2, 2-3, 3-4, 4-5, and 5-6 cm respectively. Tower cuts have been applied .*

Further studies of the $\Delta\phi_{DC}$ correlation functions were made as a function of centrality and p_T in order to investigate possible p_T and centrality dependent variations. Figs. 12, 13, 14, and 15 show representative examples of the p_T dependence of $\Delta\phi_{DC}$ for the centrality cut 0-30%. They do not show a strong dependence on k_T. Similar studies performed at different centralities for a fixed

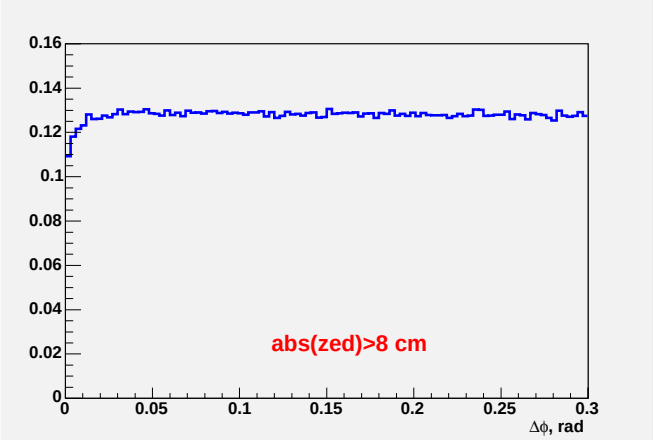

FIG. 11: $\Delta\phi_{DC}$ *correlation function for* $\Delta zed > 8cm$ *(after applying the tower cut).*

k_T indicated very little, if any, centrality dependence.

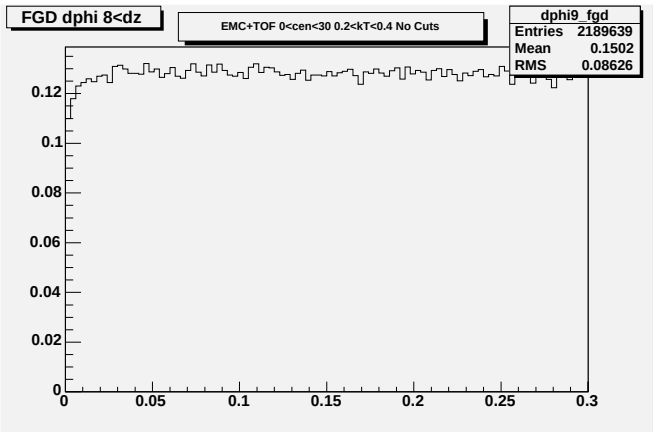

FIG. 12: $\Delta\phi_{DC}$ *correlation function for* $0.2 < k_T < 0.4$ GeV/c *and* $\Delta zed < 8$ *cm. Results are shown for the centrality cut 0-30% and with tower/slat cuts applied .*

Careful inspection of Figs. 10, 11, 12, 13, 14, and 15 indicate the following *tentative* best cuts for removing ghosts and some of the inefficiencies visible at low $\Delta\phi$ and Δzed:

- $\Delta\phi > 0.03$ for $0 < \Delta zed < 5$ cm
- $\Delta\phi > 0.01$ for $\Delta zed > 5$ cm

Hereafter, we refer to these cuts as multi-cut. Fig. 16 gives a pictorial representation of this multi-cut. We note here that Fig. 6 gives the same 2D-distribution but without the multi-cut. The multi-cut is used to make additional studies of the track merging cuts as discussed below.

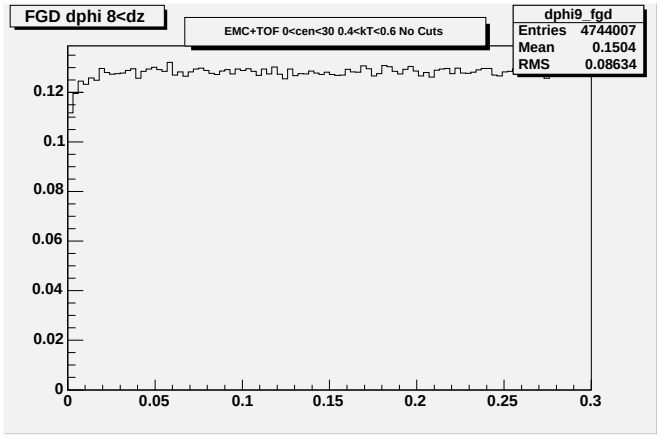

FIG. 13: $\Delta\phi_{DC}$ *correlations (real events divided by mixed events) for* $0.4 < k_T < 0.6$ GeV/c *and* $\Delta zed < 8$ *cm. Results are shown for the centrality cut 0-30% and with tower/slat cuts applied .*

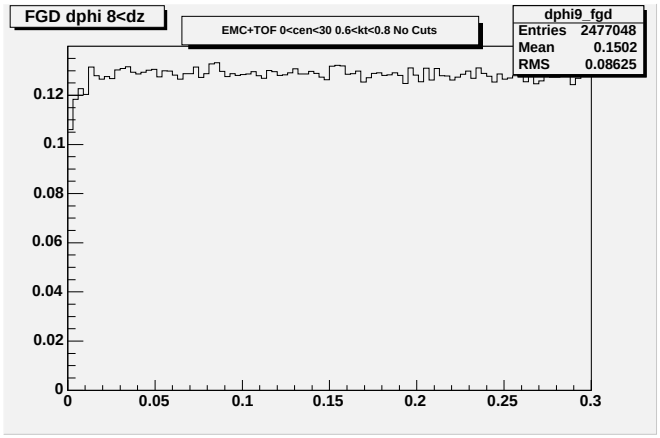

FIG. 14: $\Delta\phi_{DC}$ *correlation function for* $0.6 < k_T < 0.8$ GeV/c *and* $\Delta zed < 8$ *cm. Results are shown for the centrality cut 0-30% and with tower/slat cuts applied .*

3.2.2. Inside-out Track merging cuts

Due to finite detector resolution, one cannot measure track-pairs in real events that are closer than a certain distance (track merging). On the other hand, particle-pairs obtained from mixed events have no such constraint because they belong to different events and thus, can cluster below the two-track resolution limit. Such pairs, if included in the analysis, would lead to distortions in the correlation functions, so it is important to suppress them. To do this we establish and apply the same track merging cuts to both correlated and mixed event track pairs. We quantify the degree of track merging via the distribution of the distance between track positions (ΔR) in PC1 and EMC or TOF.

To establish a reliable set of track-merging cuts, we have carried out an extensive study of ΔR correlations for different selections of k_T, centrality, etc. Several rep-

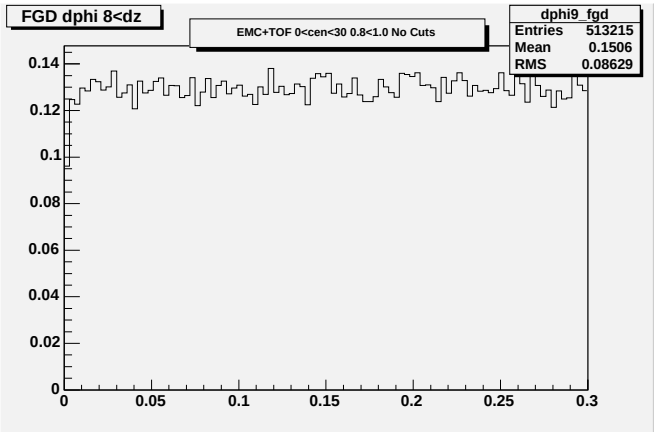

FIG. 15: *$\Delta\phi_{DC}$ correlation function for $0.8 < k_T < 1.0$ GeV/c and $\Delta zed < 8$ cm. Results are shown for the centrality cut 0-30% and with tower/slat cuts applied .*

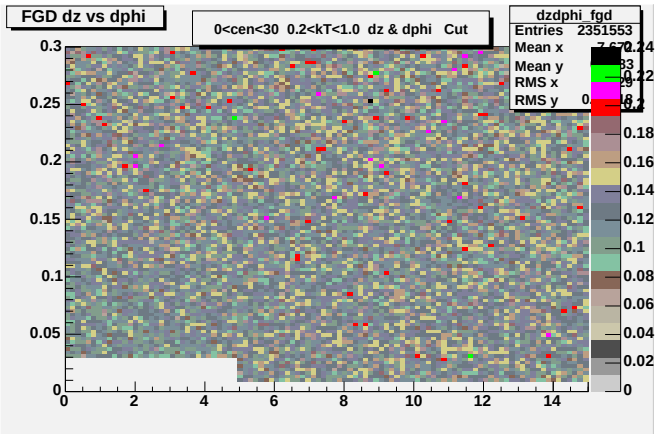

FIG. 16: *Two dimensional correlation function in Δzed - $\Delta\phi_{DC}$ for ++ pairs with multi-cut applied. Multi-cut is used to remove ghosting and some amount of inefficiency due to track merging (see text).*

resentative results from this study follow.

Figures 17 and 18 show ΔR correlation functions for PC1 and the EMC after application of the multi-cut. They were obtained for a centrality selection of 0-30% and the cut $0.2 < p_T < 1.0$. Both correlation functions indicate the presence of inefficiencies or track-merging below $\sim$ 8 and 18 cm for PC1 and EMC respectively. As indicated earlier, ΔR correlation functions were also studied as a function of centrality. Figs. 19, 20, 21 and 22 summarize results obtained for the EMC for centralities of 0-90, 0-10, 10-20 and 20-50% respectively. They show the same track-merging alluded to earlier but with little, if any, centrality dependence. A similar centrality study for ΔR_{PC1} indicated little or no centrality dependence as well.

After careful study of ΔR_{PC1} and ΔR_{EMC} the following *tentative* best cuts for track merging were obtained.

- $\Delta R_{PC1} = 7$ cm

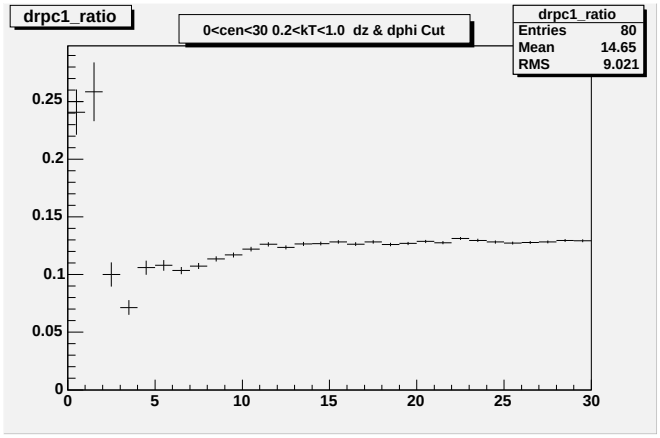

FIG. 17: *ΔR_{PC1} correlation function with multi-cut applied (see text).*

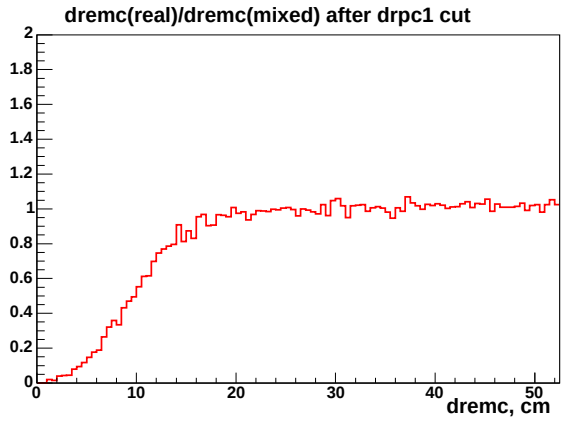

FIG. 18: *ΔR_{EMC} correlation function with multi-cut applied (see text).*

- $\Delta R_{EMC} = 16$ cm

Further study of these cuts are made in the next section.

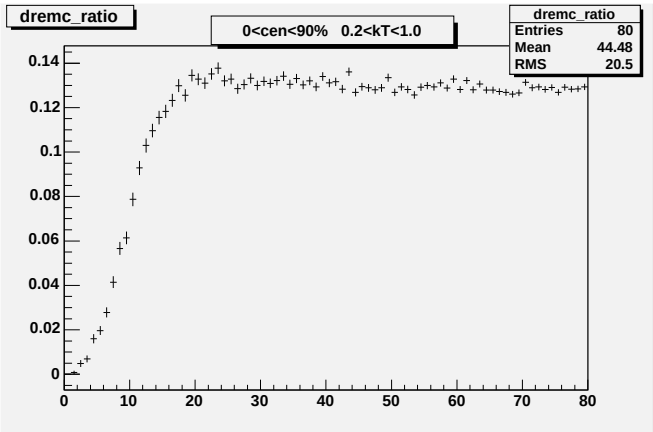

FIG. 19: ΔR_{EMC} *correlation function with multi-cut applied (see text). Results are shown for a centrality cut of 0-90%.*

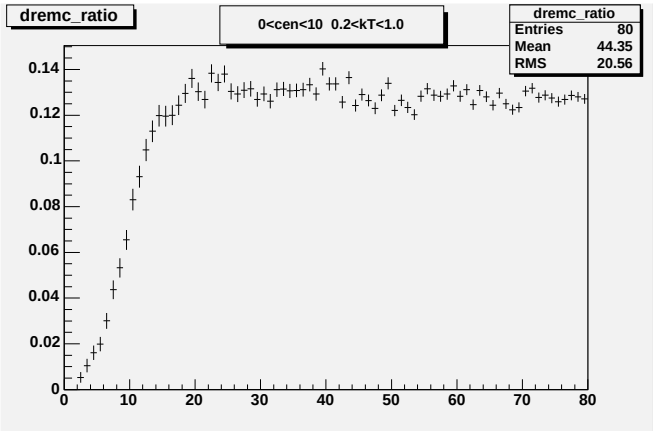

FIG. 20: ΔR_{EMC} *correlation function with multi-cut applied (see text). Results are shown for a centrality cut of 0-10%.*

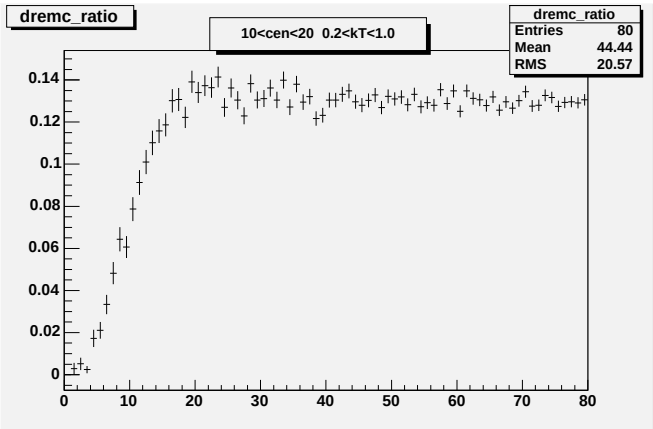

FIG. 21: ΔR_{EMC} *correlation function with multi-cut applied (see text). Results are shown for a centrality cut of 10-20%.*

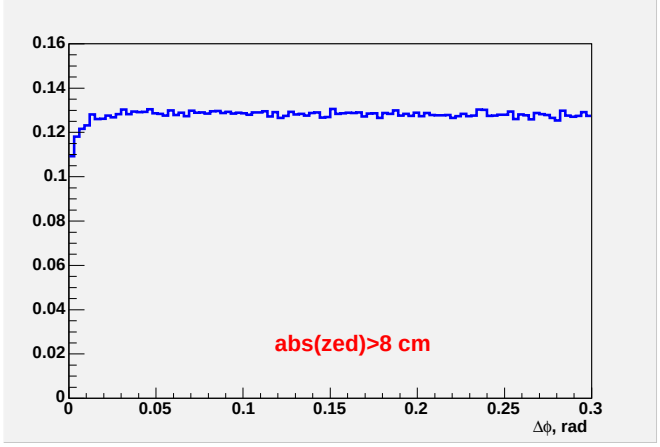

FIG. 22: ΔR_{EMC} *correlation function with multi-cut applied (see text). Results are shown for a centrality cut of 20-50%.*

3.3. Outside-in track-pair cuts for track splitting/merging

As indicated in Sec. 3 track-pair cuts were evaluated by way of both an "inside-out" and an "outside-in" approach, ie. cuts were evaluated and applied in the order DCH→ PC1 → EMC/TOF (inside-out) and in the order EMC/TOF→ PC1 → DCH (outside-in). In the previous subsection we described the procedures employed to arrive at a set of *tentative* best cuts following the "inside-out" approach. In this subsection we follow the "outside-in" approach to establish another set of cuts. Following this, an optimized set of cuts is established and used for further study.

Figures 23 and 23 shows 2D correlation functions, ΔR_{PC1} - ΔR_{EMC}, for positively charged pion pairs obtained in Au+Au and d+Au collisions respectively. In each case the only tower/slat cuts have been applied. The figure shows clear evidence for regions of enhancement due to ghosting as well as regions of inefficiency due to track merging. Such regions are much better illustrated in Figs. 25 and 26 which show one dimensional projections for ΔR_{PC1} and ΔR_{EMC} respectively for Au+Au collisions. A similar set of results for d+Au is shown in Figs. 27 and 28 Following close inspection of a variety of such correlation functions the following ΔR cuts were assigned:

- $\Delta R_{PC1} = 7$ cm
- $\Delta R_{TOF} = 14$ cm
- $\Delta R_{EMC} = 16$ cm

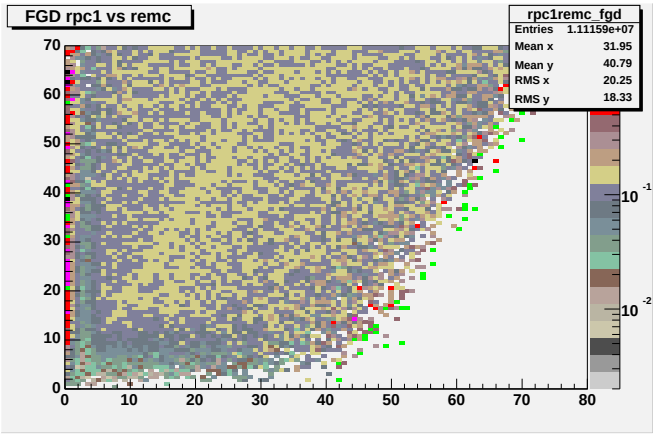

FIG. 23: *Two dimensional correlation function in* ΔR_{PC1} - ΔR_{EMC} *for Au+Au. Results are shown for positive pion pairs. No pair cuts are applied .*

Figure 29 gives a 2D view of these cuts as applied to PC1 and the EMC.

After establishing pair cuts for PC1, EMC and TOF (ΔR_{PC1}, ΔR_{EMC} and ΔR_{TOF}), we applied them along with the tower/slat cuts, and generated a large assortment of two dimensional (Δzed - $\Delta\phi_{DC}$) and one dimensional ($\Delta\phi_{DC}$) correlation functions. These latter

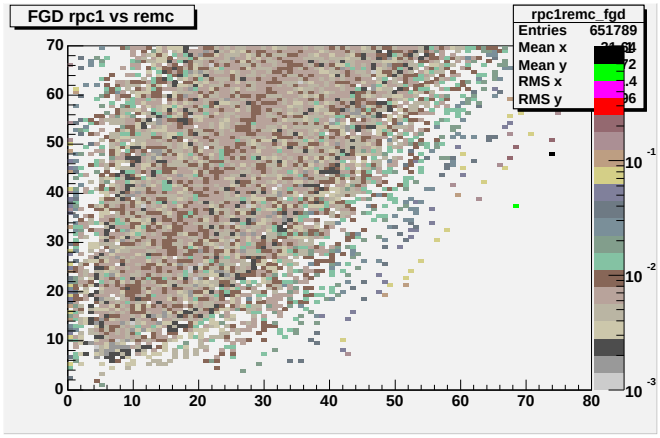

FIG. 24: *Two dimensional correlation function in* ΔR_{PC1} - ΔR_{EMC} *for d+Au. Results are shown for positive pion pairs. No pair cuts have been applied .*

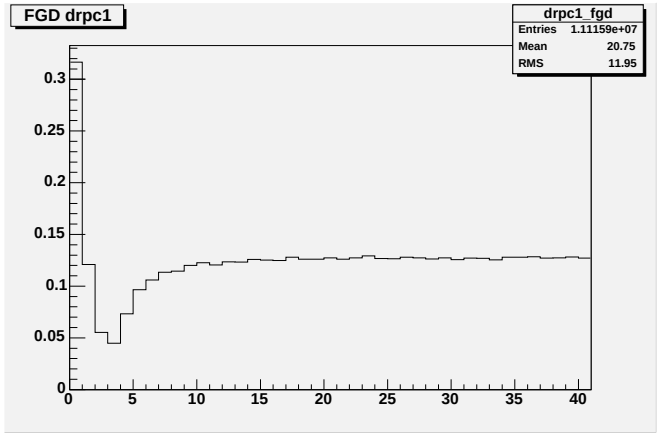

FIG. 25: ΔR_{PC1} *correlation function for Au+Au positive pion pairs. Tower/slat cuts have been applied but no pair cuts are applied .*

correlation functions were used to determine appropriate $\Delta\phi_{DC}$ cuts. Fig. 30 shows a representative 2D correlation function which clearly points to the absence of very strong pathological signals due to track splitting and merging. Figs. 31 - 38 show $\Delta\phi_{DC}$ correlation functions for Δzed cuts of 0-1, 1-2, 2-3, 3-4, 4-5, 5-6 and Δzed >8 cm respectively for Au+Au. Unlike their counterparts which were shown in Fig.10 and Fig.11, these correlation functions do not show glaring ghost peaks nor very large deficits due to track merging. After careful study of these correlation functions as a function of centrality and p_T, the following $\Delta\phi_{DC}$ cuts were assigned in addition to the slat/tower cuts:

- $\Delta\phi > 0.02$ for $0 < \Delta zed < 5$ cm
- $\Delta\phi > 0.01$ for $\Delta zed > 5$ cm

It is important to note here that both the "inside-out" and the "outside-in" cut-evaluation procedures give the same ΔR pair-cut values. However, the the $\Delta\phi$ cuts

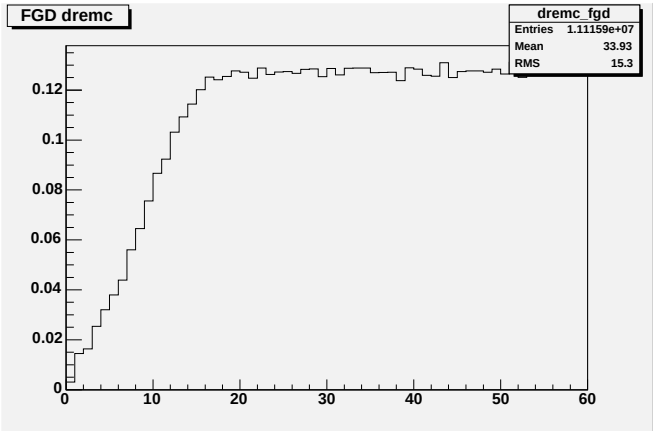

FIG. 26: ΔR_{EMC} *correlation function for Au+Au positive pion pairs. Tower/slat cuts have been applied but no pair cuts are applied .*

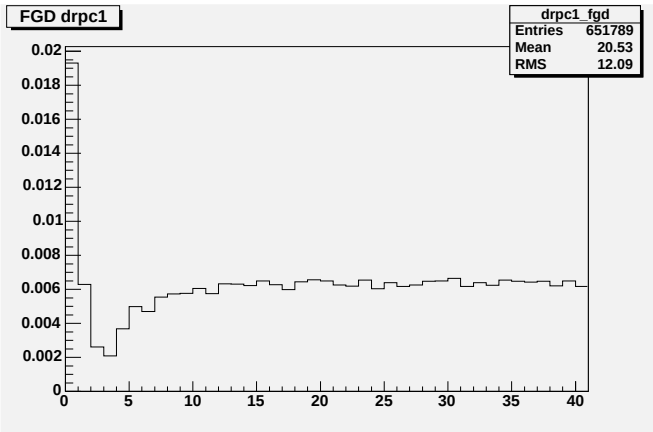

FIG. 27: ΔR_{PC1} *correlation function for d+Au positive pion pairs. Tower/slat cuts have been applied but no pair cuts are applied .*

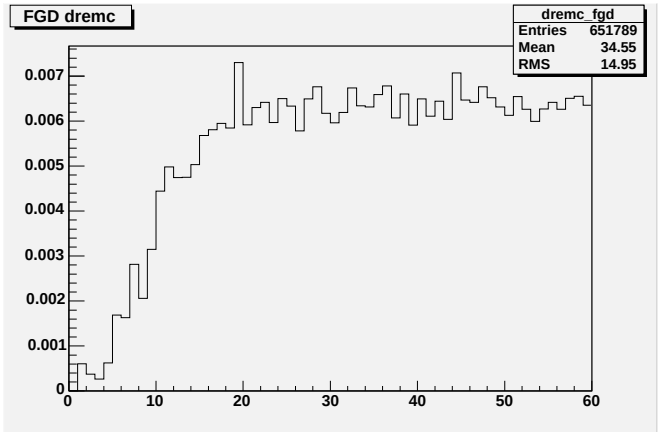

FIG. 28: ΔR_{EMC} *correlation function for d+Au positive pion pairs. Tower/slat cuts have been applied but no pair cuts are applied .*

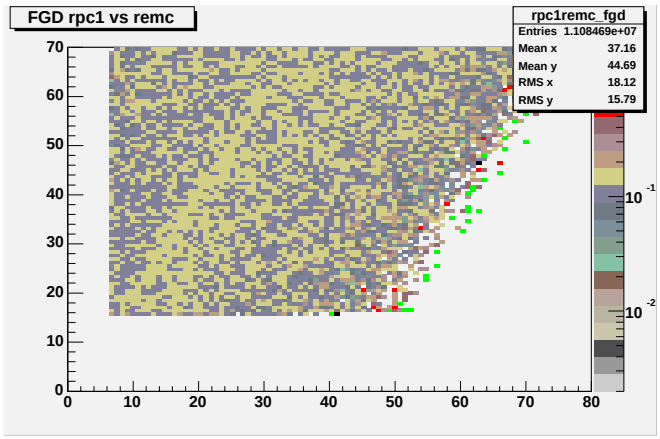

FIG. 29: *Two dimensional correlation function in* ΔR_{PC1} - ΔR_{EMC} *for ++ pairs with* ΔR_{PC1} *and* ΔR_{EMC} *pair cuts applied .*

obtained from the "outside-in" procedure are much less constraining than the ones obtained in the "inside-out" procedure. This being the case, we choose these latter cuts as part of our standard set used for final analysis of the data.

3.4. Summary of track merging and track splitting cuts

The resulting cuts used to remove the effects of track splitting (ghosting) and track merging for both Au+Au and d+Au are as follows:

3.4.1. EMC

- $\Delta\phi_{DC} > 0.02$ *for* $0 < \Delta zed < 5$ cm
- $\Delta\phi_{DC} > 0.01$ *for* $\Delta zed > 5$ cm
- A merging cut for PC1: $\Delta R_{PC1} = 7$ cm
- A merging cut for EMC: $\Delta R_{EMC} = 16$ cm

3.4.2. TOF

- $\Delta\phi_{DC} > 0.02$ *for* $0 < \Delta zed < 5$ cm
- $\Delta\phi_{DC} > 0.01$ *for* $\Delta zed > 5$ cm
- A merging cut for PC1: $\Delta R_{PC1} = 6$ cm
- A merging cut for EMC: $\Delta R_{TOF} = 14$ cm

These are the pair cuts which were applied in conjunction with slat/tower cuts for final generation of the correlation functions.

In the next section we investigate the effect of several cut variations on the extracted correlation functions.

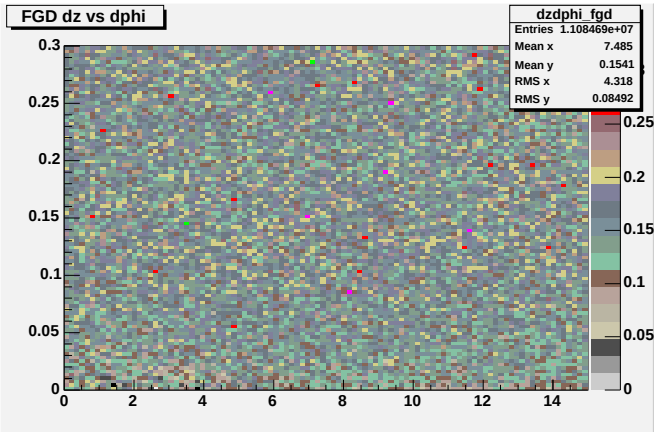

FIG. 30: *Two dimensional* Δzed - $\Delta\phi_{DC}$ *correlation function for ++ pairs with* ΔR_{PC1} *and* ΔR_{EMC} *pair cuts applied .*

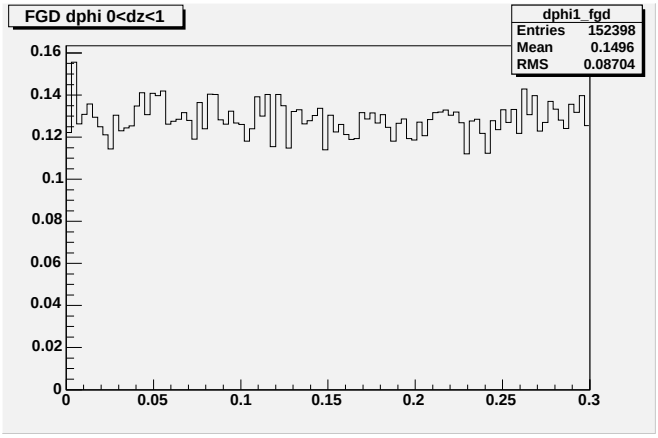

FIG. 31: $\Delta\phi_{DC}$ *correlation function for* $0 < \Delta zed < 1$ *cm (after application of* ΔR_{PC1} *and* ΔR_{EMC} *pair cuts).*

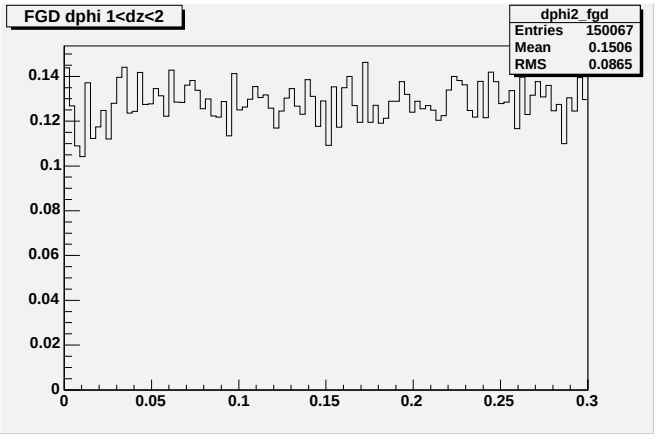

FIG. 32: $\Delta\phi_{DC}$ *correlation function for* $1 < \Delta zed < 2$ *cm (after application of* ΔR_{PC1} *and* ΔR_{EMC} *pair cuts).*

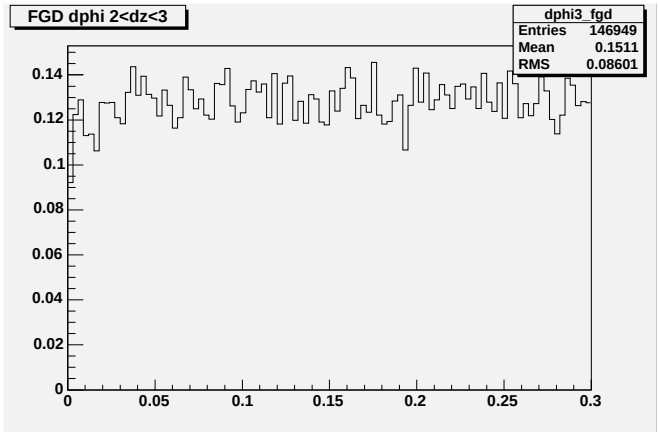

FIG. 33: $\Delta\phi_{DC}$ *correlation function for* $2 < \Delta zed < 3$ *cm (after application of* ΔR_{PC1} *and* ΔR_{EMC} *pair cuts).*

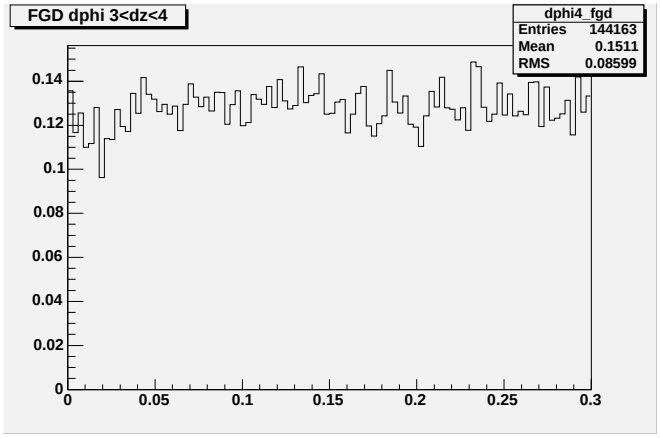

FIG. 34: $\Delta\phi_{DC}$ *correlation function for* $3 < \Delta zed < 4$ *cm (after application of* ΔR_{PC1} *and* ΔR_{EMC} *pair cuts).*

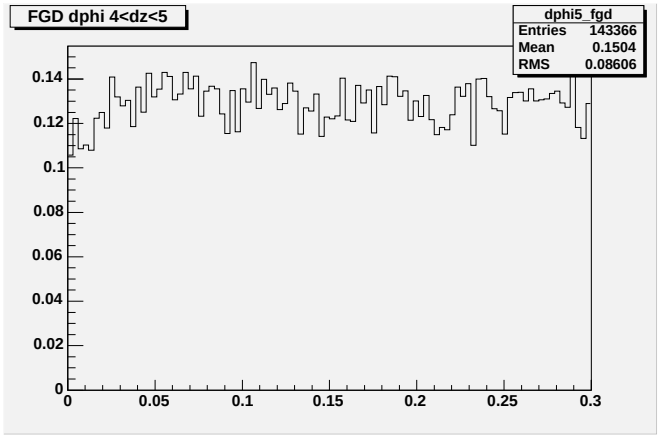

FIG. 35: $\Delta\phi_{DC}$ *correlation function for* $4 < \Delta zed < 5$ *cm (after application of* ΔR_{PC1} *and* ΔR_{EMC} *pair cuts).*

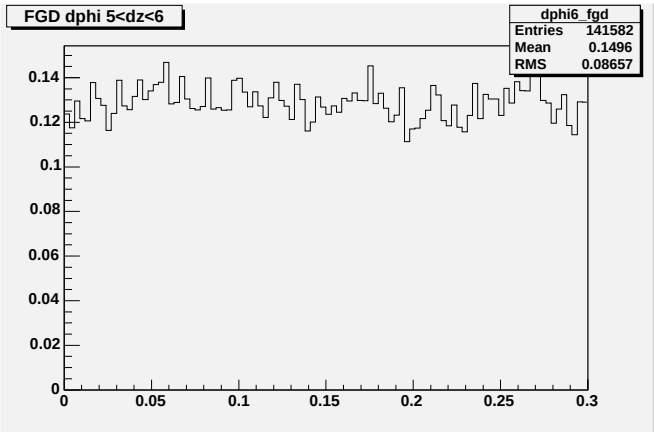

FIG. 36: *$\Delta\phi_{DC}$ correlation function for $5 < \Delta zed < 6$ cm (after application of ΔR_{PC1} and ΔR_{EMC} pair cuts).*

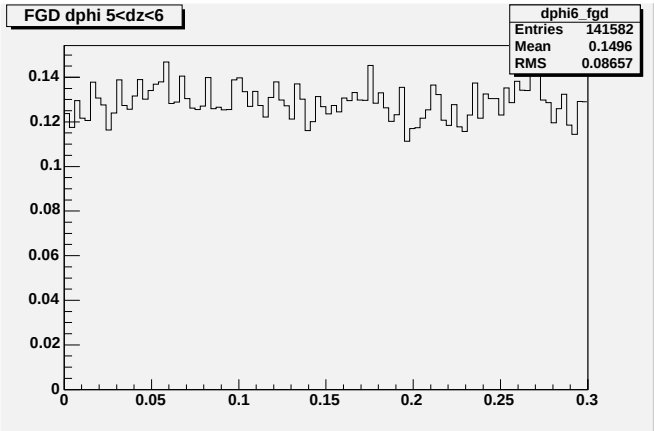

FIG. 37: *$\Delta\phi_{DC}$ correlation function for $6 < \Delta zed < 7$ cm (after application of ΔR_{PC1} and ΔR_{EMC} pair cuts).*

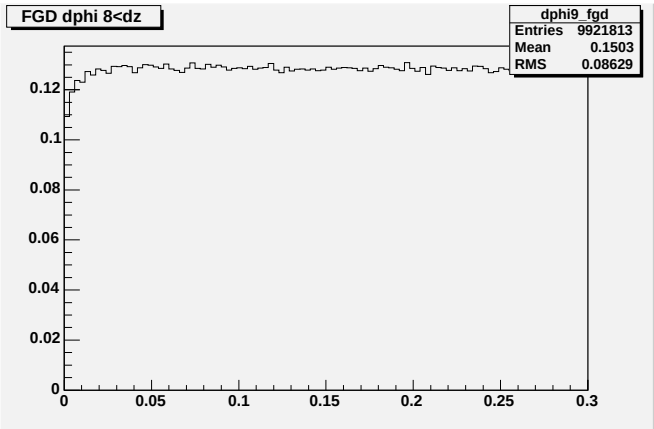

FIG. 38: *$\Delta\phi_{DC}$ correlation function for $8 < \Delta zed$ cm (after application of ΔR_{PC1} and ΔR_{EMC} pair cuts).*

4. CONSISTENCY CHECKS OF THE MEASURED CORRELATION FUNCTIONS

The track-pair cuts obtained from the "inside-out" and "outside-in" procedures described earlier in Sec. 3 were used to generate and study a large array of correlation functions for different selections of k_T, centrality, charge type, subsystem (EMC/TOF), cut variations, etc, for both Au+Au and d+Au. In what follows we show representative results and use a series of comparisons to show many of the salient features of these studies. The comparisons indicate very good agreement between the correlation functions obtained for different charge pions in each subsystem as well as across subsystems.

4.1. $\pi^+\pi^+$ and $\pi^-\pi^-$ pairs detected in EMC East

Figures 39, 40, 41, 42, 43, 44, 45 and 46 compare correlation functions for positive and negative pion pairs detected in the EMC. The comparisons are made for a centrality selection of 0-30% and several k_T selections. They indicate rather good agreement between the correlation functions obtained for $\pi^+\pi^+$ and $\pi^-\pi^-$.

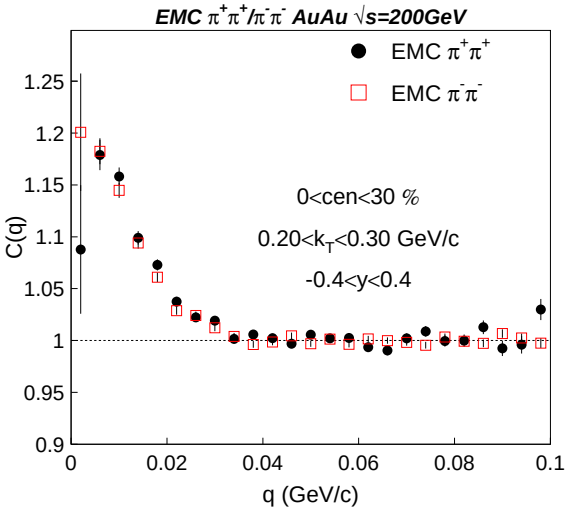

FIG. 39: *Comparison of correlation functions for negative and positive pion pairs detected in the EMC east. Results are shown for* $0 <$ *centrality* < 30 *and* $0.2 < k_T < 0.3$ *GeV/c.*

4.2. π^+ and π^- pairs detected in the TOF

Figures 47, 48, 49, 50, 51, 52, 53 and 54 compare correlation functions for positive and negative pions pairs

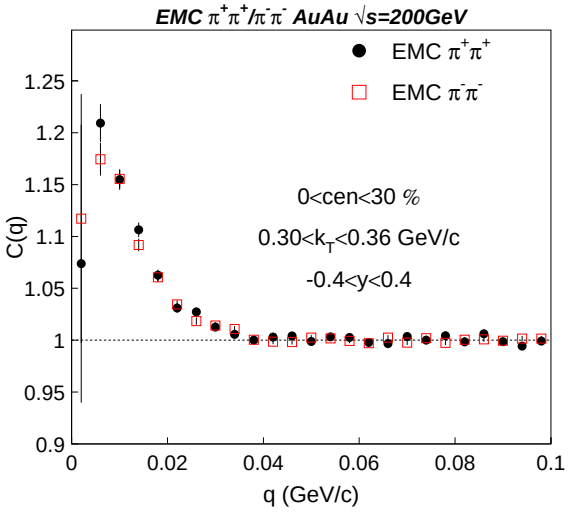

FIG. 40: *Comparison of correlation functions for negative and positive pion pairs detected in the EMC east. Results are shown for* $0 <$ *centrality* < 30 *and* $0.3 < k_T < 0.36$ *GeV/c.*

detected in the TOF. The comparisons which are shown for several k_T selections indicate similarly good agreement for $\pi^+\pi^+$ and $\pi^-\pi^-$ correlation functions measured in the TOF.

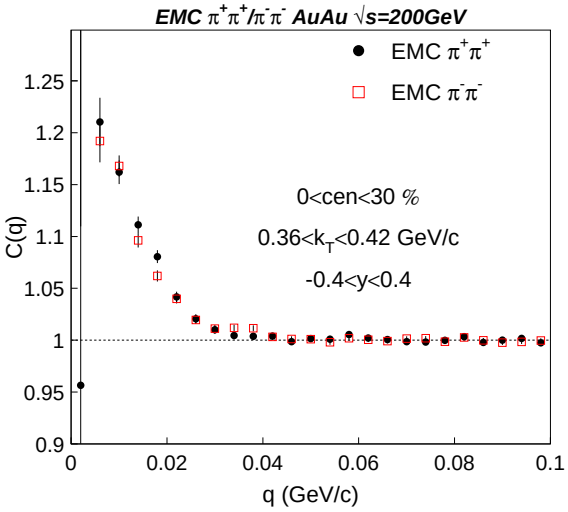

FIG. 41: *Comparison of correlation functions for negative and positive pion pairs detected in the EMC east. Results are shown for* $0 <$ *centrality* < 30 *and* $0.36 < k_T < 0.42$ *GeV/c.*

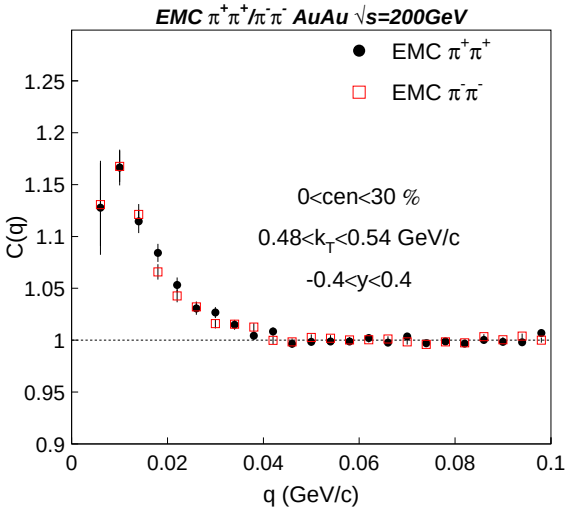

FIG. 43: *Comparison of correlation functions for negative and positive pion pairs detected in the EMC east. Results are shown for* $0 <$ *centrality* < 30 *and* $0.48 < k_T < 0.54$ *GeV/c.*

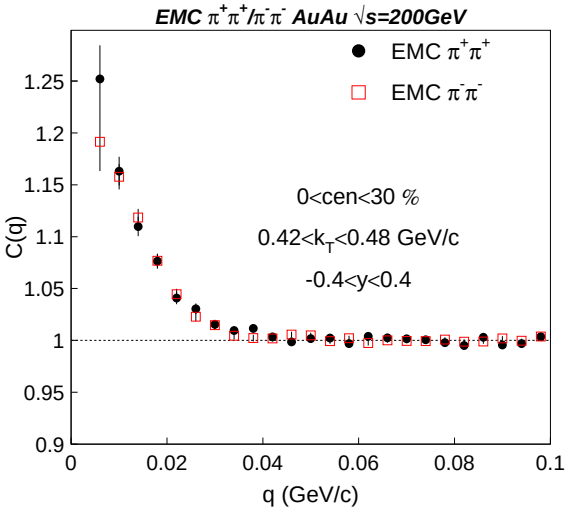

FIG. 42: *Comparison of correlation functions for negative and positive pion pairs detected in the EMC east. Results are shown for* $0 <$ *centrality* < 30 *and* $0.42 < k_T < 0.48$ *GeV/c.*

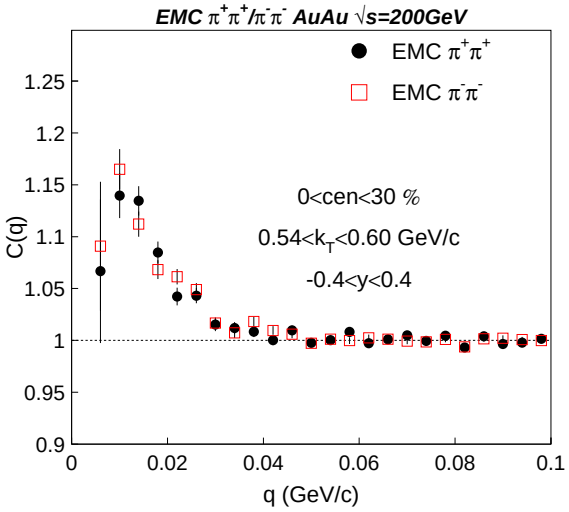

FIG. 44: *Comparison of correlation functions for negative and positive pion pairs detected in the EMC east. Results are shown for* $0 <$ *centrality* < 30 *and* $0.54 < k_T < 0.60$ *GeV/c.*

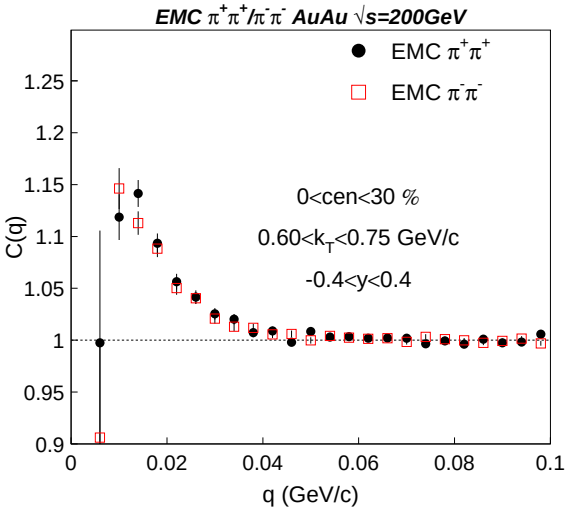

FIG. 45: *Comparison of correlation functions for negative and positive pion pairs detected in the EMC east. Results are shown for* $0 <$ *centrality* < 30 *and* $0.60 < k_T < 0.75$ *GeV/c.*

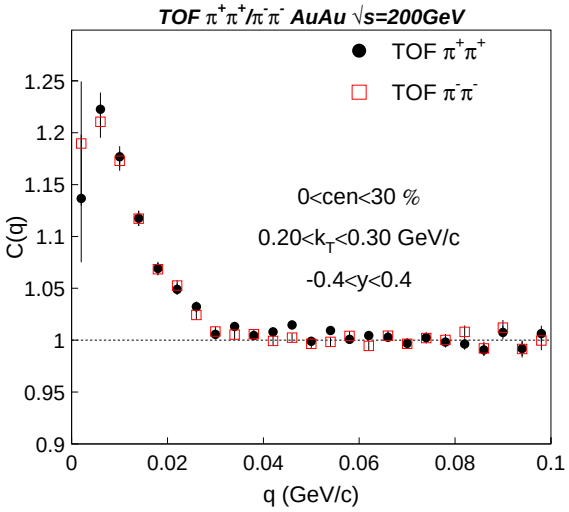

FIG. 47: *Comparison of correlation functions for negative and positive pion pairs detected in the TOF. Results are shown for* $0 <$ *centrality* < 30 *and* $0.2 < k_T < 0.3$ *GeV/c.*

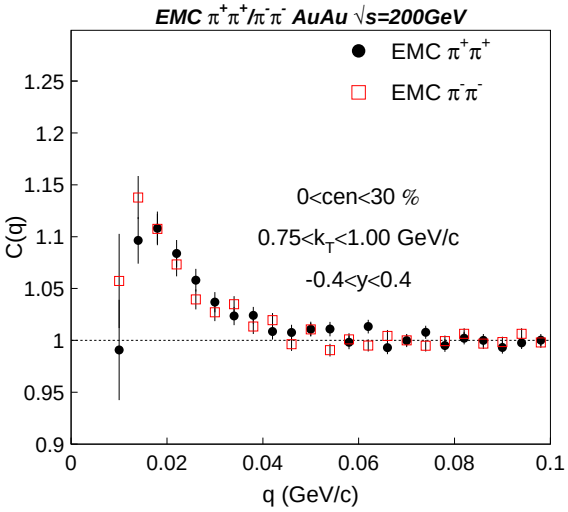

FIG. 46: *Comparison of correlation functions for negative and positive pion pairs detected in the EMC east. Results are shown for* $0 <$ *centrality* < 30 *and* $0.75 < k_T < 1.0$ *GeV/c.*

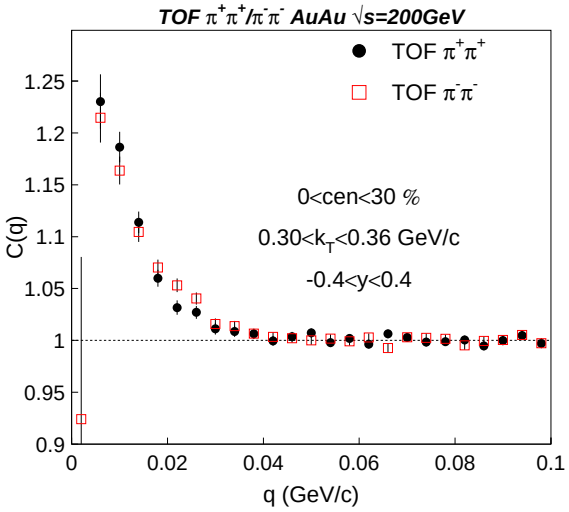

FIG. 48: *Comparison of correlation functions for negative and positive pion pairs detected in the TOF. Results are shown for* $0 <$ *centrality* < 30 *and* $0.3 < k_T < 0.36$ *GeV/c.*

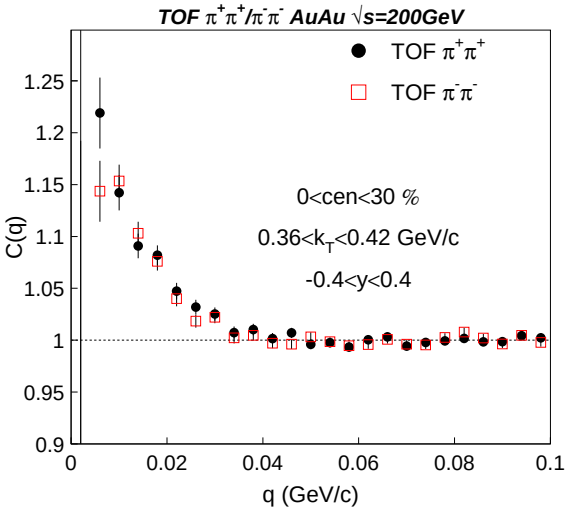

FIG. 49: *Comparison of correlation functions for negative and positive pion pairs detected in the TOF. Results are shown for* $0 <$ *centrality* < 30 *and* $0.36 < k_T < 0.42$ *GeV/c.*

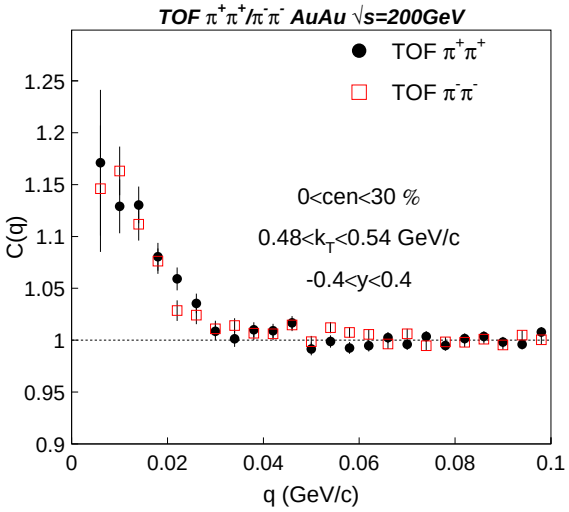

FIG. 51: *Comparison of correlation functions for negative and positive pion pairs detected in the TOF. Results are shown for* $0 <$ *centrality* < 30 *and* $0.48 < k_T < 0.54$ *GeV/c.*

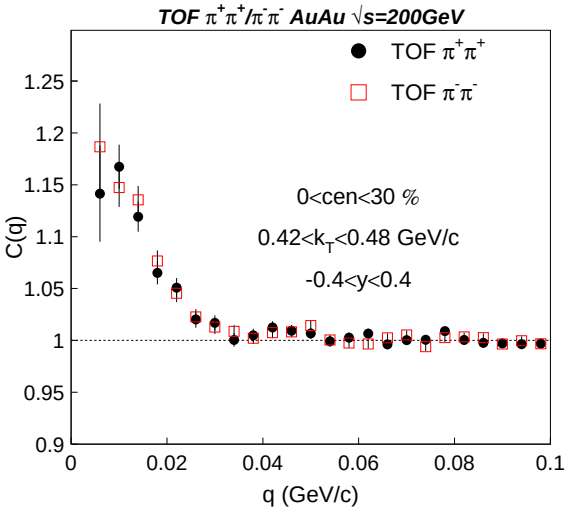

FIG. 50: *Comparison of correlation functions for negative and positive pion pairs detected in the TOF. Results are shown for* $0 <$ *centrality* < 30 *and* $0.42 < k_T < 0.48$ *GeV/c.*

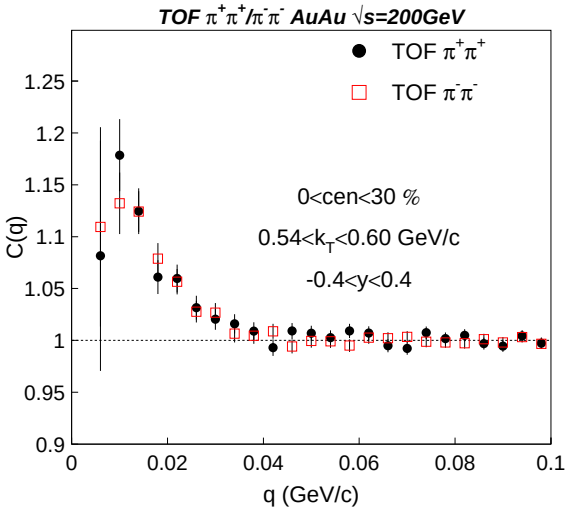

FIG. 52: *Comparison of correlation functions for negative and positive pion pairs detected in the TOF. Results are shown for* $0 <$ *centrality* < 30 *and* $0.54 < k_T < 0.60$ *GeV/c.*

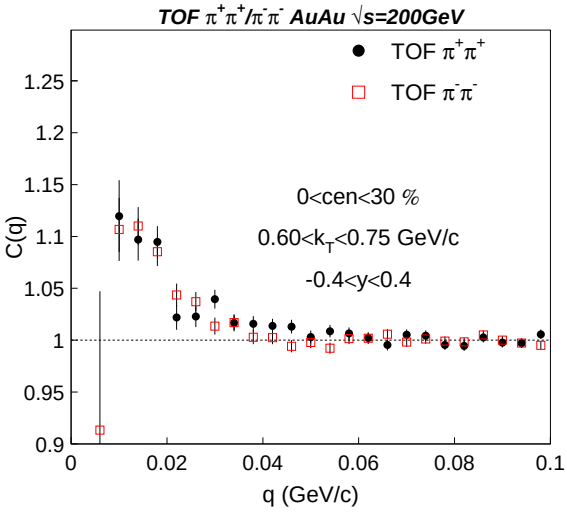

FIG. 53: *Comparison of correlation functions for negative and positive pion pairs detected in the TOF. Results are shown for* $0 <$ *centrality* < 30 *and* $0.60 < k_T < 0.75$ *GeV/c.*

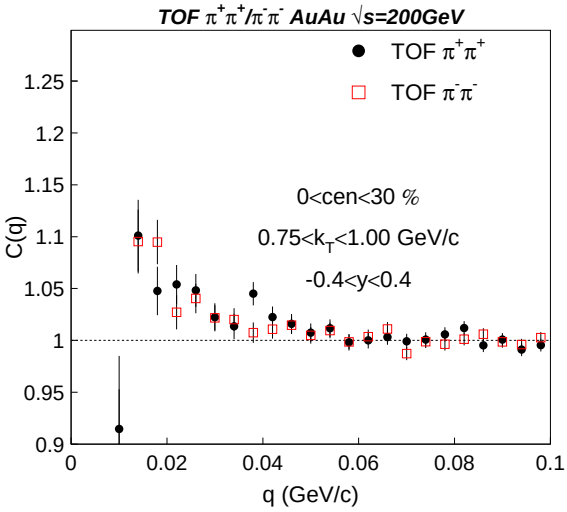

FIG. 54: *Comparison of correlation functions for negative and positive pion pairs detected in the TOF. Results are shown for* $0 <$ *centrality* < 30 *and* $0.75 < k_T < 1.0$ *GeV/c.*

4.3. Sensitivity to cut variations of σ PC3 association

In Sec. 2 we pointed out the fact that random associations between reconstructed tracks and clusters/hits in EMC/TOF results in a background contribution. For the EMC, this background is important at low momentum and decreases with increasing k_T. For the TOF, this background does not appear to be significant at any k_T providing appropriate mass-squared cuts are applied (see mass-squared plots for pions in Figs. 3 and 4).

In what follows, we illustrate the effect of PC3 matching cuts on the correlation functions obtained for several k_T selections.

4.3.1. EMC vs. TOF Correlations no PC3 association

Figures 55, 56, 57, 58, 59, 60, and 61 show comparisons of correlation functions measured in the EMC and the TOF without PC3 association. The filled symbols show results for measurements in the EMC and the open symbols show results for measurements in the TOF. The comparisons which are shown for several k_T selections indicates that the background contributions [at low k_T] serve to reduce the magnitude of the correlation function. Such a distortion can serve to influence the extraction of reliable information about the emitting source.

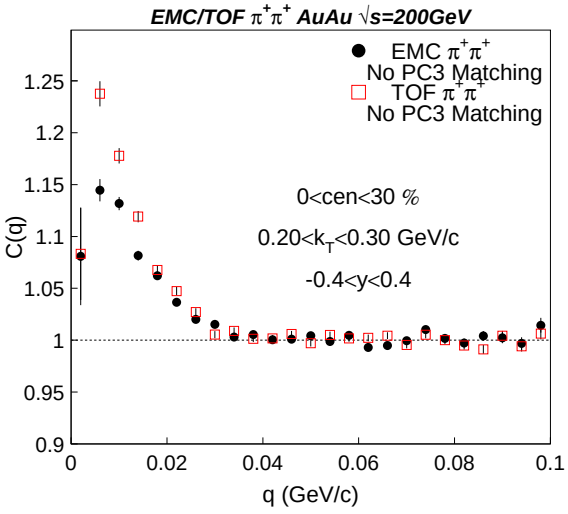

FIG. 55: *Comparison of correlation functions measured in the EMC and TOF without PC3 association. Results are shown for positively charged pions for* $0 <$ *centrality* < 30 *and* $0.2 < k_T < 0.3$ *GeV/c.*

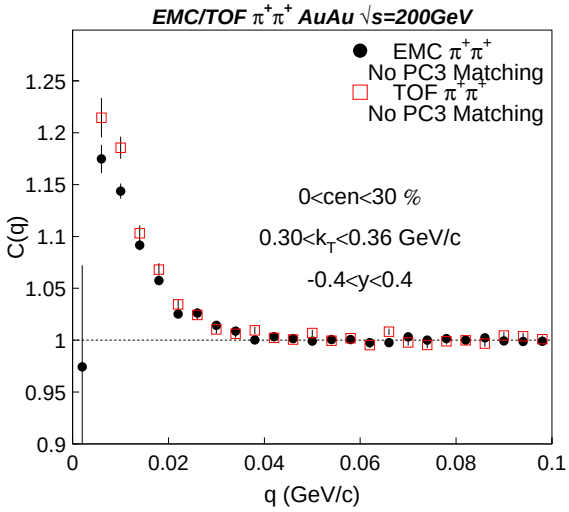

FIG. 56: *Comparison of correlation functions measured in the EMC and TOF without PC3 association. Results are shown for positively charged pions for* $0 <$ *centrality* < 30 *and* $0.3 < k_T < 0.36$ *GeV/c.*

4.3.2. EMC vs. TOF Correlations with PC3 association

In order to optimize the suppression of random background in the EMC, we made studies in which we varied the σ-matching cut in PC3. Except for statistics, the resulting correlation functions obtained from the TOF were essentially insensitive to this cut. By contrast, the correlation functions obtained from the EMC showed significant sensitivity for low k_T selections. As k_T is increased, little if any sensitivity was observed for $k_T \geq 0.4$ GeV/c.

Figures 62, 63, 64, 65, 66, 67, and 68 show comparisons of correlation functions measured in the EMC and the TOF with 2 and 3 σ PC3 association respectively. The filled symbols show results for measurements in the EMC and the open symbols show results for measurements in the TOF. The comparisons which are shown for several k_T selections clearly indicates that the background contributions in the EMC [at low k_T] can be efficiently suppressed by a 2σ cut.

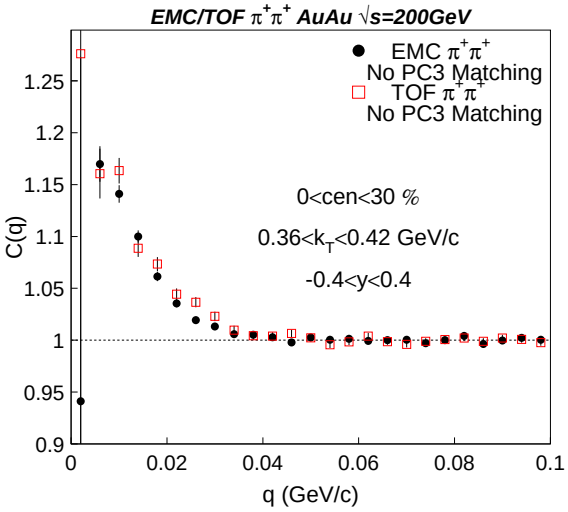

FIG. 57: *Comparison of correlation functions measured in the EMC and TOF without PC3 association. Results are shown for positively charged pions for* $0 < centrality < 30$ *and* $0.36 < k_T < 0.42$ *GeV/c.*

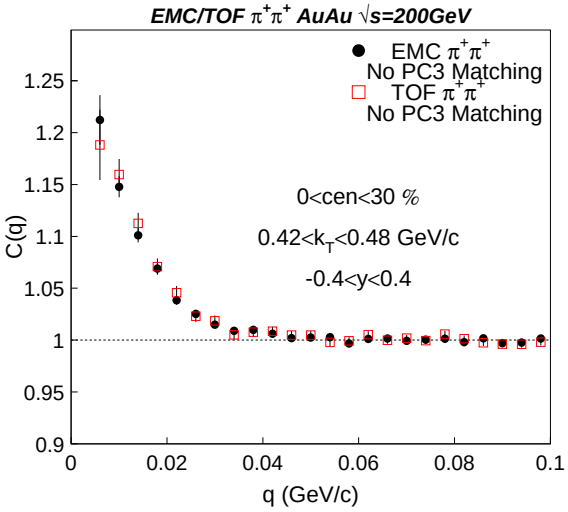

FIG. 58: *Comparison of correlation functions measured in the EMC and TOF without PC3 association. Results are shown for positively charged pions for* $0 < centrality < 30$ *and* $0.42 < k_T < 0.48$ *GeV/c.*

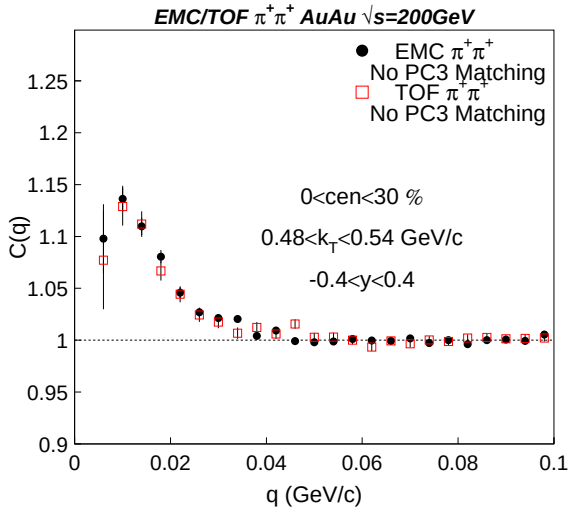

FIG. 59: *Comparison of correlation functions measured in the EMC and TOF without PC3 association. Results are shown for positively charged pions for* $0 < centrality < 30$ *and* $0.48 < k_T < 0.54$ *GeV/c.*

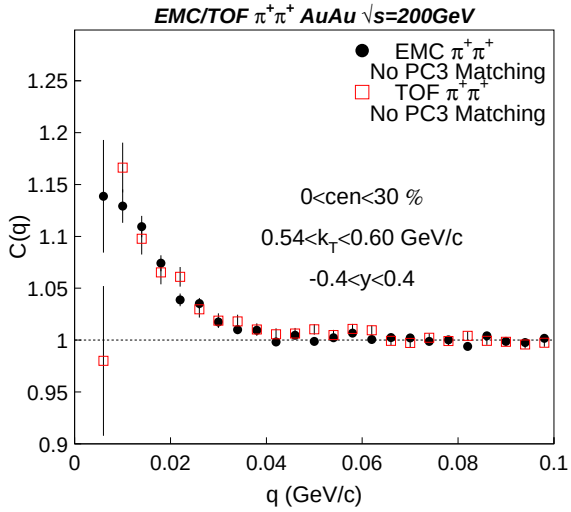

FIG. 60: *Comparison of correlation functions measured in the EMC and TOF without PC3 association. Results are shown for positively charged pions for* $0 < centrality < 30$ *and* $0.54 < k_T < 0.60$ *GeV/c.*

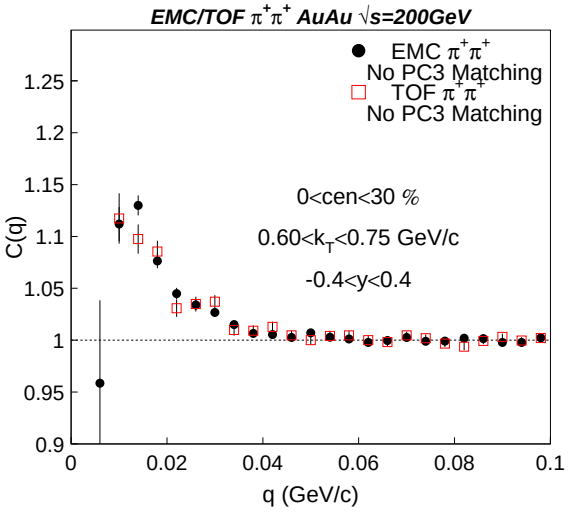

FIG. 61: *Comparison of correlation functions measured in the EMC and TOF without PC3 association. Results are shown for positively charged pions for* $0 < centrality < 30$ *and* $0.60 < k_T < 0.75$ *GeV/c.*

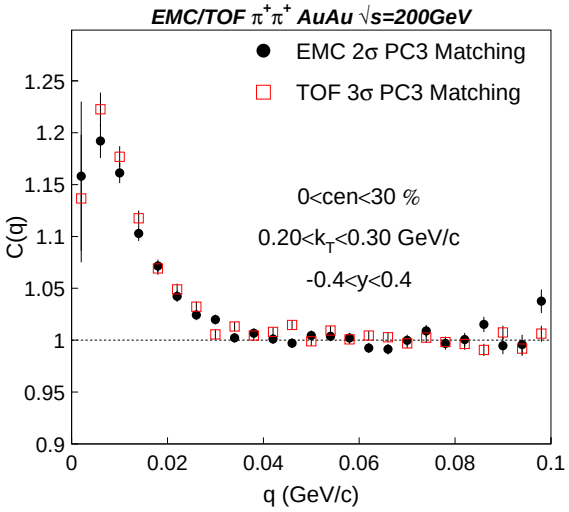

FIG. 63: *Comparison of correlation functions measured in the EMC and TOF with 2 and 3* σ *PC3 association respectively. Results are shown for positively charged pions for* $0 < centrality < 30$ *and* $0.3 < k_T < 0.36$ *GeV/c.*

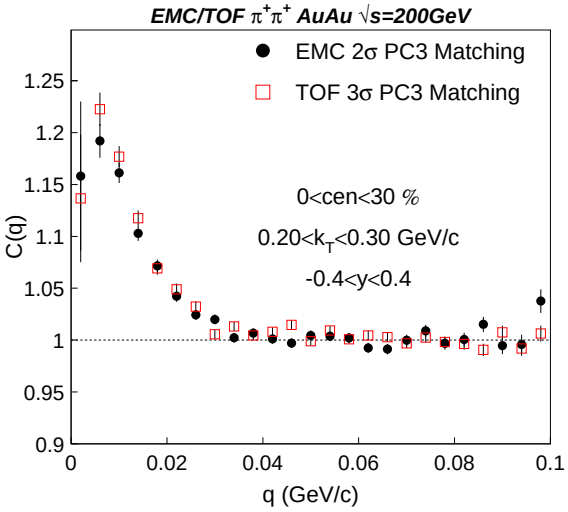

FIG. 62: *Comparison of correlation functions measured in the EMC and TOF with 2 and 3* σ *PC3 association respectively. Results are shown for positively charged pions for* $0 < centrality < 30$ *and* $0.2 < k_T < 0.3$ *GeV/c.*

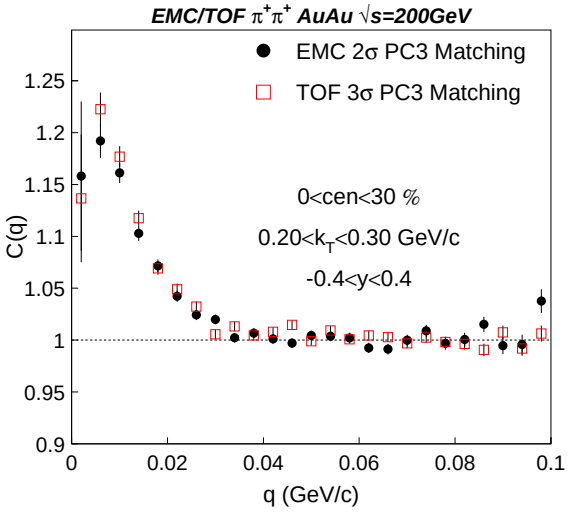

FIG. 64: *Comparison of correlation functions measured in the EMC and TOF with 2 and 3* σ *PC3 association respectively. Results are shown for positively charged pions for* $0 < centrality < 30$ *and* $0.36 < k_T < 0.42$ *GeV/c.*

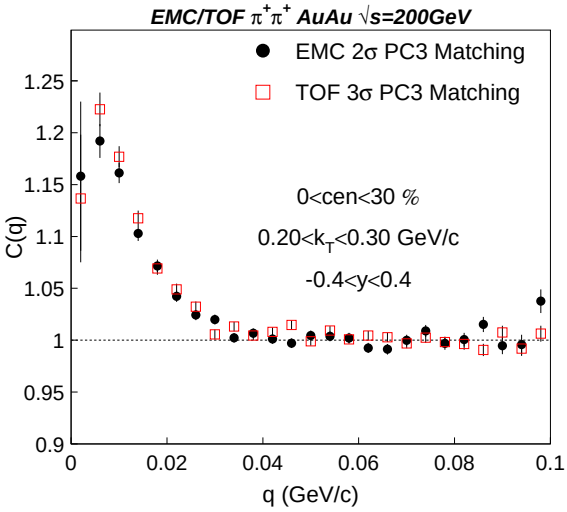

FIG. 65: *Comparison of correlation functions measured in the EMC and TOF with 2 and 3 σ PC3 association respectively. Results are shown for positively charged pions for* $0 <$ *centrality* < 30 *and* $0.42 < k_T < 0.48$ *GeV/c.*

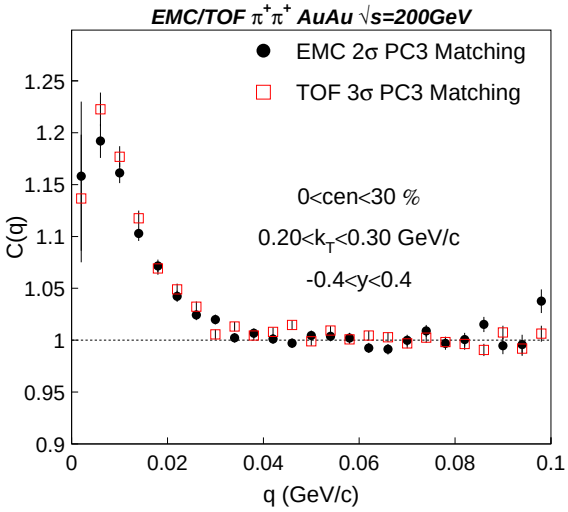

FIG. 67: *Comparison of correlation functions measured in the EMC and TOF with 2 and 3 σ PC3 association respectively. Results are shown for positively charged pions for* $0 <$ *centrality* < 30 *and* $0.54 < k_T < 0.60$ *GeV/c.*

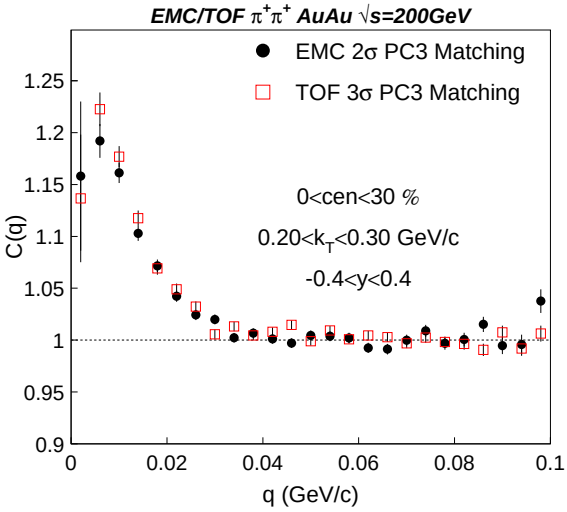

FIG. 66: *Comparison of correlation functions measured in the EMC and TOF with 2 and 3 σ PC3 association respectively. Results are shown for positively charged pions for* $0 <$ *centrality* < 30 *and* $0.48 < k_T < 0.54$ *GeV/c.*

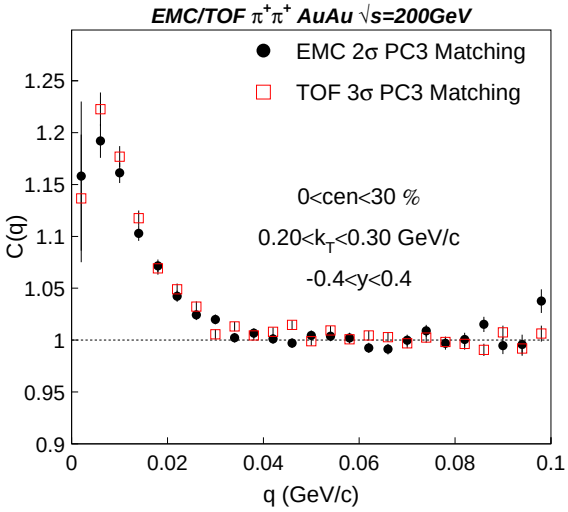

FIG. 68: *Comparison of correlation functions measured in the EMC and TOF with 2 and 3 σ PC3 association respectively. Results are shown for positively charged pions for* $0 <$ *centrality* < 30 *and* $0.60 < k_T < 0.75$ *GeV/c.*

4.4. Comparison of $\pi^-\pi^-$ pairs detected in EMC East and TOF

Figures 69, 70, 71, 72, 73, 74, 75 and 76 compare correlation functions for negatively charged pion pairs detected in the EMC and TOF respectively. A 2.5 σ PC3 association was used for detections in the EMC. The comparisons which are shown for several k_T selections indicate rather good agreement between the correlation functions generated from the EMC and TOF respectively.

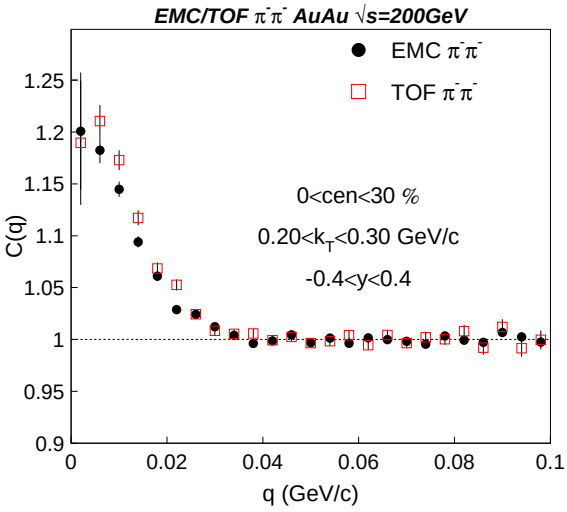

FIG. 69: *Comparison of correlation functions for negatively charged pion pairs detected in the EMC east and TOF. Results are shown for* $0 < centrality < 30$ *and* $0.2 < k_T < 0.3$ *GeV/c.*

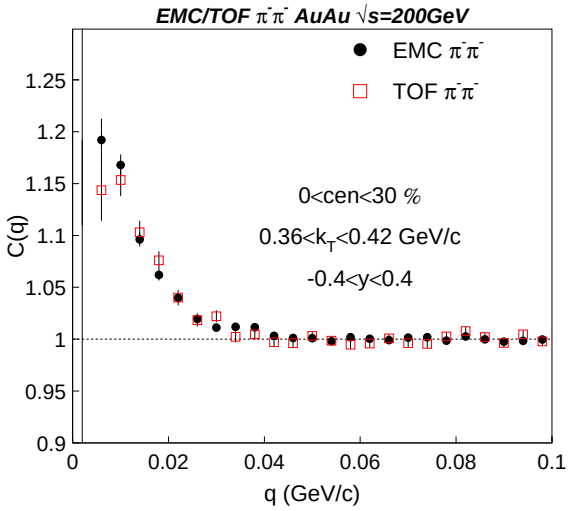

FIG. 70: *Comparison of correlation functions for negatively charged pion pairs detected in the EMC east and TOF. Results are shown for* $0 < centrality < 30$ *and* $0.3 < k_T < 0.36$ *GeV/c.*

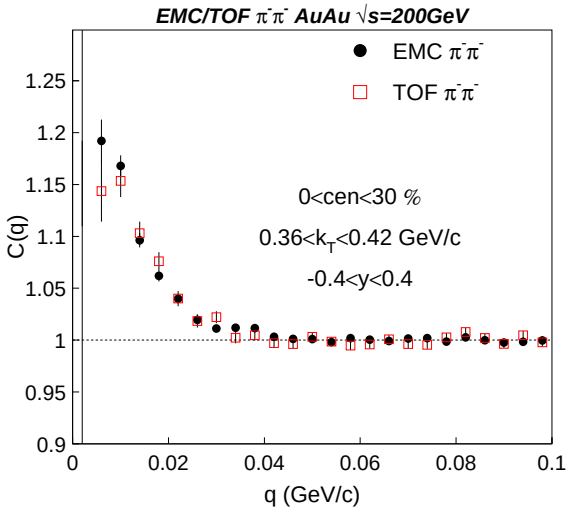

FIG. 71: *Comparison of correlation functions for negatively charged pion pairs detected in the EMC east and TOF. Results are shown for* $0 < centrality < 30$ *and* $0.36 < k_T < 0.42$ *GeV/c.*

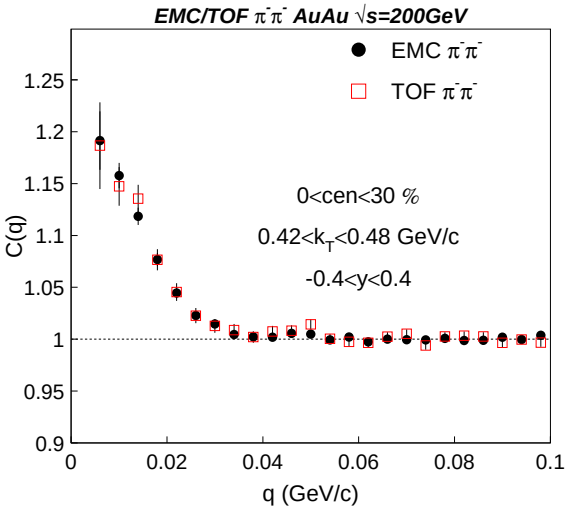

FIG. 72: *Comparison of correlation functions for negatively charged pion pairs detected in the EMC east and TOF. Results are shown for* $0 < centrality < 30$ *and* $0.42 < k_T < 0.48$ *GeV/c.*

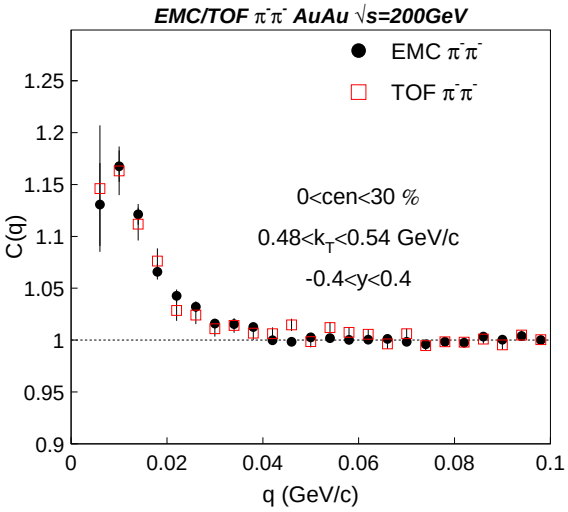

FIG. 73: *Comparison of correlation functions for negatively charged pion pairs detected in the EMC east and TOF. Results are shown for* $0 < centrality < 30$ *and* $0.48 < k_T < 0.54$ *GeV/c.*

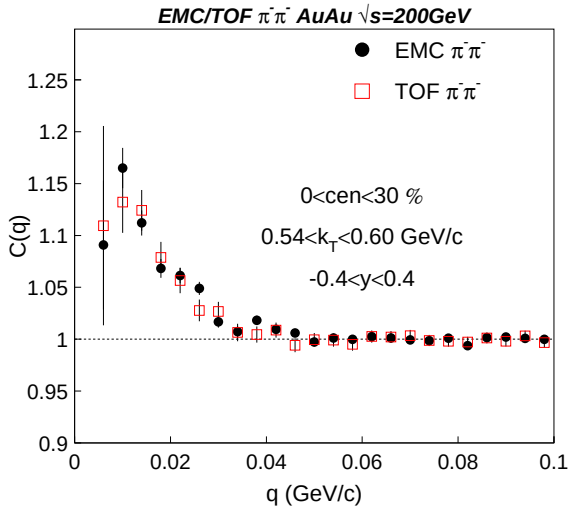

FIG. 74: *Comparison of correlation functions for negatively charged pion pairs detected in the EMC east and TOF. Results are shown for* $0 < centrality < 30$ *and* $0.54 < k_T < 0.60$ *GeV/c.*

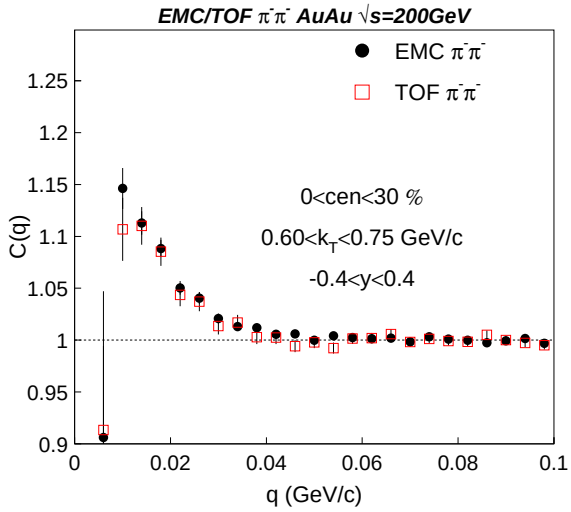

FIG. 75: *Comparison of correlation functions for negatively charged pion pairs detected in the EMC east and TOF. Results are shown for* $0 < centrality < 30$ *and* $0.60 < k_T < 0.75$ *GeV/c.*

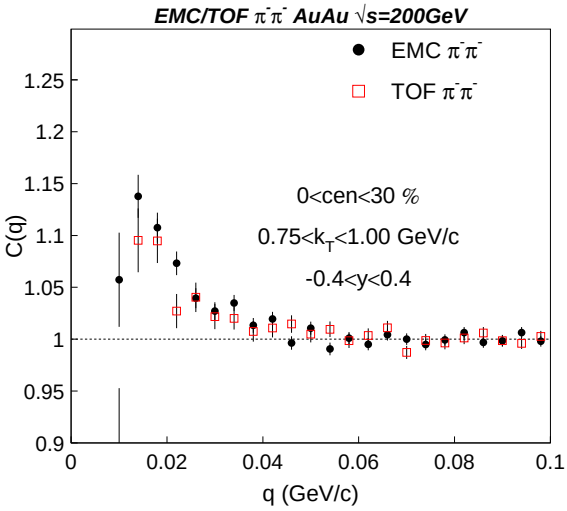

FIG. 76: *Comparison of correlation functions for negatively charged pion pairs detected in the EMC east and TOF. Results are shown for* $0 < centrality < 30$ *and* $0.75 < k_T < 1.0$ *GeV/c.*

4.5. Comparison of $\pi^+\pi^+$ pairs detected in EMC East and TOF

Figures 77, 78, 79, 80, 81, 82, 83 and 84 compare correlation functions for positively charged pion pairs detected in the EMC and TOF respectively. A 2.5 σ PC3 association was used for detections in the EMC. The comparisons which are shown for several k_T selections indicate rather good agreement between the correlation functions generated from the EMC and TOF respectively.

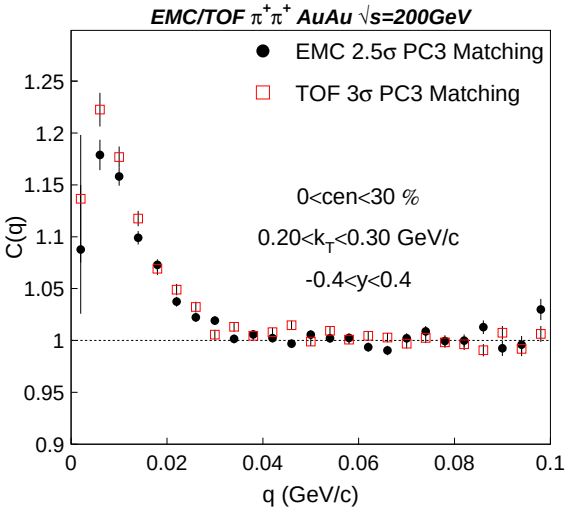

FIG. 77: *Comparison of correlation functions for positively charged pion pairs detected in the EMC east and TOF. Results are shown for* $0 < centrality < 30$ *and* $0.2 < k_T < 0.3$ *GeV/c.*

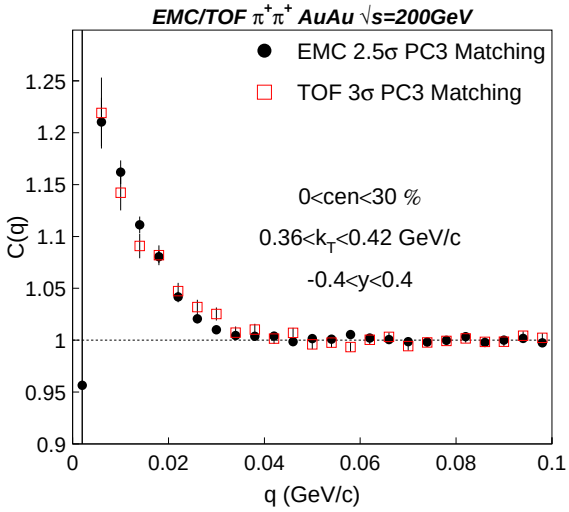

FIG. 78: *Comparison of correlation functions for positively charged pion pairs detected in the EMC east and TOF. Results are shown for* $0 < centrality < 30$ *and* $0.3 < k_T < 0.36$ *GeV/c.*

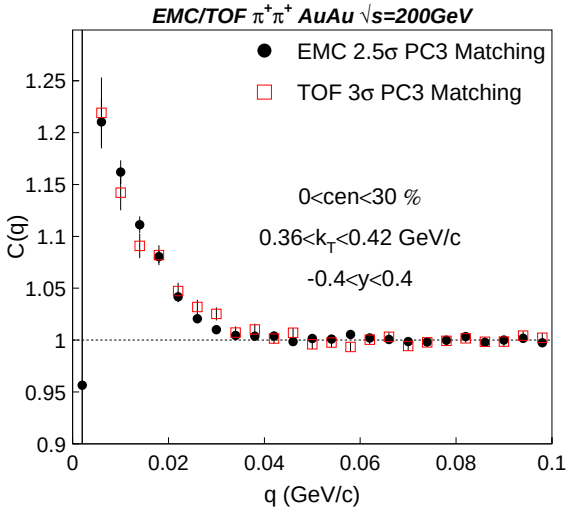

FIG. 79: *Comparison of correlation functions for positively charged pion pairs detected in the EMC east and TOF. Results are shown for* $0 < centrality < 30$ *and* $0.36 < k_T < 0.42$ *GeV/c.*

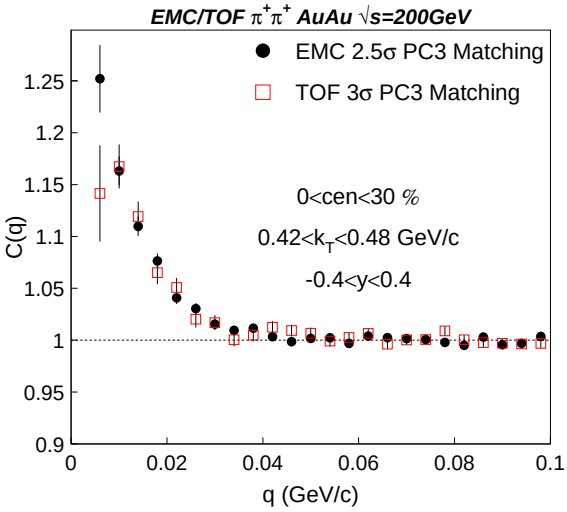

FIG. 80: *Comparison of correlation functions for positively charged pion pairs detected in the EMC east and TOF. Results are shown for* $0 < centrality < 30$ *and* $0.42 < k_T < 0.48$ *GeV/c.*

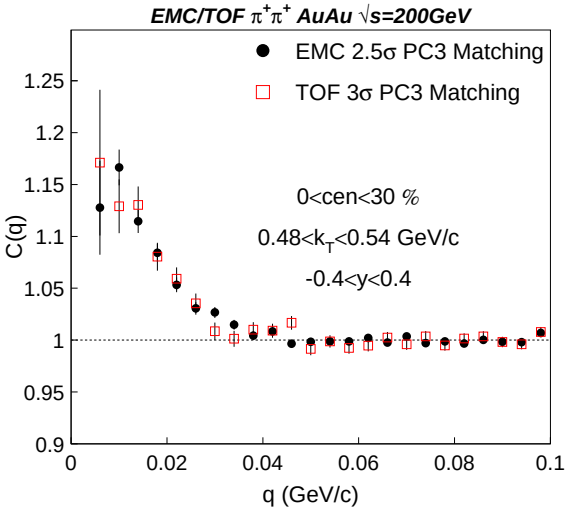

FIG. 81: *Comparison of correlation functions for positively charged pion pairs detected in the EMC east and TOF. Results are shown for* $0 < centrality < 30$ *and* $0.48 < k_T < 0.54$ *GeV/c.*

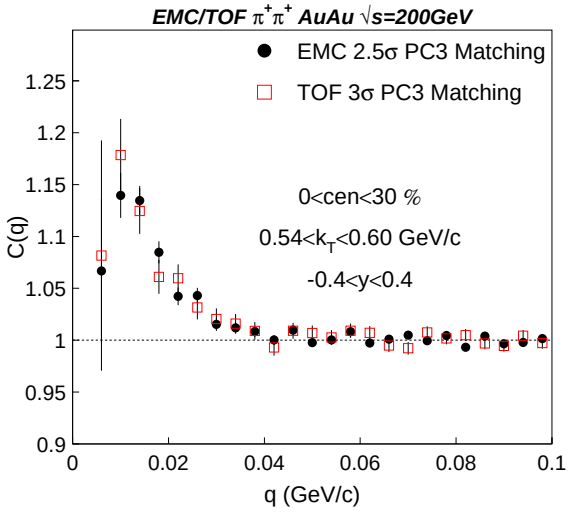

FIG. 82: *Comparison of correlation functions for positively charged pion pairs detected in the EMC east and TOF. Results are shown for* $0 < centrality < 30$ *and* $0.54 < k_T < 0.60$ *GeV/c.*

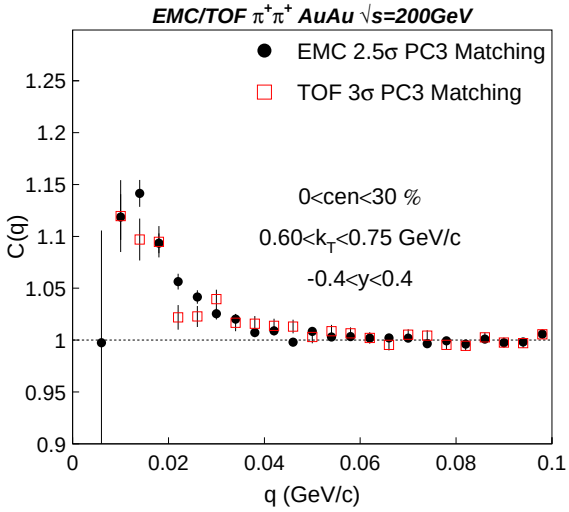

FIG. 83: *Comparison of correlation functions for positively charged pion pairs detected in the EMC east and TOF. Results are shown for* $0 < centrality < 30$ *and* $0.60 < k_T < 0.75$ *GeV/c.*

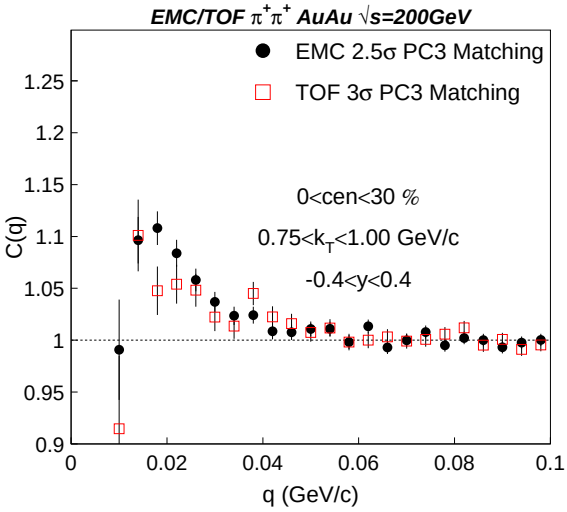

FIG. 84: *Comparison of correlation functions for positively charged pion pairs detected in the EMC east and TOF. Results are shown for* $0 < centrality < 30$ *and* $0.75 < k_T < 1.0$ *GeV/c.*

4.6. EMC correlation functions: East vs. West

Figures 85, 86, 87, 88, 89, 90, 91 and 92 compare correlation functions for positively charged pion pairs detected in EMC East and West respectively. The comparisons which are shown for several k_T selections indicate rather good agreement between the correlation functions generated from both arms of PHENIX.

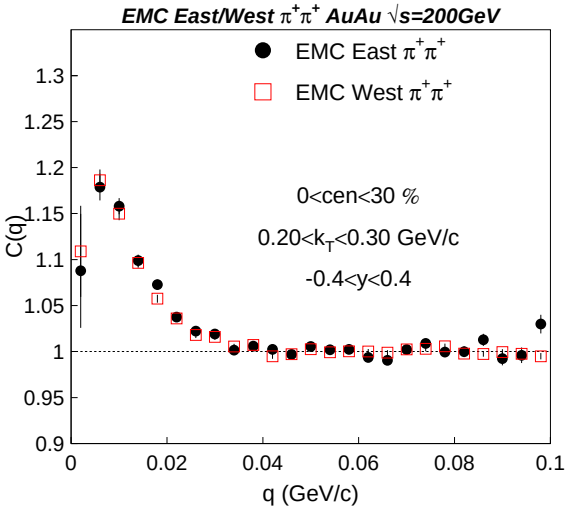

FIG. 85: *Comparison of correlation functions for positively charged pion pairs detected in the EMC East and EMC West. Results are shown for* $0 < centrality < 30$ *and* $0.2 < k_T < 0.3$ *GeV/c.*

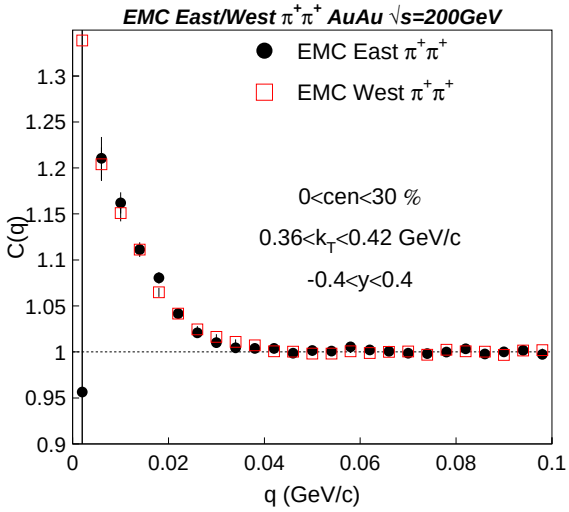

FIG. 86: *Comparison of correlation functions for positively charged pion pairs detected in the EMC East and EMC West. Results are shown for* $0 < centrality < 30$ *and* $0.3 < k_T < 0.36$ *GeV/c.*

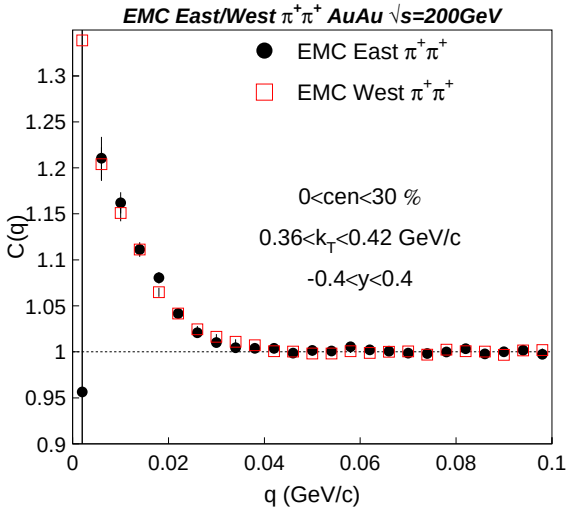

FIG. 87: *Comparison of correlation functions for positively charged pion pairs detected in the EMC East and EMC West. Results are shown for* $0 < centrality < 30$ *and* $0.36 < k_T < 0.42$ *GeV/c.*

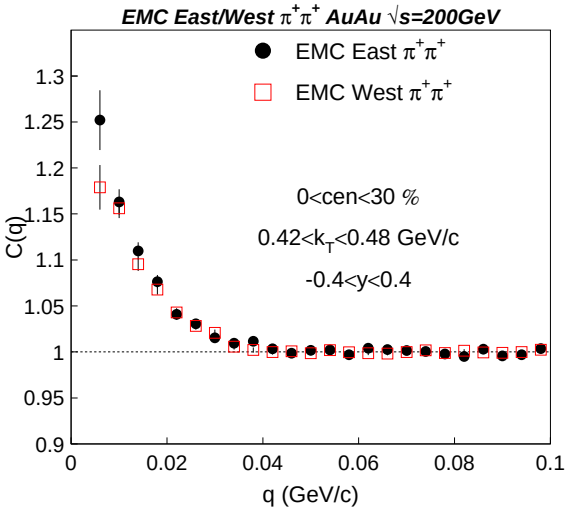

FIG. 88: *Comparison of correlation functions for positively charged pion pairs detected in the EMC East and EMC West. Results are shown for* $0 < centrality < 30$ *and* $0.42 < k_T < 0.48$ *GeV/c.*

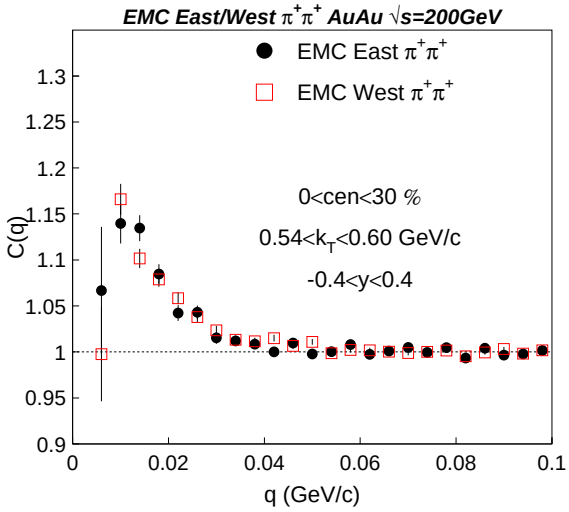

FIG. 90: *Comparison of correlation functions for positively charged pion pairs detected in the EMC East and EMC West. Results are shown for* $0 < centrality < 30$ *and* $0.54 < k_T < 0.60$ *GeV/c.*

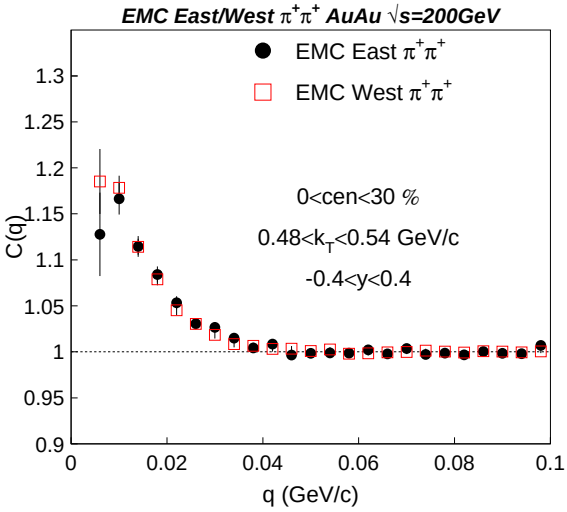

FIG. 89: *Comparison of correlation functions for positively charged pion pairs detected in the EMC East and EMC West. Results are shown for* $0 < centrality < 30$ *and* $0.48 < k_T < 0.54$ *GeV/c.*

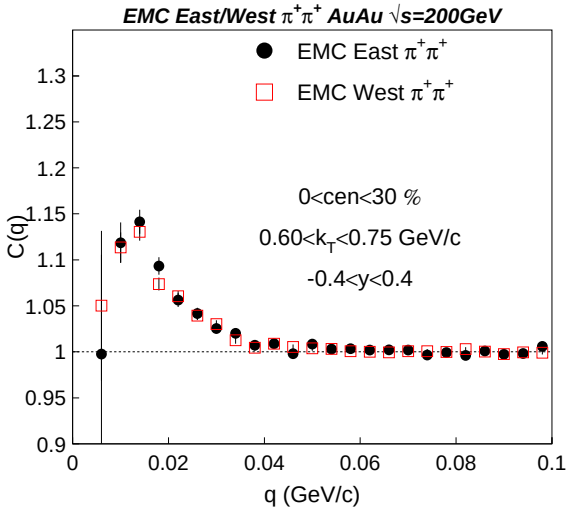

FIG. 91: *Comparison of correlation functions for positively charged pion pairs detected in the EMC East and EMC West. Results are shown for* $0 < centrality < 30$ *and* $0.60 < k_T < 0.75$ *GeV/c.*

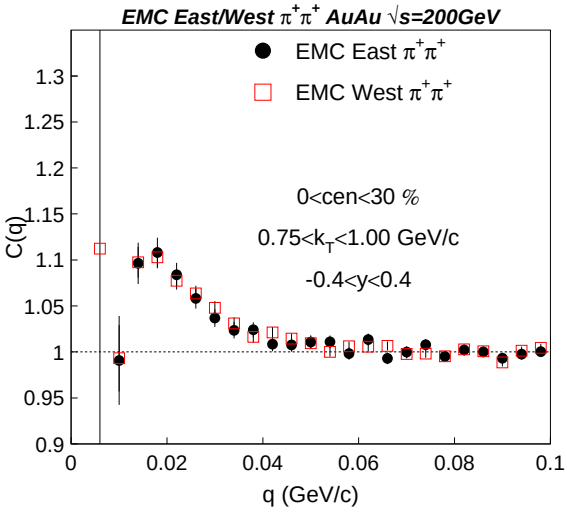

FIG. 92: *Comparison of correlation functions for positively charged pion pairs detected in the EMC East and EMC West. Results are shown for* $0 < centrality < 30$ *and* $0.75 < k_T < 1.0$ *GeV/c.*

4.7. EMC-East correlation functions for $\pi^+\pi^+$: This work vs. PPG021

Figures 93, 94, 95, 96, 97, 98, 99 and 100 compare correlation functions from this work with those reported in PPG021. Results are shown for positively charged pion pairs detected in EMC East for several k_T selections. They indicate good overall agreement except for the lowest k_T selections.

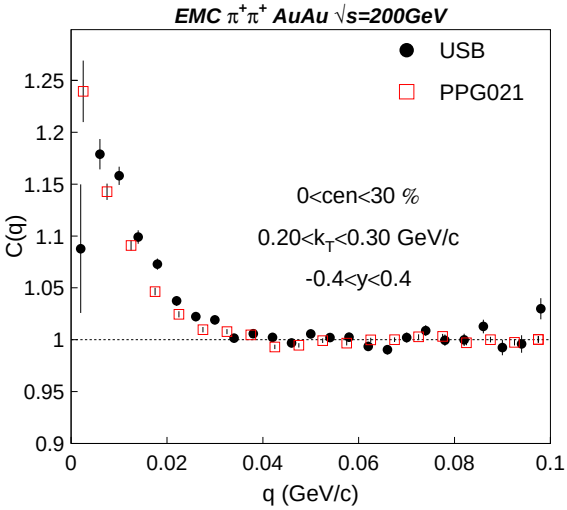

FIG. 93: *Comparison of correlation functions for positively charged pion pairs detected in the EMC East with similar correlation functions reported in PPG021. Results are shown for* $0 <$ *centrality* < 30 *and* $0.2 < k_T < 0.3$ *GeV/c.*

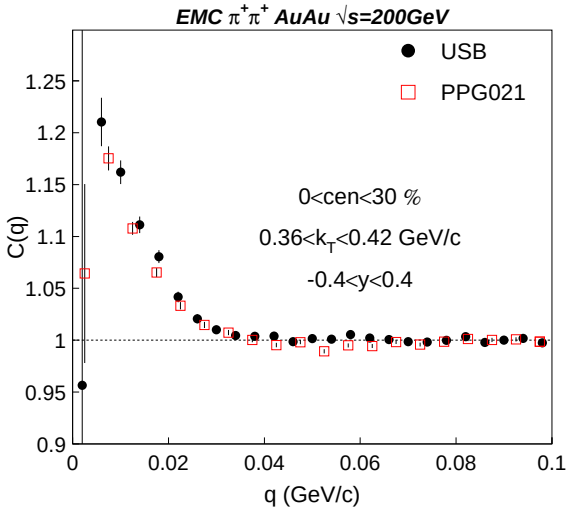

FIG. 94: *Comparison of correlation functions for positively charged pion pairs detected in the EMC East with similar correlation functions reported in PPG021. Results are shown for* $0 <$ *centrality* < 30 *and* $0.3 < k_T < 0.36$ *GeV/c.*

4.8. EMC-East correlation functions for $\pi^-\pi^-$: This work vs. PPG021

Figures 101, 102, 103, 104, 105, 106, 107 and 108 compare correlation functions from this work with those reported in PPG021. Results are shown for negatively charged pion pairs detected in EMC East for several k_T selections. They indicate good overall agreement except for the lowest k_T selections.

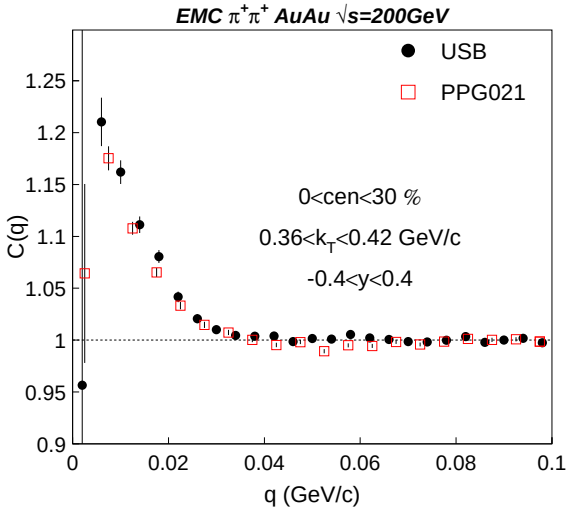

FIG. 95: *Comparison of correlation functions for positively charged pion pairs detected in the EMC East with similar correlation functions reported in PPG021. Results are shown for* $0 <$ *centrality* < 30 *and* $0.36 < k_T < 0.42$ *GeV/c.*

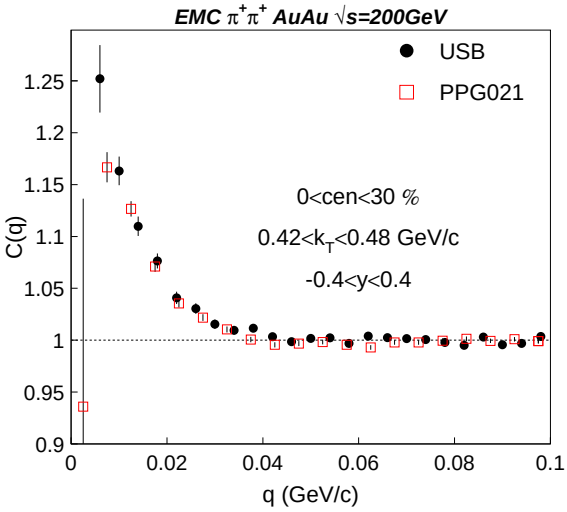

FIG. 96: *Comparison of correlation functions for positively charged pion pairs detected in the EMC East with similar correlation functions reported in PPG021. Results are shown for* $0 <$ *centrality* < 30 *and* $0.42 < k_T < 0.48$ *GeV/c.*

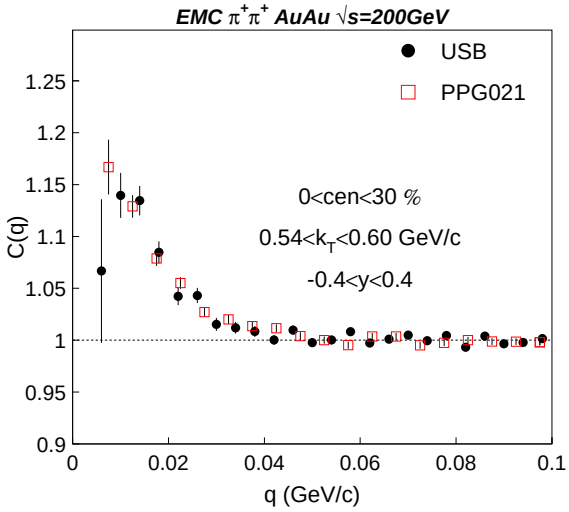

FIG. 98: *Comparison of correlation functions for positively charged pion pairs detected in the EMC East with similar correlation functions reported in PPG021. Results are shown for* $0 <$ *centrality* < 30 *and* $0.54 < k_T < 0.60$ *GeV/c.*

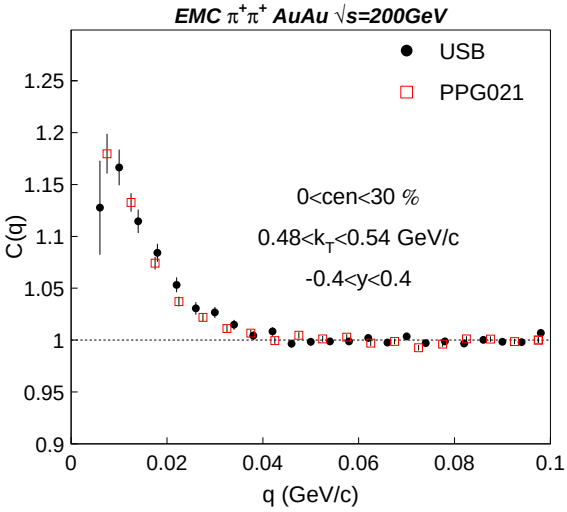

FIG. 97: *Comparison of correlation functions for positively charged pion pairs detected in the EMC East with similar correlation functions reported in PPG021. Results are shown for* $0 <$ *centrality* < 30 *and* $0.48 < k_T < 0.54$ *GeV/c.*

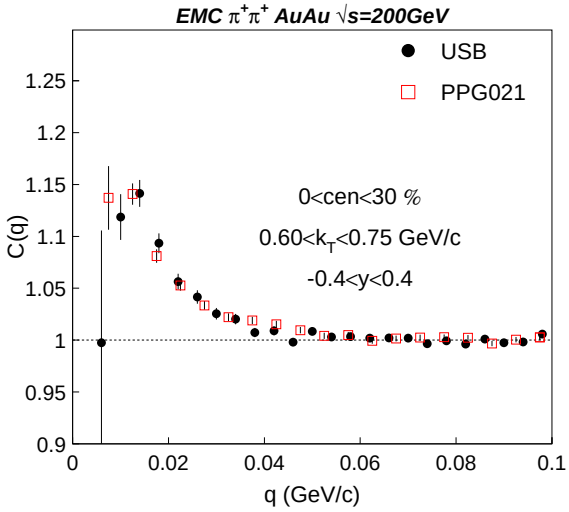

FIG. 99: *Comparison of correlation functions for positively charged pion pairs detected in the EMC East with similar correlation functions reported in PPG021. Results are shown for* $0 <$ *centrality* < 30 *and* $0.60 < k_T < 0.75$ *GeV/c.*

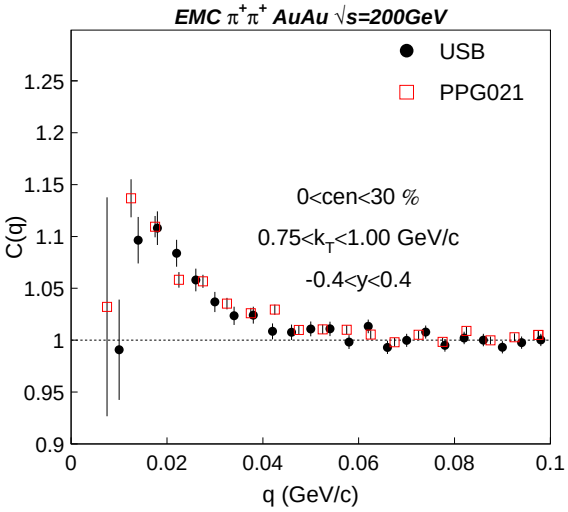

FIG. 100: *Comparison of correlation functions for positively charged pion pairs detected in the EMC East with similar correlation functions reported in PPG021. Results are shown for* $0 <$ *centrality* < 30 *and* $0.75 < k_T < 1.0$ *GeV/c.*

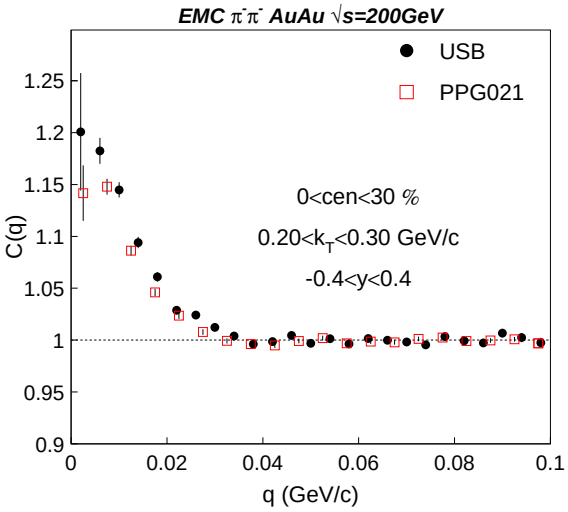

FIG. 101: *Comparison of correlation functions for negatively charged pion pairs detected in the EMC East with similar correlation functions reported in PPG021. Results are shown for* $0 <$ *centrality* < 30 *and* $0.2 < k_T < 0.3$ *GeV/c.*

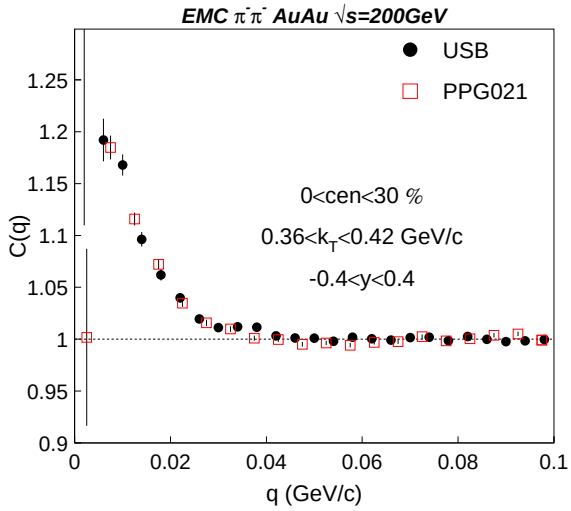

FIG. 102: *Comparison of correlation functions for negatively charged pion pairs detected in the EMC East with similar correlation functions reported in PPG021. Results are shown for* $0 <$ *centrality* < 30 *and* $0.3 < k_T < 0.36$ *GeV/c.*

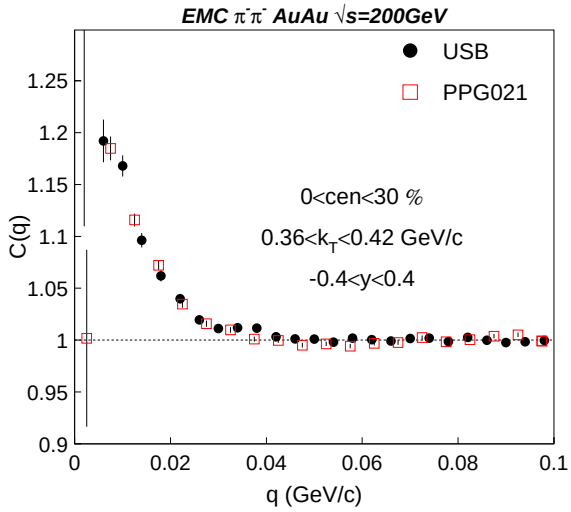

FIG. 103: *Comparison of correlation functions for negatively charged pion pairs detected in the EMC East with similar correlation functions reported in PPG021. Results are shown for* $0 <$ *centrality* < 30 *and* $0.36 < k_T < 0.42$ *GeV/c.*

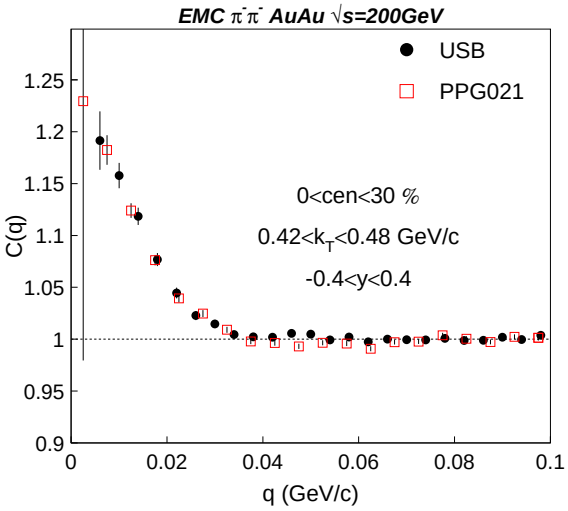

FIG. 104: *Comparison of correlation functions for negatively charged pion pairs detected in the EMC East with similar correlation functions reported in PPG021. Results are shown for* $0 <$ *centrality* < 30 *and* $0.42 < k_T < 0.48$ *GeV/c.*

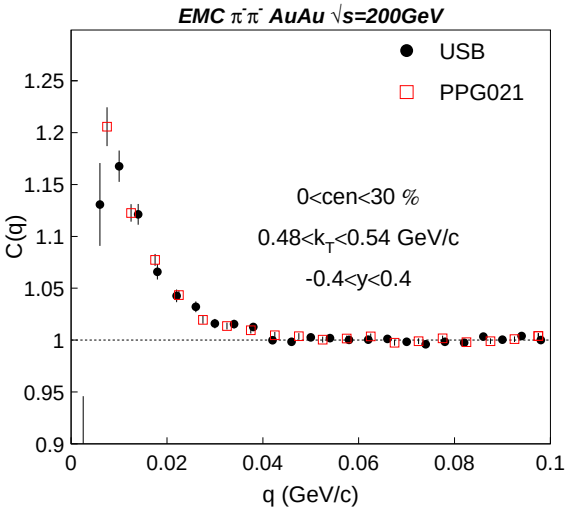

FIG. 105: *Comparison of correlation functions for negatively charged pion pairs detected in the EMC East with similar correlation functions reported in PPG021. Results are shown for* $0 <$ *centrality* < 30 *and* $0.48 < k_T < 0.54$ *GeV/c.*

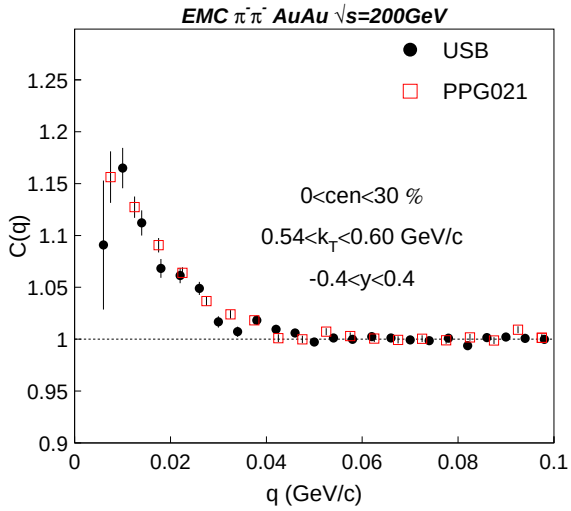

FIG. 106: *Comparison of correlation functions for negatively charged pion pairs detected in the EMC East with similar correlation functions reported in PPG021. Results are shown for* $0 <$ *centrality* < 30 *and* $0.54 < k_T < 0.60$ *GeV/c.*

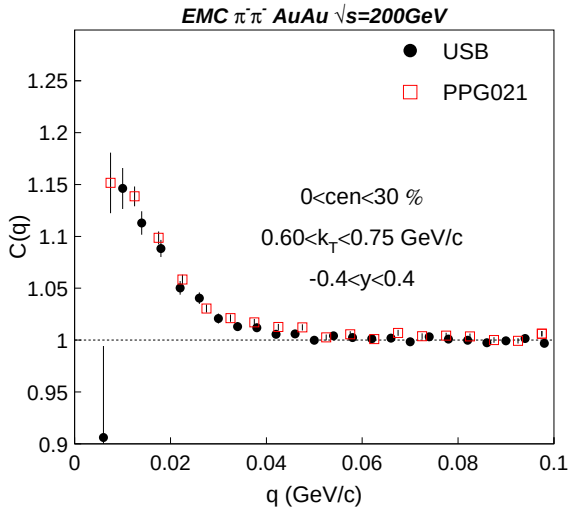

FIG. 107: *Comparison of correlation functions for negatively charged pion pairs detected in the EMC East with similar correlation functions reported in PPG021. Results are shown for* $0 <$ *centrality* < 30 *and* $0.60 < k_T < 0.75$ *GeV/c.*

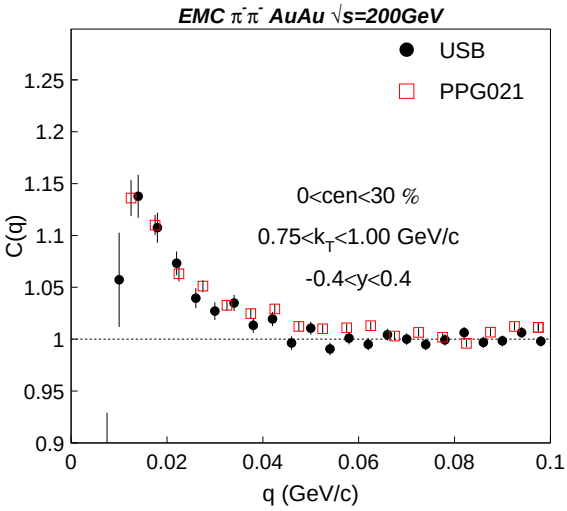

FIG. 108: *Comparison of correlation functions for negatively charged pion pairs detected in the EMC East with similar correlation functions reported in PPG021. Results are shown for* $0 <$ *centrality* < 30 *and* $0.75 < k_T < 1.0$ *GeV/c.*

4.9. Comparison of Mixed-pair Correlation functions for $\pi^+\pi^-$

Mixed charged-pair ($\pi^+\pi^-$ pairs) correlation functions were also generated for particle pairs detected in the combined acceptance of EMC+TOF. Figs. 119, 120, compare these correlation functions to those reported in PPG021 for two k_T selections as indicated. Results are shown for positively charged pion pairs for $0 <$ centrality $< 30\%$. The comparison indicates reasonable agreement.

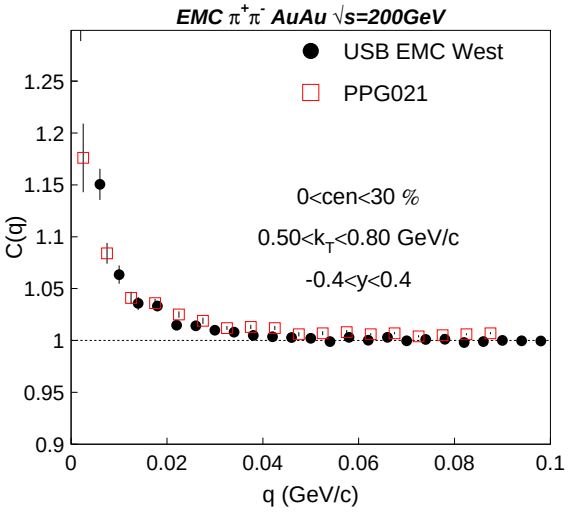

FIG. 109: *Comparison of correlation functions for mixed-charged pion pairs detected in the EMC West (PPG021) with similar correlation functions obtained from a combination of the EMC and TOF (this work). Results are shown for* $0 <$ *centrality* < 30 *and* $0.5 < k_T < 0.8$ *GeV/c.*

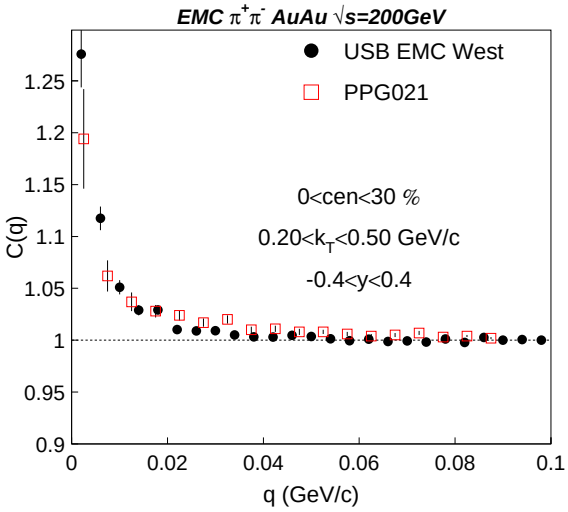

FIG. 110: *Comparison of correlation functions for mixed-charged pion pairs detected in the EMC West (PPG021) with similar correlation functions obtained from a combination of the EMC and TOF (this work). Results are shown for* $0 <$ *centrality* $< 30\%$ *and* $0.2 < k_T < 0.5$ *GeV/c.*

5. CORRELATION FUNCTIONS FROM COMBINED DETECTIONS IN EMC (E&W) AND TOF

In order to improve the statistical significance of the correlation measurements, charged pions detected in the EMC (East and West) and the TOF were combined to generate correlation functions. In what follows, we show the correlation functions which result from this combination of subsystems, and compare them to the correlation functions obtained from the EMC and TOF separately.

5.1. Correlation functions from EMC (E&W)+TOF

The combined particle pairs detected in EMC East, EMC West and the TOF were used to generate correlation functions with significantly improved statistical significance. Figs. 111, 112, 113, 114, 115, 116, 117 and 118 show the resulting correlation functions obtained for positively charged pions for for $0 <$ centrality < 30 and several k_T selections; they show a much smoother pattern as would be expected for the improved statistics. A comparison between these correlation functions and the ones obtained from the EMC and TOF respectively is given below.

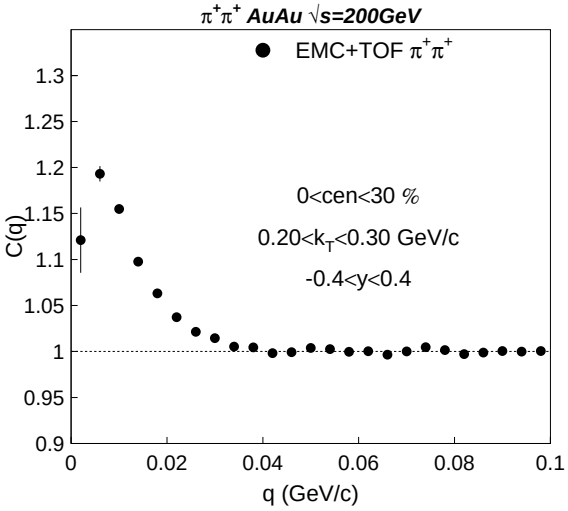

FIG. 111: *Correlation functions for positively charged pion pairs detected in the combined acceptance of the EMC and TOF. Results are shown for* $0 <$ *centrality* < 30 *and* $0.2 < k_T < 0.3$ *GeV/c.*

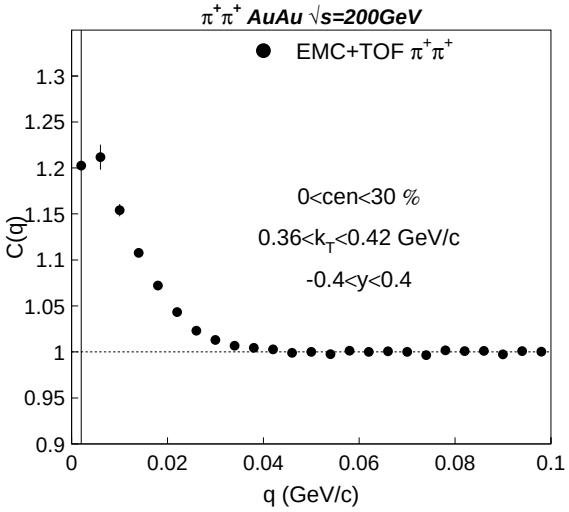

FIG. 112: *Correlation functions for positively charged pion pairs detected in the combined acceptance of the EMC and TOF. Results are shown for* $0 <$ *centrality* < 30 *and* $0.3 < k_T < 0.36$ *GeV/c.*

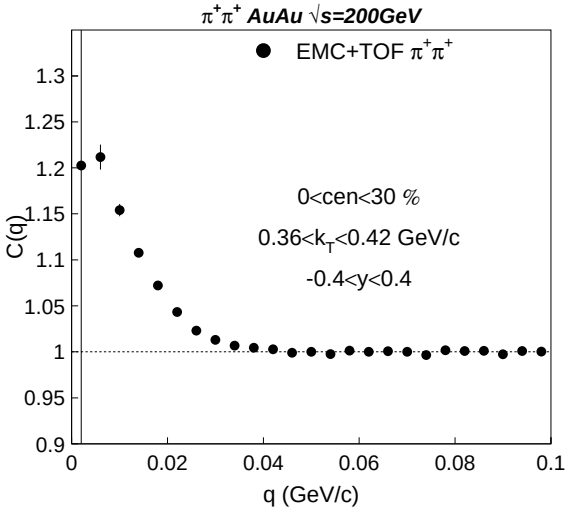

FIG. 113: *Correlation functions for positively charged pion pairs detected in the combined acceptance of the EMC and TOF. Results are shown for* $0 <$ *centrality* < 30 *and* $0.36 < k_T < 0.42$ *GeV/c.*

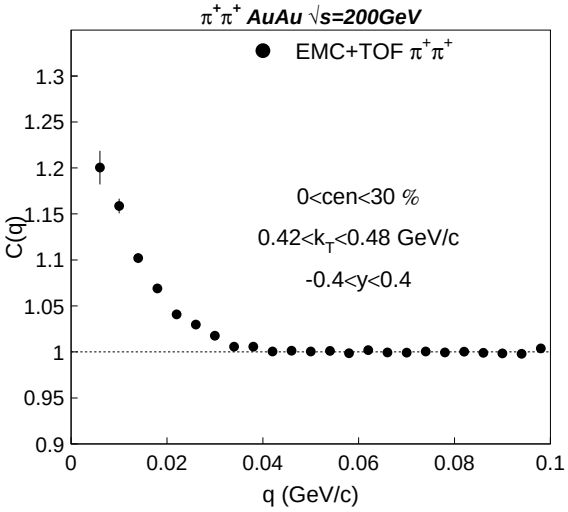

FIG. 114: *Correlation functions for positively charged pion pairs detected in the combined acceptance of the EMC and TOF. Results are shown for* $0 <$ *centrality* < 30 *and* $0.42 < k_T < 0.48$ *GeV/c.*

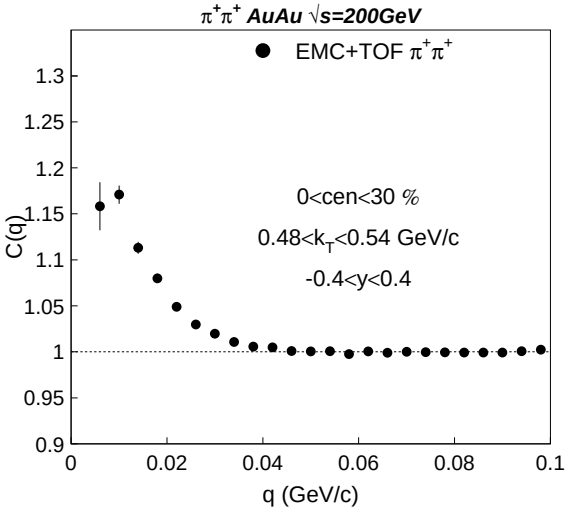

FIG. 115: *Correlation functions for positively charged pion pairs detected in the combined acceptance of the EMC and TOF. Results are shown for* $0 <$ *centrality* < 30 *and* $0.48 < k_T < 0.54$ *GeV/c.*

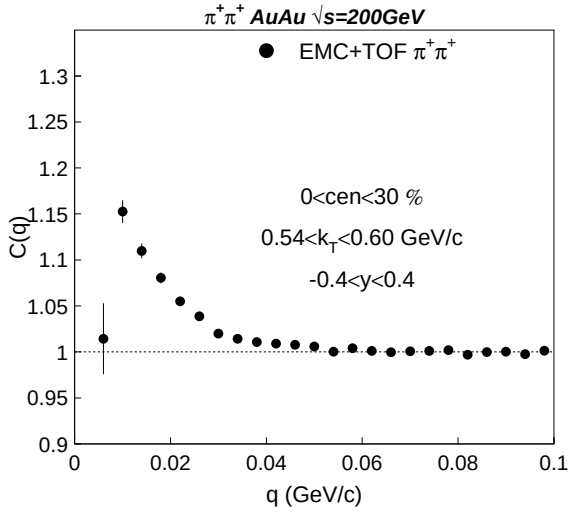

FIG. 116: *Correlation functions for positively charged pion pairs detected in the combined acceptance of the EMC and TOF. Results are shown for* $0 <$ *centrality* < 30 *and* $0.54 < k_T < 0.60$ *GeV/c.*

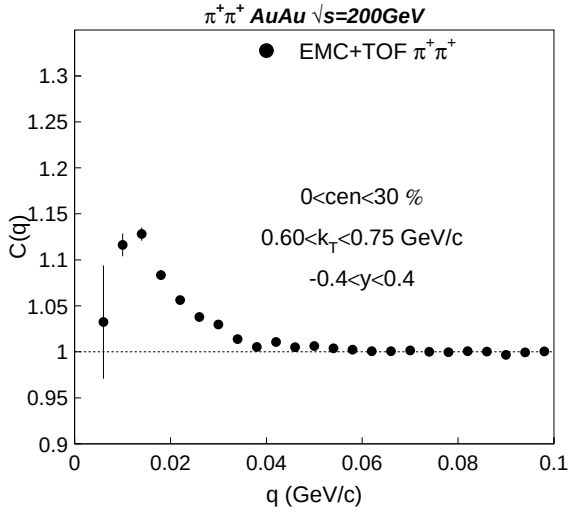

FIG. 117: *Correlation functions for positively charged pion pairs detected in the combined acceptance of the EMC and TOF. Results are shown for* $0 <$ *centrality* < 30 *and* $0.60 < k_T < 0.75$ *GeV/c.*

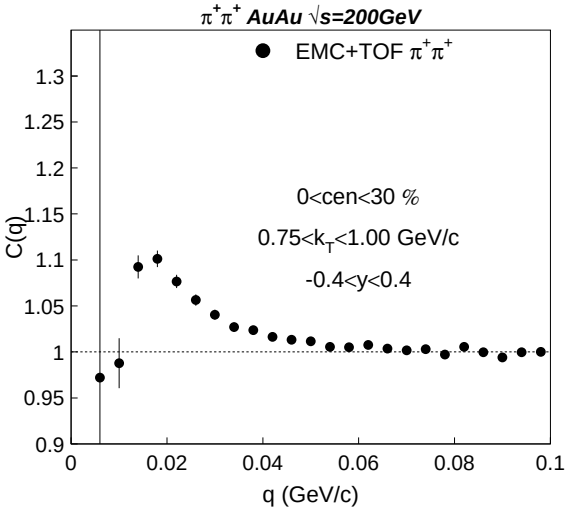

FIG. 118: *Correlation functions for positively charged pion pairs detected in the combined acceptance of the EMC and TOF. Results are shown for* $0 <$ *centrality* < 30 *and* $0.75 < k_T < 1.0$ *GeV/c.*

5.2. Consistency checks: EMC East vs EMC (E&W)+TOF

Figures 119, 120, 121, 122, 123, 124, 125 and 126 compare correlation functions obtained from EMC east with those obtained from EMC and TOF combined. Results are shown for positively charged pion pairs for several k_T selections. The comparison indicates rather good agreement as they should. Comparisons made for other centrality selections indicate a similar pattern.

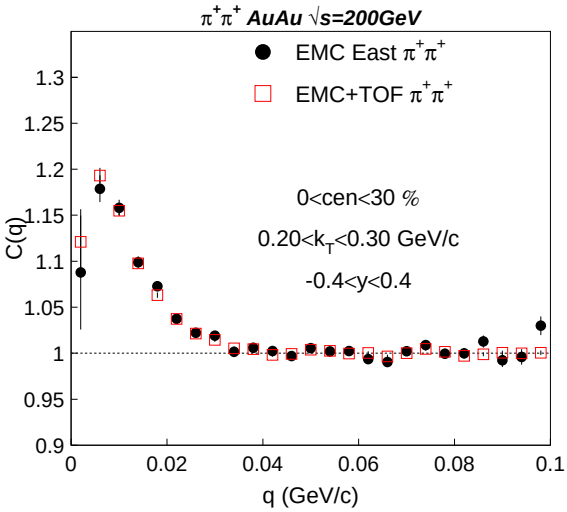

FIG. 119: *Comparison of correlation functions for positively charged pion pairs detected in the EMC East with similar correlation functions obtained from a combination of the EMC and TOF. Results are shown for* $0 < centrality < 30$ *and* $0.2 < k_T < 0.3$ *GeV/c.*

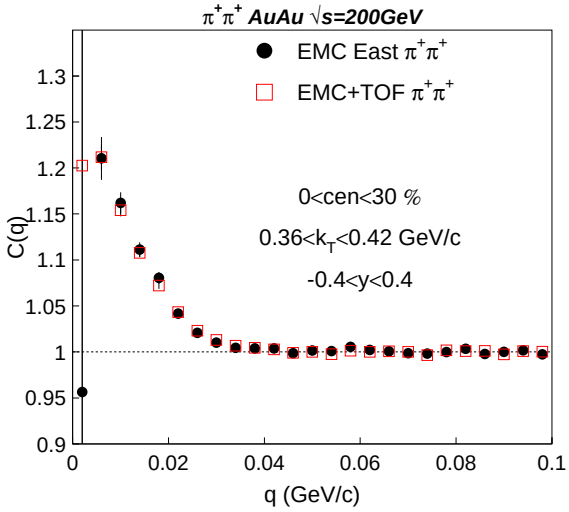

FIG. 120: *Comparison of correlation functions for positively charged pion pairs detected in the EMC East with similar correlation functions obtained from a combination of the EMC and TOF. Results are shown for* $0 < centrality < 30$ *and* $0.3 < k_T < 0.36$ *GeV/c.*

5.3. Consistency checks: TOF vs EMC (E&W)+TOF

Figures 127, 128, 129, 130, 131, 132, 133 and 134 compare correlation functions obtained from the TOF with those obtained from the the EMC and TOF combined. Results are shown for positively charged pion pairs for several k_T selections. Here again, the comparison indicates rather good agreement as they should.

Given the very good agreement between the correlation functions obtained from EMC and TOF (respectively), and those obtained from EMC + TOF (cf. Figs. 119 - 134) we use the correlation functions obtained from EMC + TOF as a basis for the imaging analysis discussed in the next section. These data have much better statistical significance and hence, allows a much more reliable extraction of source images.

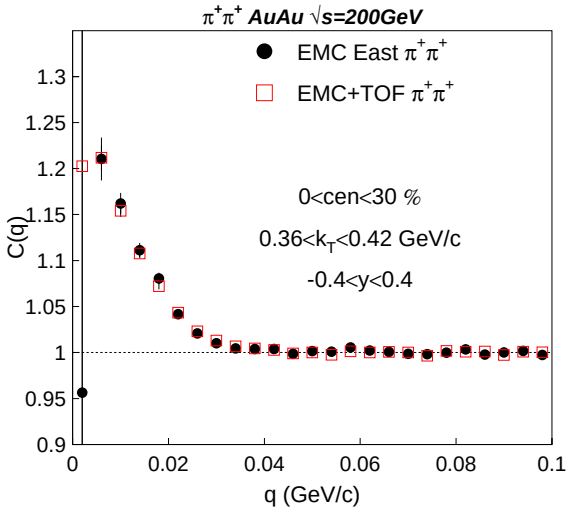

FIG. 121: *Comparison of correlation functions for positively charged pion pairs detected in the EMC East with similar correlation functions obtained from a combination of the EMC and TOF. Results are shown for* $0 < centrality < 30$ *and* $0.36 < k_T < 0.42$ *GeV/c.*

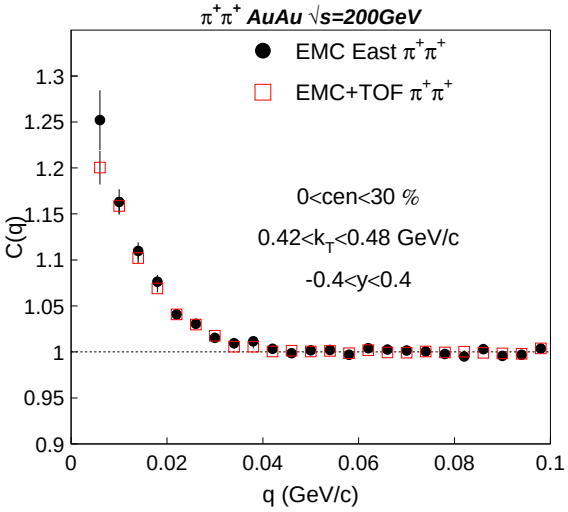

FIG. 122: *Comparison of correlation functions for positively charged pion pairs detected in the EMC East with similar correlation functions obtained from a combination of the EMC and TOF. Results are shown for* $0 < centrality < 30$ *and* $0.42 < k_T < 0.48$ *GeV/c.*

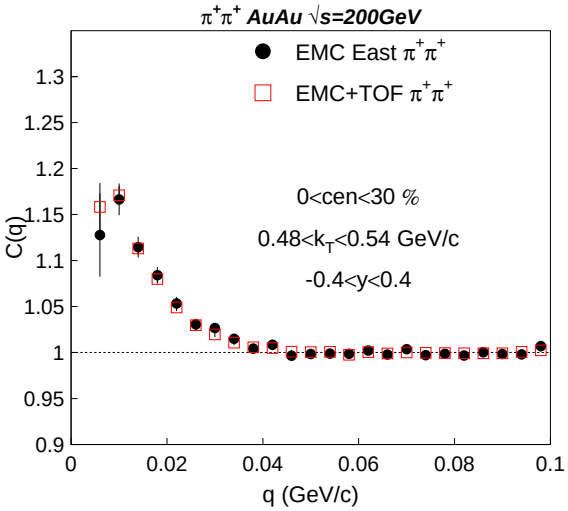

FIG. 123: *Comparison of correlation functions for positively charged pion pairs detected in the EMC East with similar correlation functions obtained from a combination of the EMC and TOF. Results are shown for* $0 < centrality < 30$ *and* $0.48 < k_T < 0.54$ *GeV/c.*

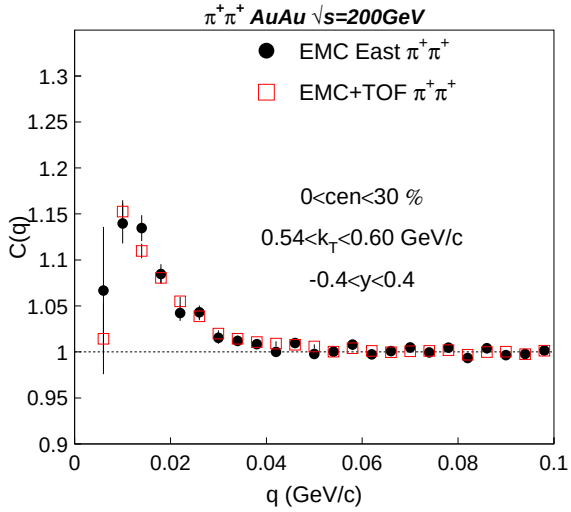

FIG. 124: *Comparison of correlation functions for positively charged pion pairs detected in the EMC East with similar correlation functions obtained from a combination of the EMC and TOF. Results are shown for* $0 < centrality < 30$ *and* $0.54 < k_T < 0.60$ *GeV/c.*

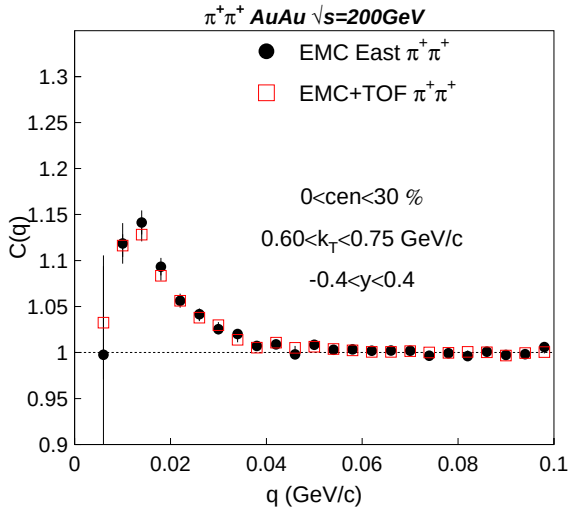

FIG. 125: *Comparison of correlation functions for positively charged pion pairs detected in the EMC East with similar correlation functions obtained from a combination of the EMC and TOF. Results are shown for* $0 < centrality < 30$ *and* $0.60 < k_T < 0.75$ *GeV/c.*

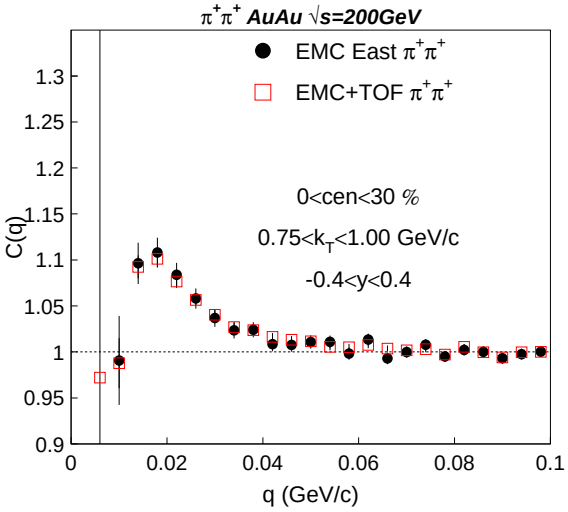

FIG. 126: *Comparison of correlation functions for positively charged pion pairs detected in the EMC East with similar correlation functions obtained from a combination of the EMC and TOF. Results are shown for* $0 < centrality < 30$ *and* $0.75 < k_T < 1.0$ *GeV/c.*

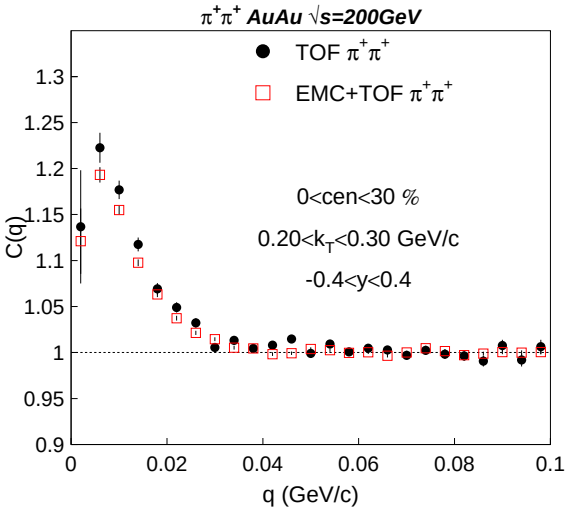

FIG. 127: *Comparison of correlation functions for positively charged pion pairs detected in the TOF with similar correlation functions obtained from a combination of the EMC and TOF. Results are shown for* $0 < centrality < 30$ *and* $0.2 < k_T < 0.3$ *GeV/c.*

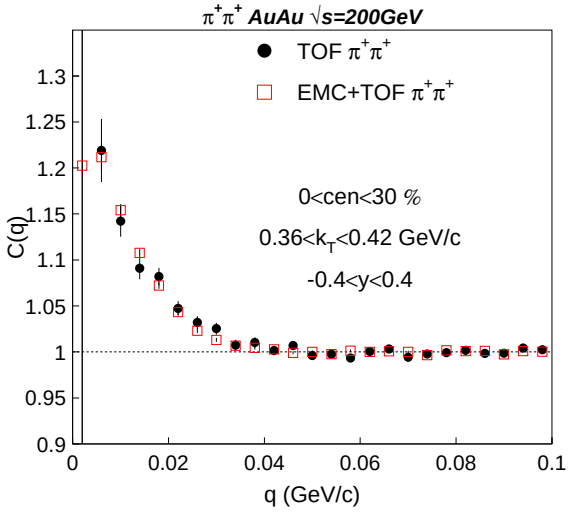

FIG. 128: *Comparison of correlation functions for positively charged pion pairs detected in the TOF with similar correlation functions obtained from a combination of the EMC and TOF. Results are shown for* $0 < centrality < 30$ *and* $0.3 < k_T < 0.36$ *GeV/c.*

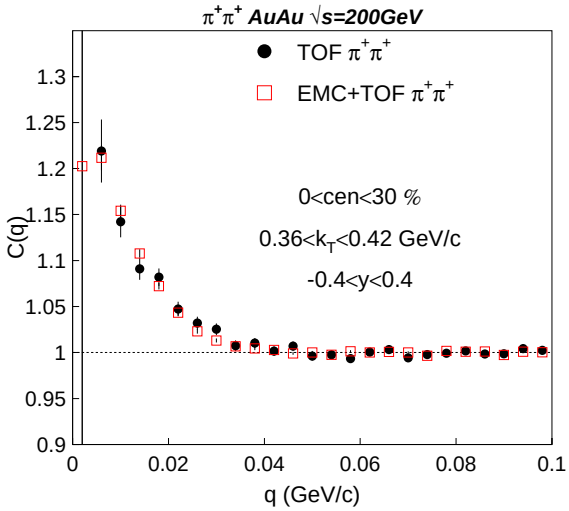

FIG. 129: *Comparison of correlation functions for positively charged pion pairs detected in the TOF with similar correlation functions obtained from a combination of the EMC and TOF. Results are shown for* $0 < centrality < 30$ *and* $0.36 < k_T < 0.42$ *GeV/c.*

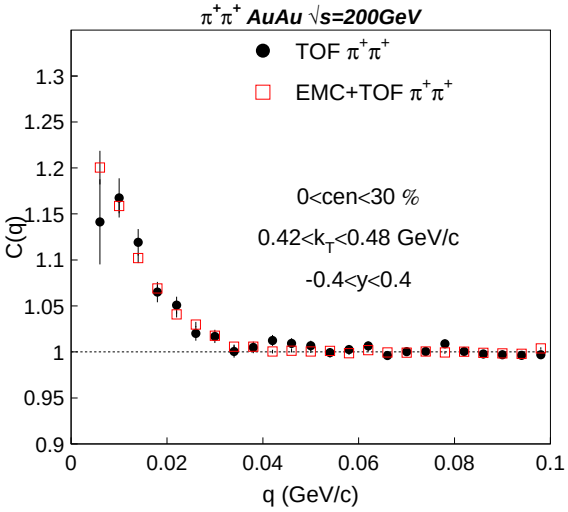

FIG. 130: *Comparison of correlation functions for positively charged pion pairs detected in the TOF with similar correlation functions obtained from a combination of the EMC and TOF. Results are shown for* $0 <$ *centrality* < 30 *and* $0.42 < k_T < 0.48$ *GeV/c.*

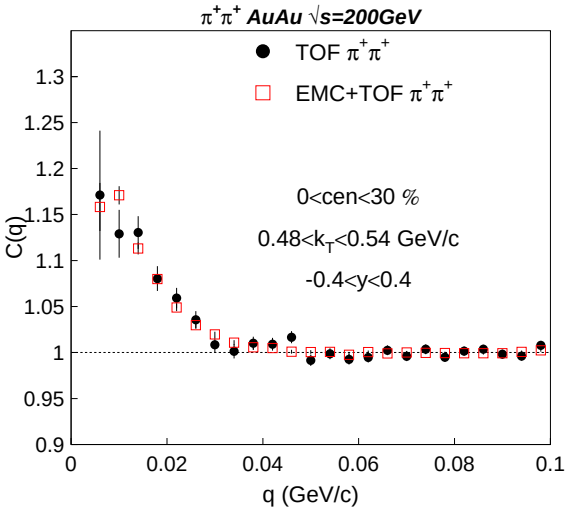

FIG. 131: *Comparison of correlation functions for positively charged pion pairs detected in the TOF with similar correlation functions obtained from a combination of the EMC and TOF. Results are shown for* $0 <$ *centrality* < 30 *and* $0.48 < k_T < 0.54$ *GeV/c.*

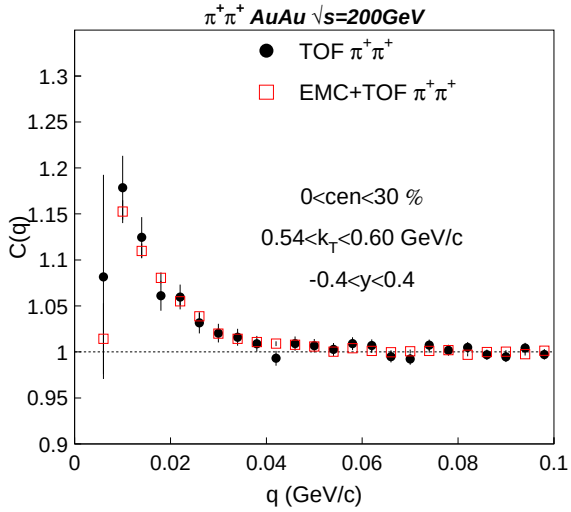

FIG. 132: *Comparison of correlation functions for positively charged pion pairs detected in the TOF with similar correlation functions obtained from a combination of the EMC and TOF. Results are shown for* $0 <$ *centrality* < 30 *and* $0.54 < k_T < 0.60$ *GeV/c.*

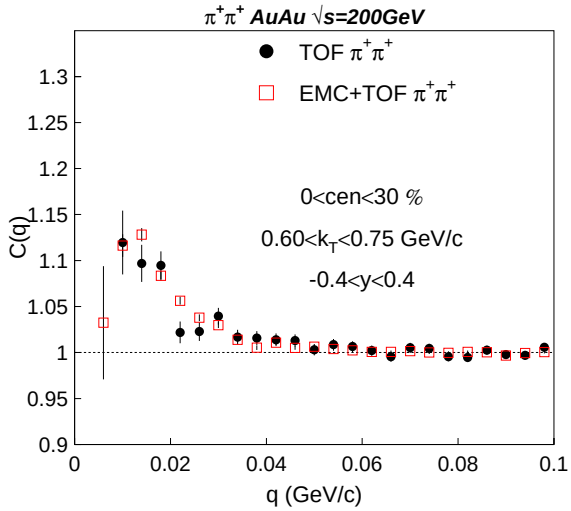

FIG. 133: *Comparison of correlation functions for positively charged pion pairs detected in the TOF with similar correlation functions obtained from a combination of the EMC and TOF. Results are shown for* $0 <$ *centrality* < 30 *and* $0.60 < k_T < 0.75$ *GeV/c.*

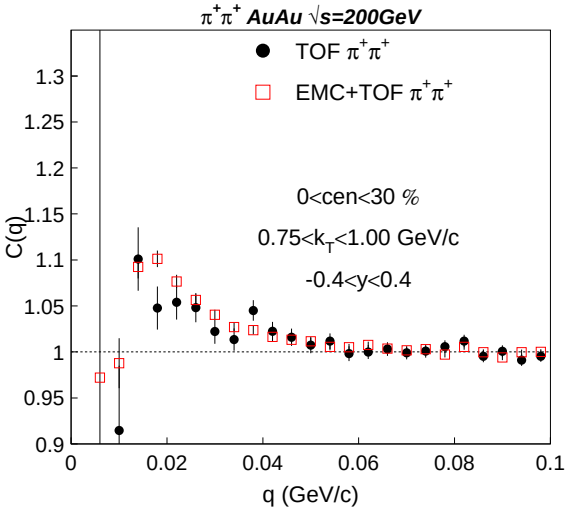

FIG. 134: *Comparison of correlation functions for positively charged pion pairs detected in the TOF with similar correlation functions obtained from a combination of the EMC and TOF. Results are shown for* $0 < centrality < 30$ *and* $0.75 < k_T < 1.0$ *GeV/c.*

6. INFLUENCE OF CUTS ON THE CORRELATION FUNCTIONS

An important question which arises in all correlation analyses is whether or not "reasonable" systematic variations of track-pair cuts have a significant impact on the extracted correlation functions. This issue has been thoroughly investigated for this analysis. Here, it is important to remind the reader that the important track-pair cut variables are $\Delta\phi_{DC}$, ΔR_{PC1} and $\Delta R_{EMC/TOF}$. In what follows we show representative results which summarize the major findings from our investigations. The cut variations used for these investigations have been significantly influenced by PWG discussions and PWG convener requests.

6.1. Sensitivity to cut variations of $\Delta\Phi_{DC}$

6.1.1. $\Delta\Phi_{DC}$ variation for $\Delta zed > 5cm$

Figures 135, 136, 137, 138, 139, 140, 141 and 142 compare correlation functions for positively charged pions detected in the EMC. The focus here is to show the effect of an extreme variation of the $\Delta\phi_{DC}$ cut for $\Delta zed > 5$cm. The filled symbols show results for our standard cuts and the open symbols show results for a very large increase (factor of 2) in the $\Delta\phi_{DC}$ as indicated on each figure. The comparisons which are shown for several k_T selections indicate very little if any, change in the correlation functions for this cut variation. Thus, it can be concluded that a more reasonable (smaller) variation of this cut would not affect the correlation function.

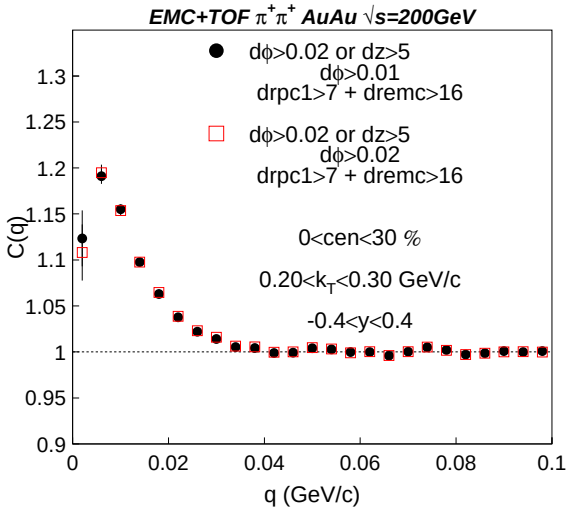

FIG. 135: *Comparison of correlation functions for 100% $\Delta\phi_{DC}$ cut variation for $\Delta zed > 5cm$. Results are shown for positively charged pions for $0 < centrality < 30$ and $0.2 < k_T < 0.3$ GeV/c.*

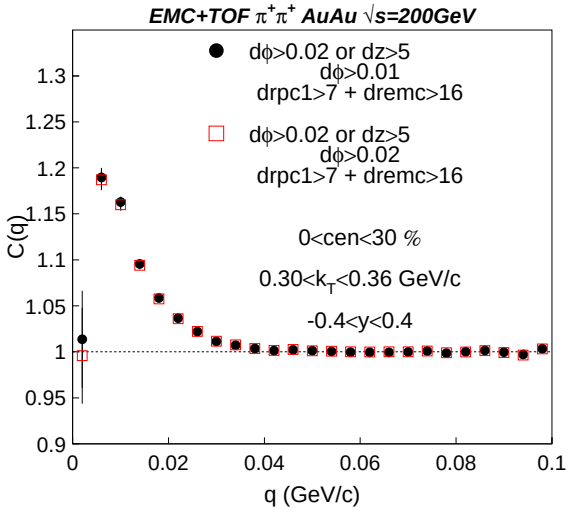

FIG. 136: *Comparison of correlation functions for 100% $\Delta\phi_{DC}$ cut variation for $\Delta zed > 5cm$. Results are shown for positively charged pions for $0 < centrality < 30$ and $0.3 < k_T < 0.36$ GeV/c.*

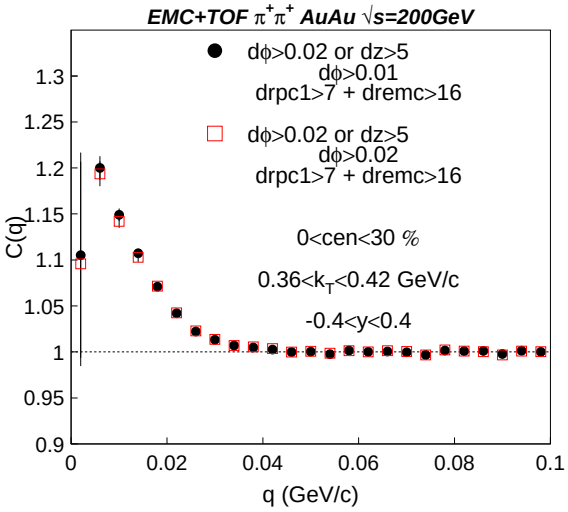

FIG. 137: *Comparison of correlation functions for 100% $\Delta\phi_{DC}$ cut variation for $\Delta zed > 5cm$. Results are shown for positively charged pions for $0 < centrality < 30$ and $0.36 < k_T < 0.42$ GeV/c.*

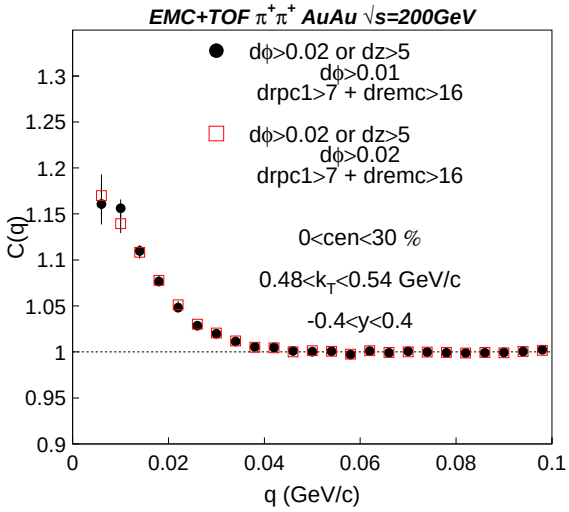

FIG. 139: *Comparison of correlation functions for 100% $\Delta\phi_{DC}$ cut variation for $\Delta zed > 5cm$. Results are shown for positively charged pions for $0 < centrality < 30$ and $0.48 < k_T < 0.54$ GeV/c.*

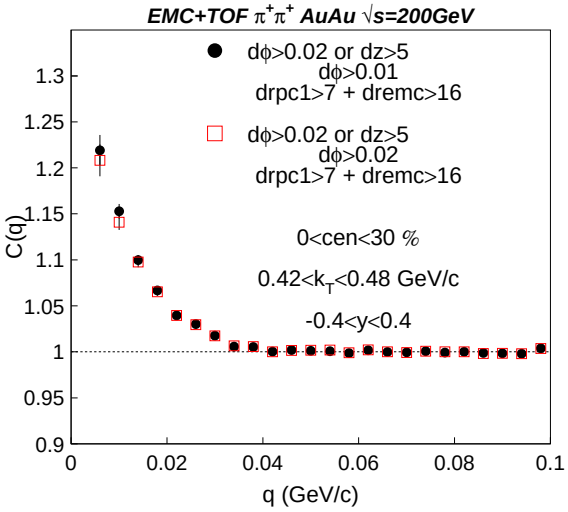

FIG. 138: *Comparison of correlation functions for 100% $\Delta\phi_{DC}$ cut variation for $\Delta zed > 5cm$. Results are shown for positively charged pions for $0 < centrality < 30$ and $0.42 < k_T < 0.48$ GeV/c.*

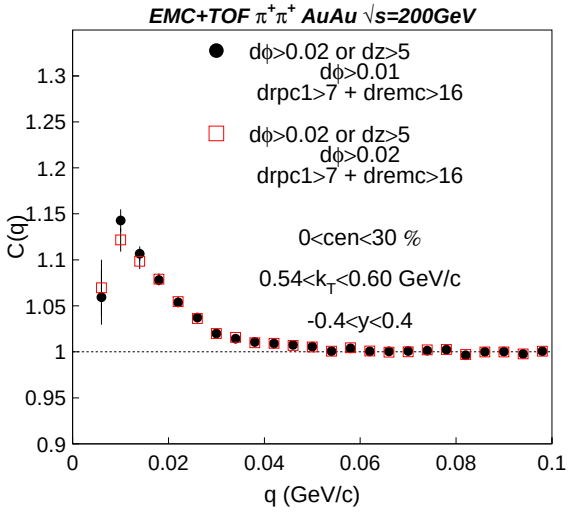

FIG. 140: *Comparison of correlation functions for 100% $\Delta\phi_{DC}$ cut variation for $\Delta zed > 5cm$. Results are shown for positively charged pions for $0 < centrality < 30$ and $0.54 < k_T < 0.60$ GeV/c.*

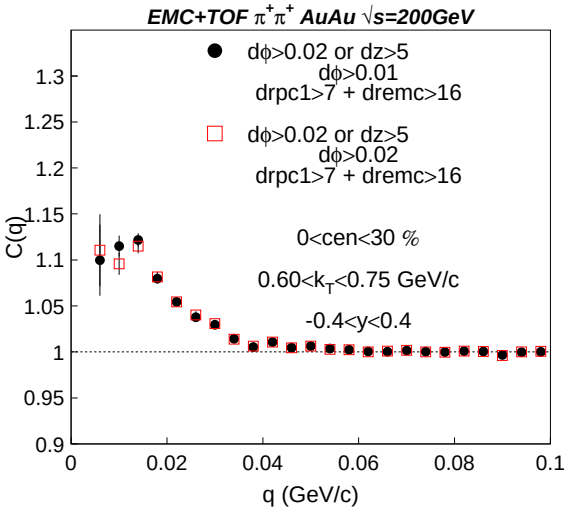

FIG. 141: *Comparison of correlation functions for $\Delta\phi_{DC}$ cut variations for $\Delta zed > 5cm$. Results are shown for positively charged pions for $0 <$ centrality < 30 and $0.60 < k_T < 0.75$ GeV/c.*

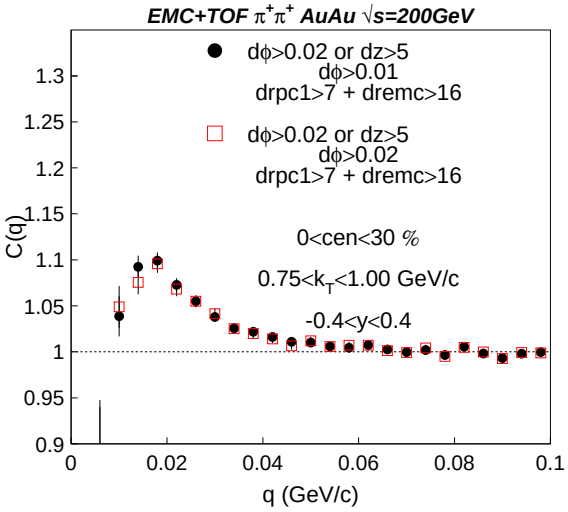

FIG. 142: *Comparison of correlation functions for 100% $\Delta\phi_{DC}$ cut variation for $\Delta zed > 5cm$. Results are shown for positively charged pions for $0 <$ centrality < 30 and $0.75 < k_T < 1.0$ GeV/c.*

6.1.2. $\Delta\Phi_{DC}$ variation for $\Delta zed < 5cm$

Figures 143, 144, 145, 146, 147, 148, 149 and 150 compare correlation functions for positively charged pions with different $\Delta\phi_{DC}$ cuts. The focus in this case is to show the effect of a really extreme variation of the $\Delta\phi_{DC}$ cut for Δzed <5 cm. The filled symbols show results for our standard cuts and the open symbols show results for a very large increase (X3) in the $\Delta\phi_{DC}$ as indicated on each figure. The comparisons which are shown for several k_T selections indicate very little if any change in the correlation functions for this cut variation. Again it can be concluded that a more reasonable (smaller) variation of this cut would not affect the correlation function.

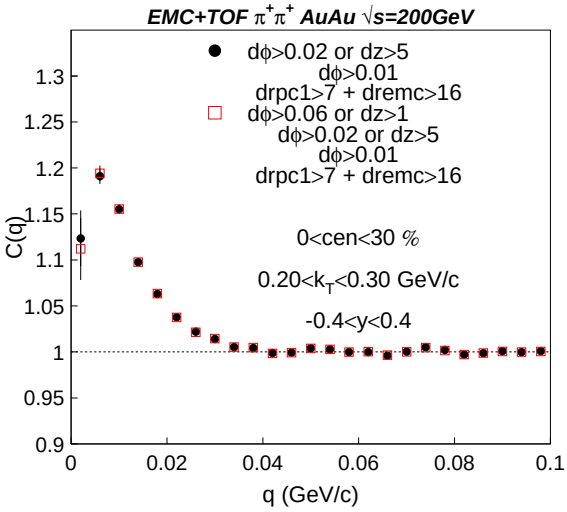

FIG. 143: *Comparison of correlation functions for $\Delta\phi_{DC}$ cut variations for dzed < 5cm. Results are shown for positively charged pions for 0 < centrality < 30 and 0.2 < k_T< 0.3 GeV/c.*

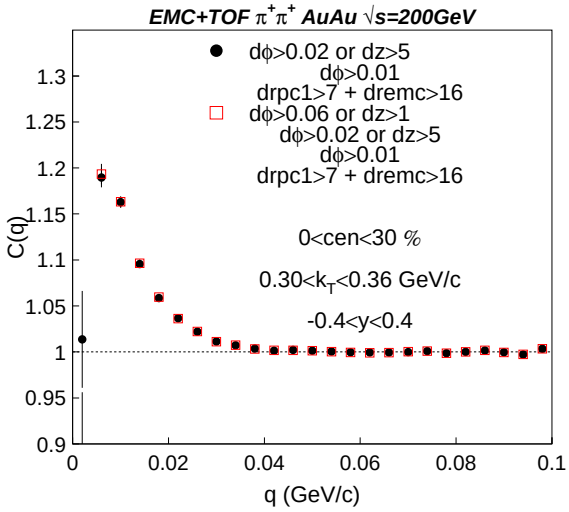

FIG. 144: *Comparison of correlation functions for $\Delta\phi_{DC}$ cut variations for dzed < 5cm. Results are shown for positively charged pions for 0 < centrality < 30 and 0.3 < k_T< 0.360 GeV/c.*

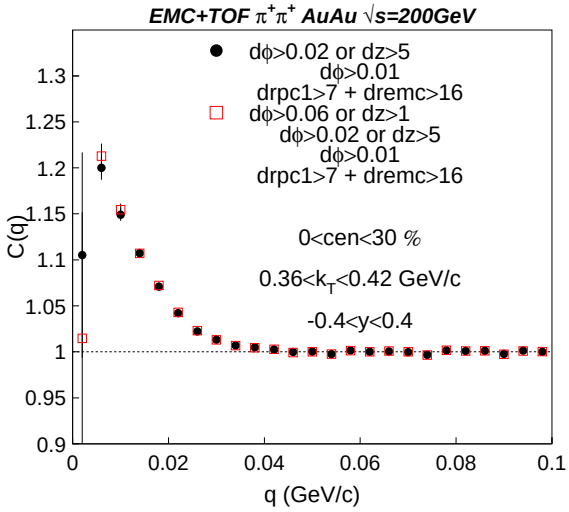

FIG. 145: *Comparison of correlation functions for $\Delta\phi_{DC}$ cut variations for dzed < 5cm. Results are shown for positively charged pions for 0 < centrality < 30 and 0.360 < k_T< 0.42 GeV/c.*

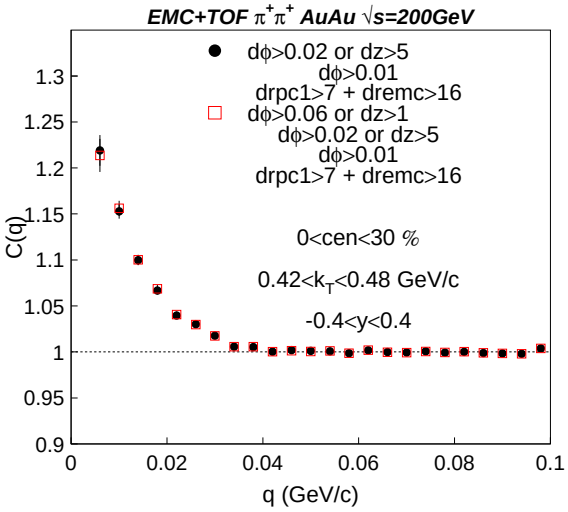

FIG. 146: *Comparison of correlation functions for $\Delta\phi_{DC}$ cut variations for dzed < 5cm. Results are shown for positively charged pions for 0 < centrality < 30 and 0.42 < k_T< 0.48 GeV/c.*

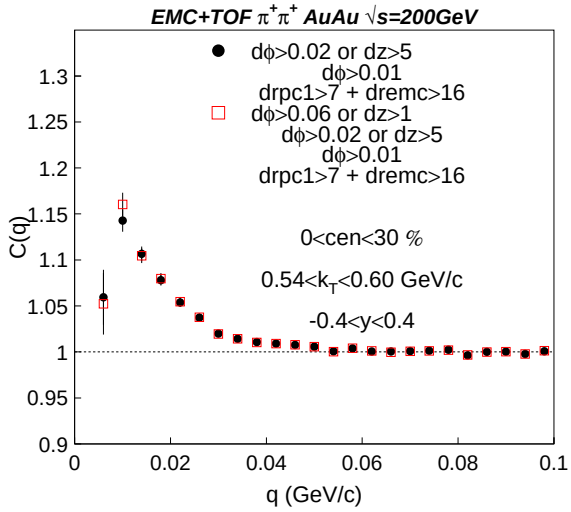

FIG. 148: *Comparison of correlation functions for $\Delta\phi_{DC}$ cut variations for dzed < 5cm. Results are shown for positively charged pions for 0 < centrality < 30 and 0.54 < k_T< 0.60 GeV/c.*

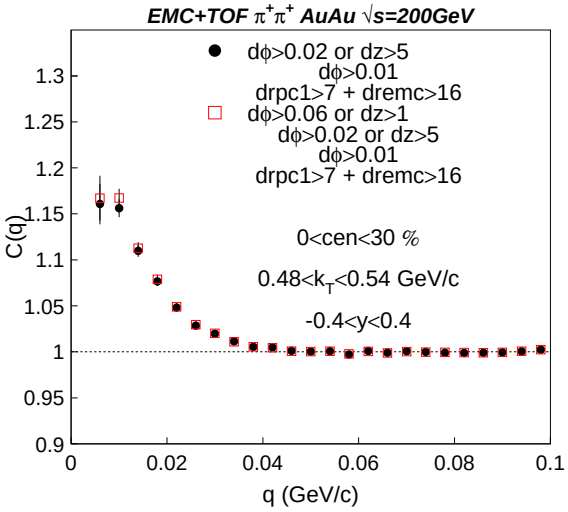

FIG. 147: *Comparison of correlation functions for $\Delta\phi_{DC}$ cut variations for dzed < 5cm. Results are shown for positively charged pions for 0 < centrality < 30 and 0.48 < k_T< 0.54 GeV/c.*

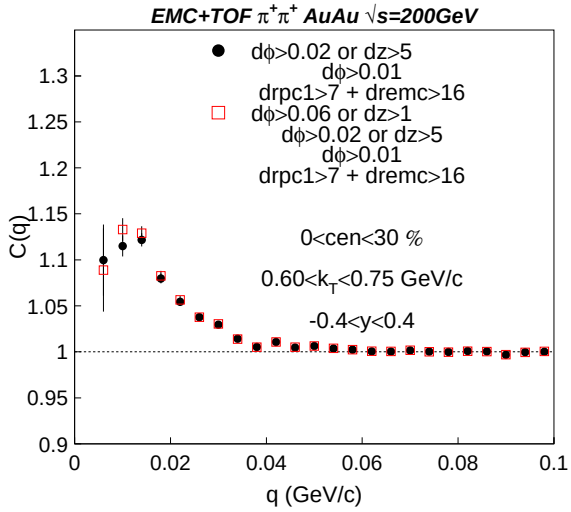

FIG. 149: *Comparison of correlation functions for $\Delta\phi_{DC}$ cut variations for dzed < 5cm. Results are shown for positively charged pions for 0 < centrality < 30 and 0.60 < k_T< 0.75 GeV/c.*

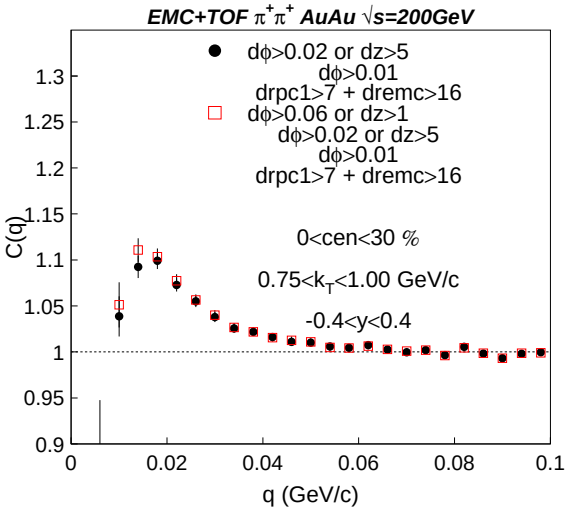

FIG. 150: *Comparison of correlation functions for* $\Delta\phi_{DC}$ *cut variations for dzed* $<$ *5cm . Results are shown for positively charged pions for* $0 <$ *centrality* < 30 *and* $0.75 < k_T < 1.0$ *GeV/c.*

6.1.3. *Simultaneous variation of $\Delta\Phi_{DC}$ for $\Delta zed < 5cm$ and $\Delta zed > 5cm$*

Figures 151, 152, 153, 154, 155, 156, 157 and 158 compare correlation functions in which we have simultaneously varied $\Delta\Phi_{DC}$. for the two Δzed regions of interest. The filled symbols show results for our standard cuts and the open symbols show results for extreme variations in $\Delta\Phi_{DC}$ for $\Delta zed < 5$cm and $\Delta zed > 5$cm (as indicated on each figure). Comparisons are shown for several k_T selections; they do not indicate significant changes for low k_T but do show some small differences for large k_T. We conclude that more reasonable variations of these cuts will not have a strong influence on the correlation functions. In a later section we will address the influence of such changes on the extracted images.

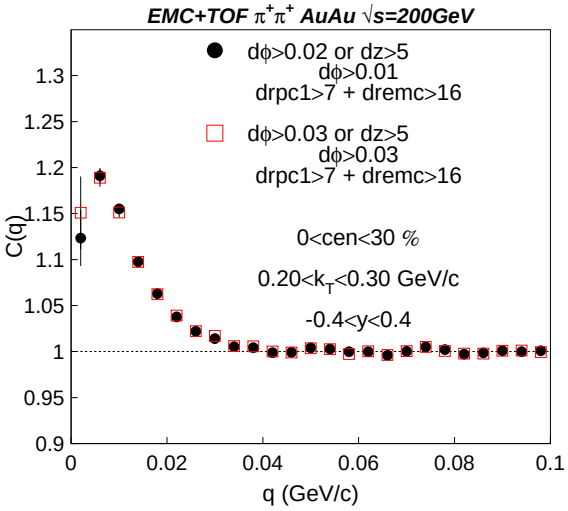

FIG. 151: *Comparison of correlation functions for simultaneous $\Delta\phi_{DC}$ variation for $\Delta zed < 5cm$ and $\Delta zed > 5cm$. Results are shown for positively charged pions for $0 <$ centrality < 30 and $0.2 < k_T < 0.3$ GeV/c.*

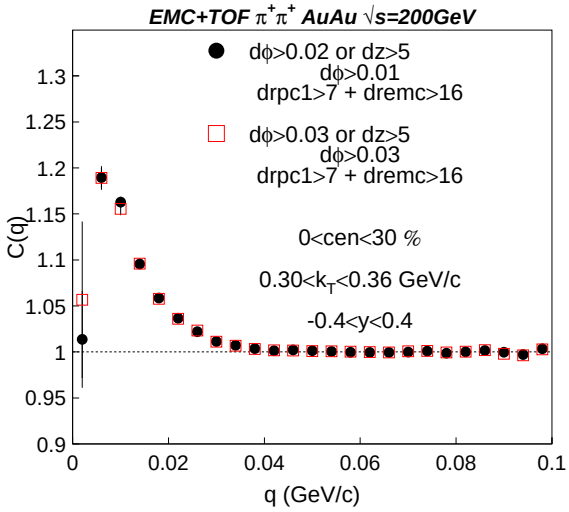

FIG. 152: *Comparison of correlation functions for simultaneous $\Delta\phi_{DC}$ variation for $\Delta zed < 5cm$ and $\Delta zed > 5cm$. Results are shown for positively charged pions for $0 <$ centrality < 30 and $0.3 < k_T < 0.360$ GeV/c.*

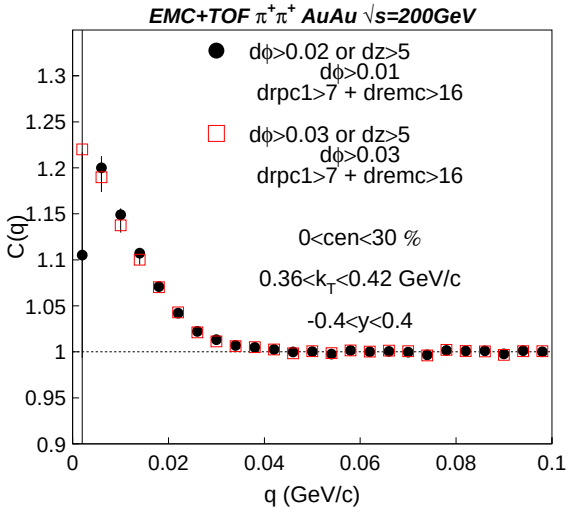

FIG. 153: *Comparison of correlation functions for simultaneous $\Delta\phi_{DC}$ variation for $\Delta zed < 5cm$ and $\Delta zed > 5cm$. Results are shown for positively charged pions for $0 <$ centrality < 30 and $0.360 < k_T < 0.42$ GeV/c.*

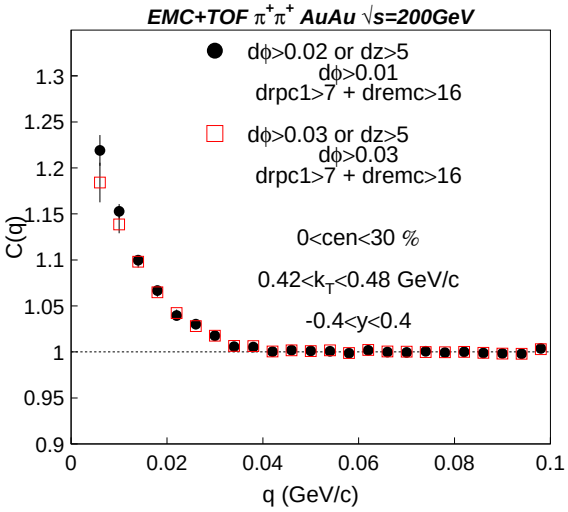

FIG. 154: *Comparison of correlation functions for simultaneous $\Delta\phi_{DC}$ variation for $\Delta zed < 5cm$ and $\Delta zed > 5cm$. Results are shown for positively charged pions for $0 <$ centrality < 30 and $0.42 < k_T < 0.48$ GeV/c.*

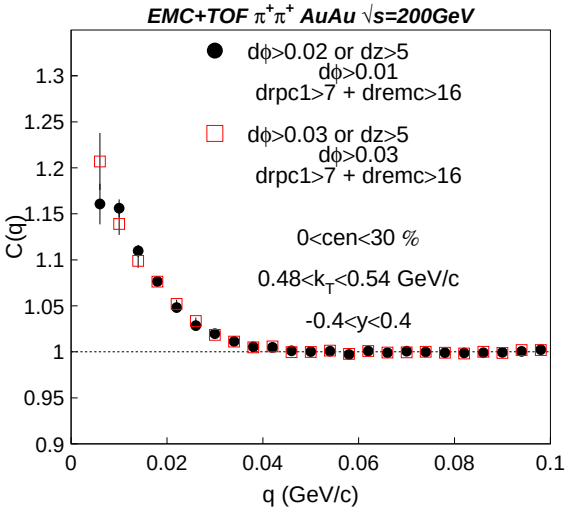

FIG. 155: *Comparison of correlation functions for simultaneous $\Delta\phi_{DC}$ variation for $\Delta zed < 5cm$ and $\Delta zed > 5cm$. Results are shown for positively charged pions for $0 <$ centrality < 30 and $0.48 < k_T < 0.54$ GeV/c.*

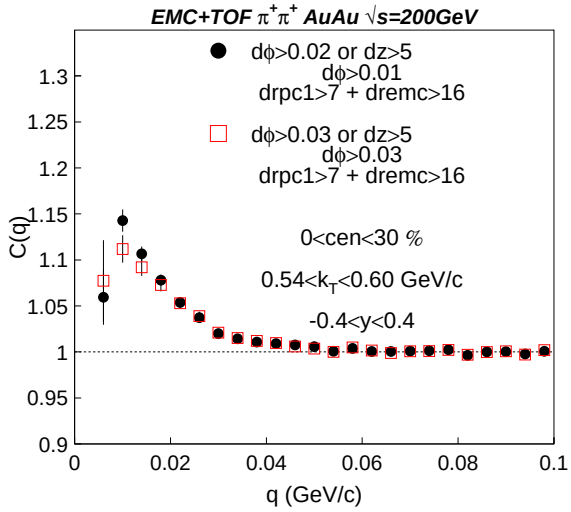

FIG. 156: *Comparison of correlation functions for simultaneous $\Delta\phi_{DC}$ variation for $\Delta zed < 5cm$ and $\Delta zed > 5cm$. Results are shown for positively charged pions for $0 <$ centrality < 30 and $0.54 < k_T < 0.60$ GeV/c.*

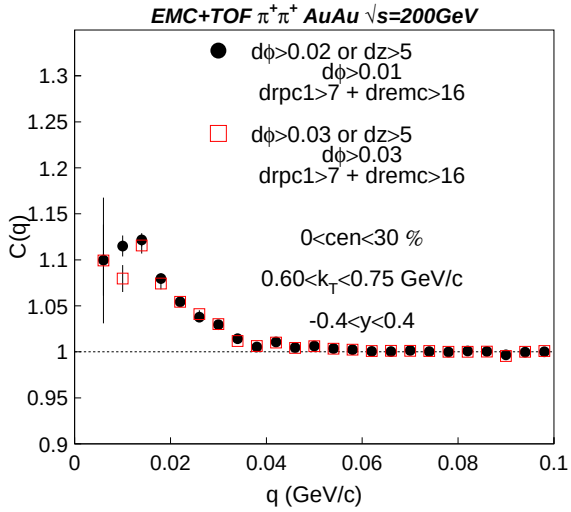

FIG. 157: *Comparison of correlation functions for simultaneous $\Delta\phi_{DC}$ variation for $\Delta zed < 5cm$ and $\Delta zed > 5cm$. Results are shown for positively charged pions for $0 <$ centrality < 30 and $0.60 < k_T < 0.75$ GeV/c.*

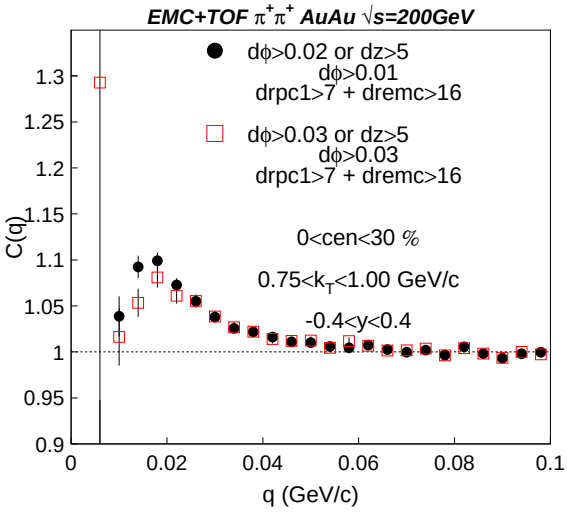

FIG. 158: *Comparison of correlation functions for simultaneous $\Delta\phi_{DC}$ variation for $\Delta zed < 5cm$ and $\Delta zed > 5cm$. Results are shown for positively charged pions for $0 <$ centrality < 30 and $0.75 < k_T < 1.0$ GeV/c.*

6.2. Sensitivity to cut variations of ΔR

6.2.1. Cut variations of ΔR_{PC1}

Figures 159, 160, 161, 162, 163, 164, 165 and 166 show comparisons of correlation functions measured in the EMC-TOF for cut variations of ΔR_{PC1}. The filled symbols show results for our standard cuts and the open symbols show results for a ∼15% increase in the ΔR_{PC1} cut. The comparisons which are shown for several k_T selections indicate very little if any, change in the correlation functions for this cut variation.

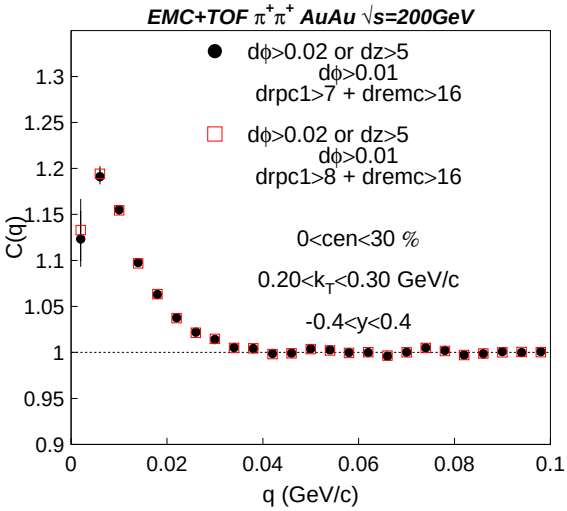

FIG. 159: *Comparison of correlation functions measured in the EMC for ∼ 15% cut variations of ΔR_{PC1}. Results are shown for positively charged pions for 0 < centrality < 30 and 0.2 < k_T < 0.3 GeV/c.*

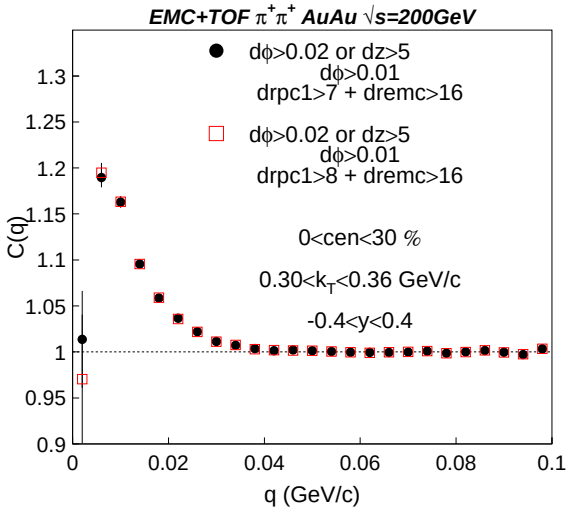

FIG. 160: *Comparison of correlation functions measured in the EMC for ∼ 15% cut variations of ΔR_{PC1}. Results are shown for positively charged pions for 0 < centrality < 30 and 0.3 < k_T < 0.36 GeV/c.*

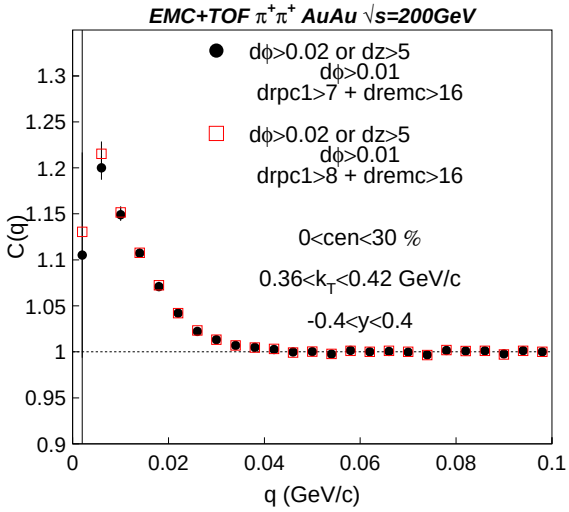

FIG. 161: *Comparison of correlation functions measured in the EMC for ∼15% cut variations of ΔR_{PC1}. Results are shown for positively charged pions for 0 < centrality < 30 and 0.36 < k_T < 0.42 GeV/c.*

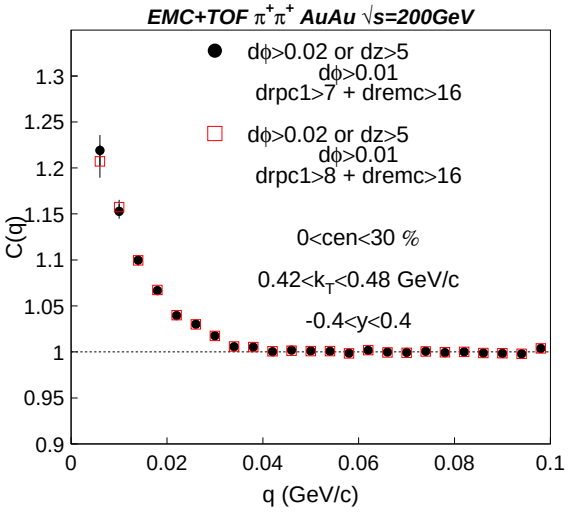

FIG. 162: *Comparison of correlation functions measured in the EMC for ∼15% cut variations of ΔR_{PC1}. Results are shown for positively charged pions for 0 < centrality < 30 and 0.42 < k_T < 0.48 GeV/c.*

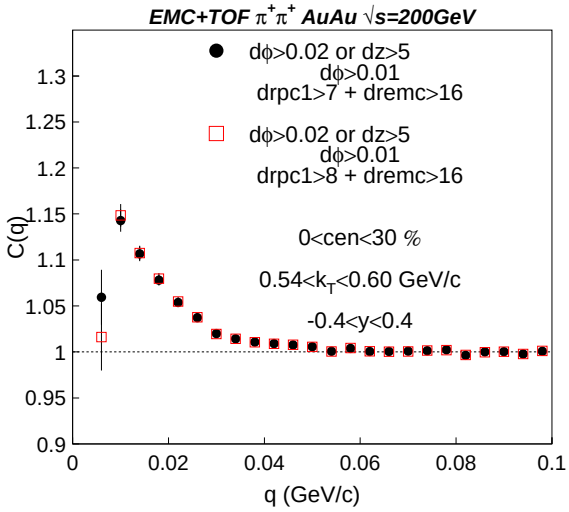

FIG. 164: *Comparison of correlation functions measured in the EMC for ∼15% cut variations of ΔR_{PC1}. Results are shown for positively charged pions for 0 < centrality < 30 and 0.54 < k_T < 0.60 GeV/c.*

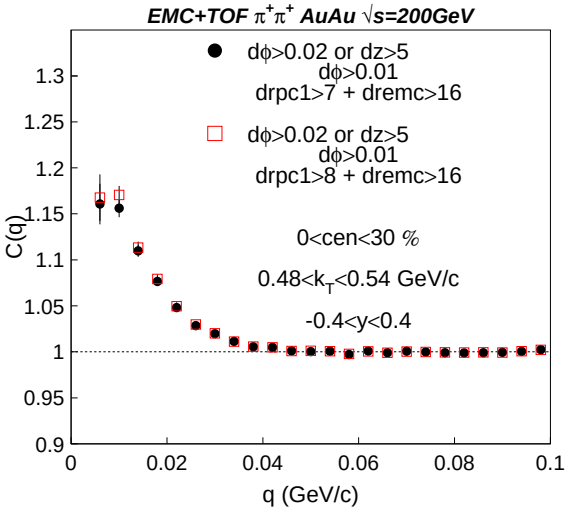

FIG. 163: *Comparison of correlation functions measured in the EMC for ∼15% cut variations of ΔR_{PC1}. Results are shown for positively charged pions for 0 < centrality < 30 and 0.48 < k_T < 0.54 GeV/c.*

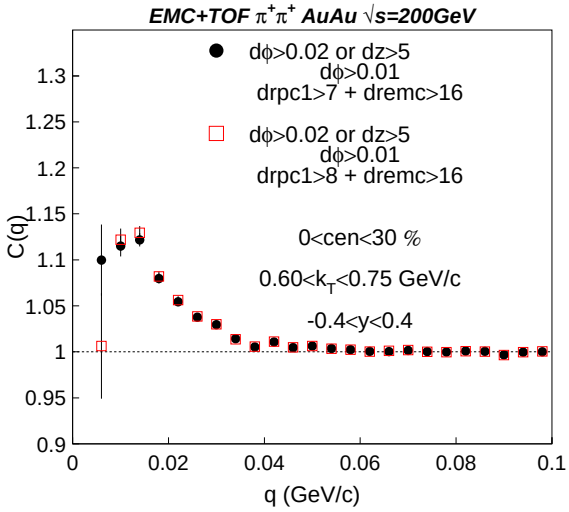

FIG. 165: *Comparison of correlation functions measured in the EMC for ∼15% cut variations of ΔR_{PC1}. Results are shown for positively charged pions for 0 < centrality < 30 and 0.60 < k_T < 0.75 GeV/c.*

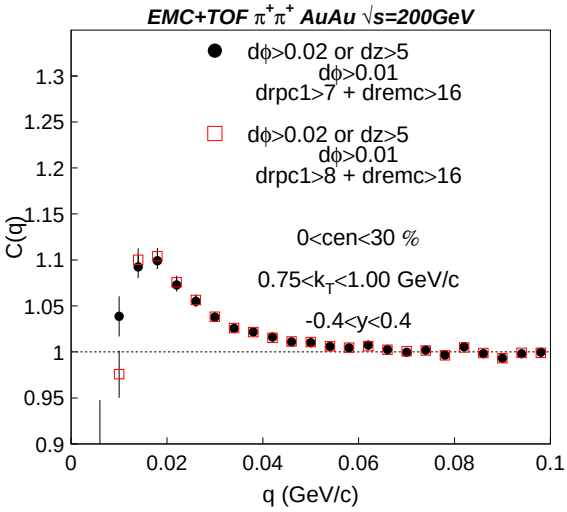

FIG. 166: *Comparison of correlation functions measured in the EMC for ∼15% cut variations of* ΔR_{PC1}. *Results are shown for positively charged pions for* $0 <$ *centrality* < 30 *and* $0.75 < k_T < 1.00$ *GeV/c.*

6.2.2. *Sensitivity to cut variations of* $\Delta R_{EMC/TOF}$

Figures 167, 168, 169, 170, 171, 172, 173 and 174 show comparisons of correlation functions measured in the EMC for cut variations of $\Delta R_{EMC/TOF}$. The filled symbols show results for our standard cuts and the open symbols show results for a ∼15% increase in the ΔR_{EMC} and ΔR_{TOF} cut. The comparisons which are shown for several k_T selections indicate very little if any, change in the correlation functions for this cut variation.

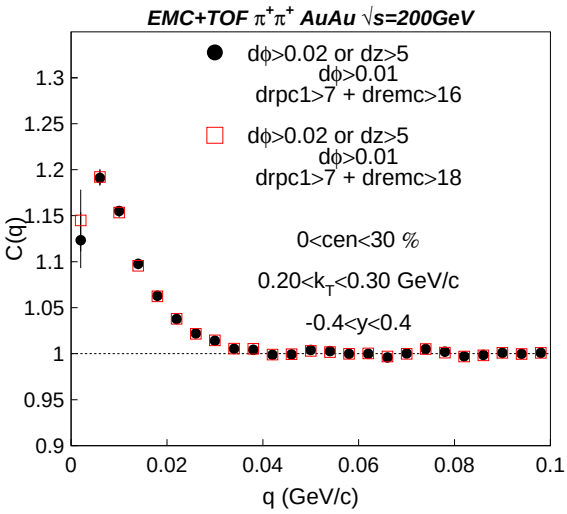

FIG. 167: *Comparison of correlation functions measured in the EMC for ∼ 15% cut variations of* ΔR_{EMC}*. Results are shown for positively charged pions for* $0 <$ *centrality* < 30 *and* $0.2 < k_T < 0.3$ *GeV/c.*

6.2.3. *Summary of sensitivity cut variations of* ΔR

The ΔR variation studies clearly indicate that if these track-pair cuts are varied systematically over a reasonable range, they do not lead to any significant influence on the correlation functions. This invariance is important for minimization of systematic errors associated with source image extraction.

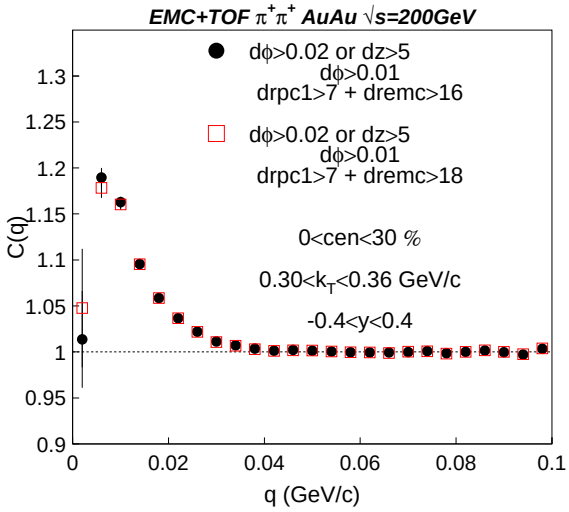

FIG. 168: *Comparison of correlation functions measured in the EMC for ∼ 15% cut variations of* ΔR_{EMC}*. Results are shown for positively charged pions for* $0 <$ *centrality* < 30 *and* $0.3 < k_T < 0.36$ *GeV/c.*

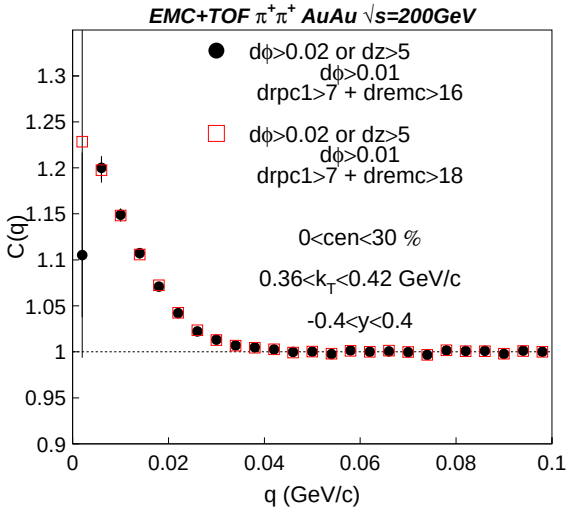

FIG. 169: *Comparison of correlation functions measured in the EMC for ∼15% cut variations of* ΔR_{EMC}*. Results are shown for positively charged pions for* $0 <$ *centrality* < 30 *and* $0.36 < k_T < 0.42$ *GeV/c.*

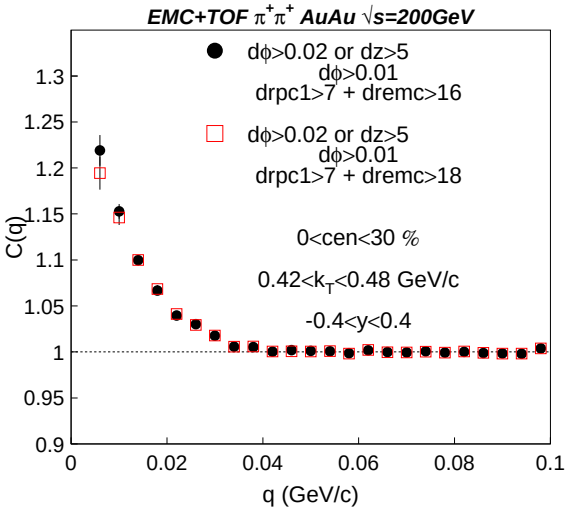

FIG. 170: *Comparison of correlation functions measured in the EMC for ∼15% cut variations of ΔR_{EMC}. Results are shown for positively charged pions for 0 < centrality < 30 and 0.42 < k_T < 0.48 GeV/c.*

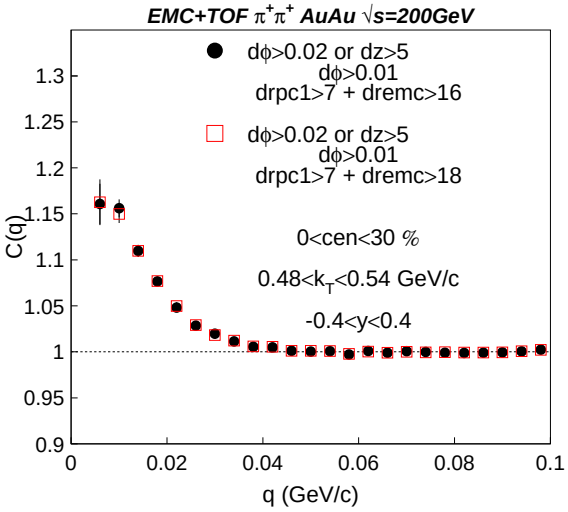

FIG. 171: *Comparison of correlation functions measured in the EMC for ∼15% cut variations of ΔR_{EMC}. Results are shown for positively charged pions for 0 < centrality < 30 and 0.48 < k_T < 0.54 GeV/c.*

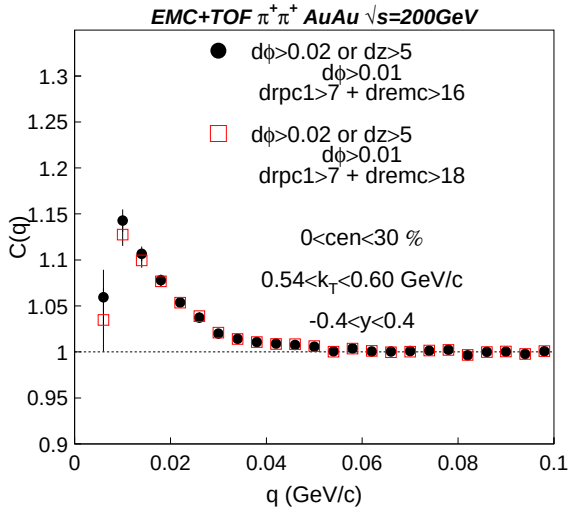

FIG. 172: *Comparison of correlation functions measured in the EMC for ∼15% cut variations of ΔR_{EMC}. Results are shown for positively charged pions for 0 < centrality < 30 and 0.54 < k_T < 0.60 GeV/c.*

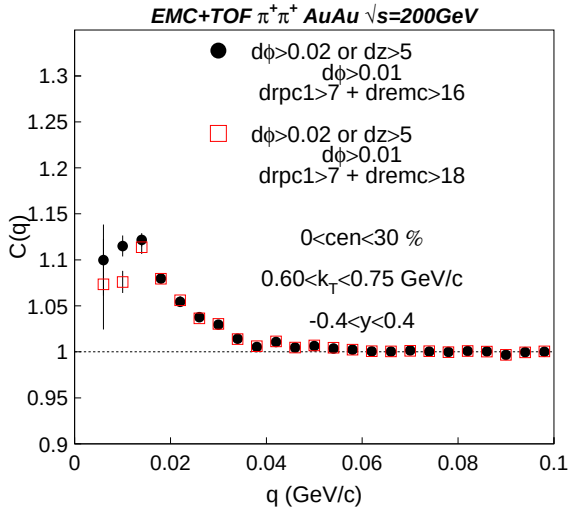

FIG. 173: *Comparison of correlation functions measured in the EMC for ∼15% cut variations of ΔR_{EMC}. Results are shown for positively charged pions for 0 < centrality < 30 and 0.60 < k_T < 0.75 GeV/c.*

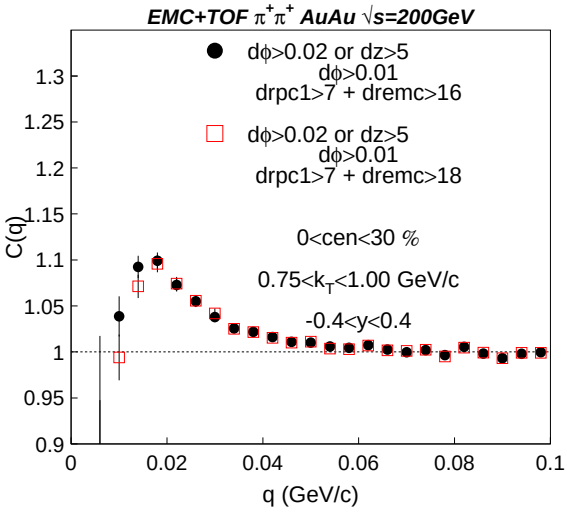

FIG. 174: *Comparison of correlation functions measured in the EMC for ∼15% cut variations of* ΔR_{EMC}. *Results are shown for positively charged pions for* $0 <$ *centrality* < 30 *and* $0.75 < k_T < 1.0$ *GeV/c.*

7. SOURCE IMAGE EXTRACTION

As indicated in section 1, the primary task of an imaging analysis is to extract the source function $S(r)$, from the measured correlation function [2, 3, 5]. The correlation function is related to the source function via the Koonin-Pratt equation [7] as follows:

$$C(\vec{q}) = 4\pi \int dr r^2 K(q,r)\ S(r). \tag{4}$$

Imaging the source means that we invert this integral equation. To do this we follow the procedures outlined in Refs. [2, 3, 5]. Carrying out this inversion is not a trivial matter because one has to take into account experimental factors, finite statistics, the widths of momentum bins, etc. as well as the intrinsic resolution of the kernel $K(q,r)$. However, if successful, this inversion has the virtue of being model independent. A brief outline of the imaging procedure follows.

The source functions $S(r)$ are expanded as a superposition of polynomial splines;

$$S(r) = \sum_j S_j \cdot B_j(r). \tag{5}$$

Following this expansion, the the Koonin-Pratt equation is discretized into a matrix equation

$$C_i^{Theory}(q) = \sum_j K_{ij} \cdot S_j \tag{6}$$

where K_{ij} is obtained from;

$$K_{ij} = \int dr \cdot K(q,r) B_j(r). \tag{7}$$

The unknown coefficients S_j, in the matrix equation (Eq. 6) are determined by minimizing the χ^2 value between the experimental correlation function and the theoretical correlation function obtained from Eq. 6;

$$\chi^2 = \left(C_i^{Expt.}(q) - \sum_j k_{ij} S_j \right)^2 / \Delta^2 C_i(q)^{Expt} \tag{8}$$

Inversion of this condition for the minimum gives an algebraic expression for the values of S_j as follows:

$$S_j = \sum_i \left[\left(K_T \left(\Delta^2 C^{Expt.}(q) \right)^{-1} K^T B \right) \right]_{ji} \left(C_i^{Expt.} - 1 \right)$$

where K^T is the transpose of the kernel matrix given by Eq. 7. The uncertainties in the source coefficients ΔS, can be obtained from the square root of the diagonal elements of the covariance matrix of the source

$$\Delta^2 S = \left(K^T \left(\Delta^2 C(q) \right)^{-1} K \right)^{-1}.$$

We have used the above procedure to image a wide array of correlation functions for several centralities, particle charge (π^+, π^-), k_T etc. A representative set of these results are presented below. It is important to note here that the imaging analysis reproduces the whole shape of the correlation function. Consequently, the extracted sources provide a measure of the entire information content that can be obtained from the correlation functions.

7.1. Extracting Source images

The correlation functions obtained from the combined particle pairs detected in EMC-East, EMC-West and the TOF were used to extract source images. Imaging followed the procedure outlined earlier. A superposition of six spline polynomials of the 3rd order (cf. Eq. 5 was used for source decomposition.

7.1.1. $\pi^-\pi^-$ images for 0 < centrality < 30 %

Figs. 175, 176, 177, 178, 179, 180, 181 and 182 show measured and restored correlation functions (top panels) and the corresponding source images (bottom panels). The results shown are for negatively charged pions for $0 <$ centrality < 30 and several k_T selections. The source images show a prominent Gaussian peak centered at $r = 0$ fm and a broad shoulder which extends out to $r \sim 35$ fm. This pattern is characteristic of the short- and long-range contributions to the source image.

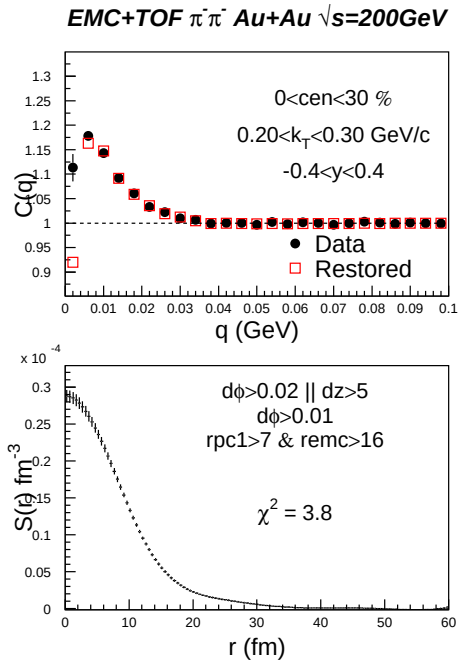

FIG. 175: *Experimental and restored correlation functions (top panel), and source image (bottom panel) for negatively charged pion pairs detected in the combined acceptance of the EMC and TOF. Results are shown for* $0 <$ *centrality* < 30 *and* $0.2 < k_T < 0.3$ *GeV/c.*

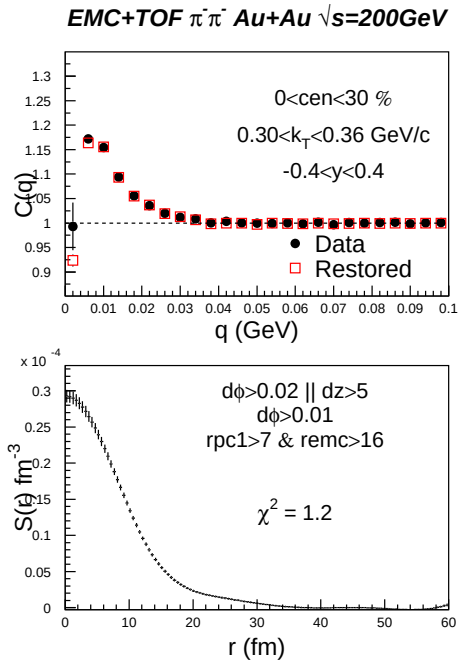

FIG. 176: *Experimental and restored correlation functions (top panel), and source image (bottom panel) for negatively charged pion pairs detected in the combined acceptance of the EMC and TOF. Results are shown for* $0 <$ *centrality* < 30 *and* $0.3 < k_T < 0.36$ *GeV/c.*

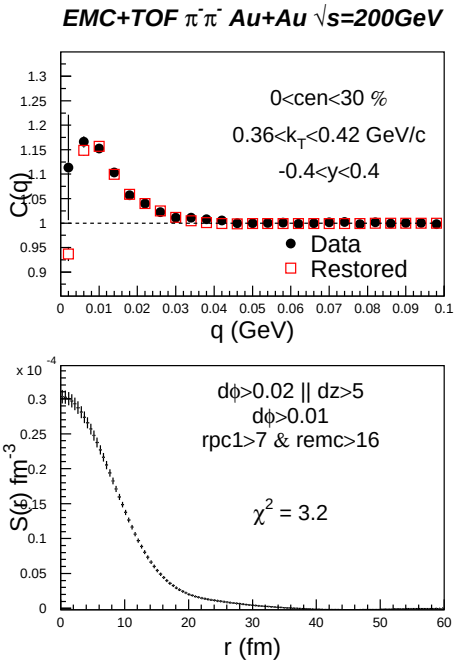

FIG. 177: *Experimental and restored correlation functions (top panel), and source image (bottom panel) for negatively charged pion pairs detected in the combined acceptance of the EMC and TOF. Results are shown for* $0 <$ *centrality* < 30 *and* $0.36 < k_T < 0.42$ *GeV/c.*

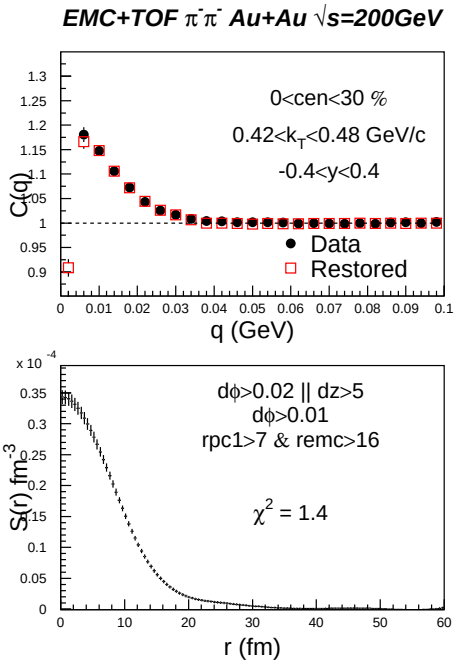

FIG. 178: *Experimental and restored correlation functions (top panel), and source image (bottom panel) for negatively charged pion pairs detected in the combined acceptance of the EMC and TOF. Results are shown for* $0 <$ *centrality* < 30 *and* $0.42 < k_T < 0.48$ *GeV/c.*

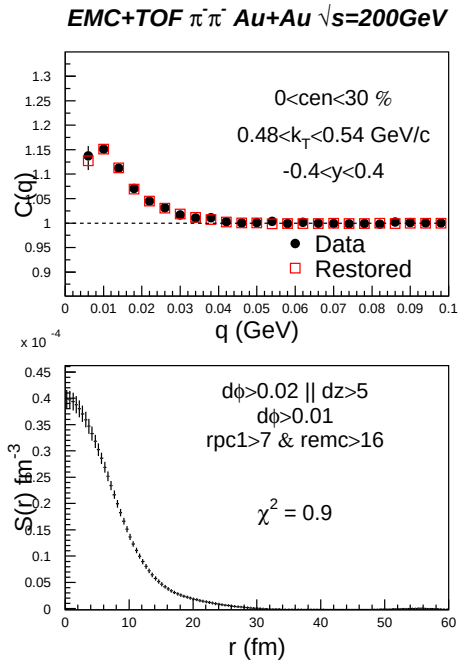

FIG. 179: *Experimental and restored correlation functions (top panel), and source image (bottom panel) for negatively charged pion pairs detected in the combined acceptance of the EMC and TOF. Results are shown for* $0 <$ *centrality* < 30 *and* $0.48 < k_T < 0.54$ *GeV/c.*

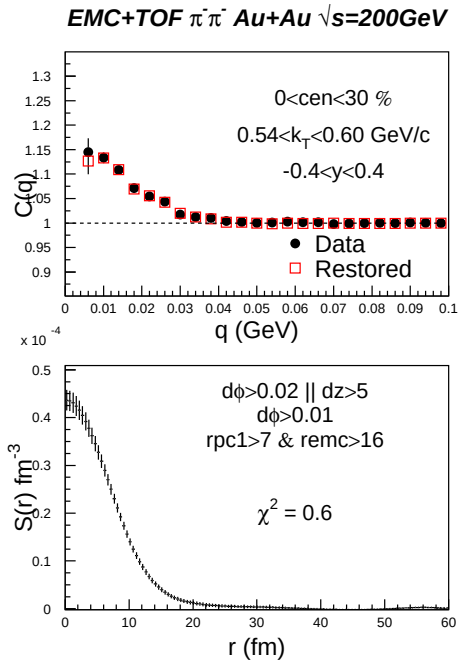

FIG. 180: *Experimental and restored correlation functions (top panel), and source image (bottom panel) for negatively charged pion pairs detected in the combined acceptance of the EMC and TOF. Results are shown for* $0 <$ *centrality* < 30 *and* $0.54 < k_T < 0.60$ *GeV/c.*

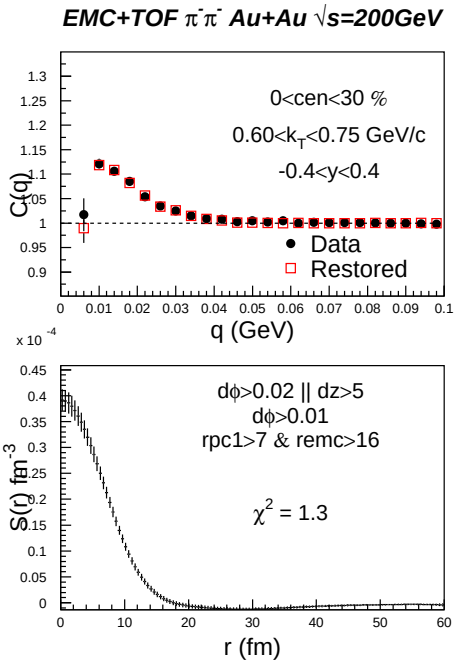

FIG. 181: *Experimental and restored correlation functions (top panel), and source image (bottom panel) for negatively charged pion pairs detected in the combined acceptance of the EMC and TOF. Results are shown for* $0 <$ *centrality* < 30 *and* $0.60 < k_T < 0.75$ *GeV/c.*

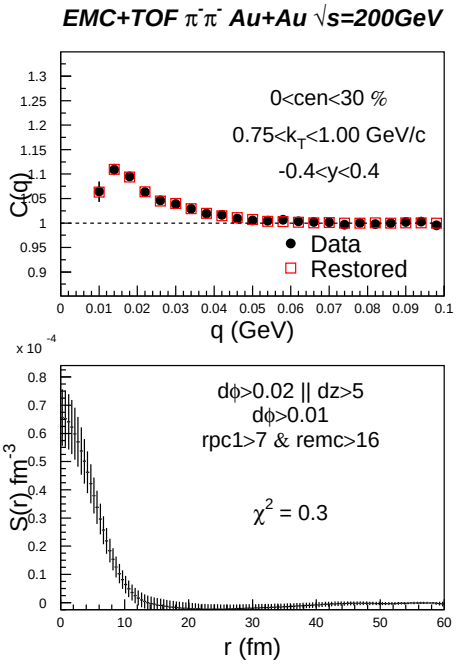

FIG. 182: *Experimental and restored correlation functions (top panel), and source image (bottom panel) for negatively charged pion pairs detected in the combined acceptance of the EMC and TOF. Results are shown for* $0 <$ *centrality* < 30 *and* $0.75 < k_T < 1.0$ *GeV/c.*

7.1.2. $\pi^+\pi^+$ images for $0 <$ centrality < 30 %

Figs. 183, 184, 185, 186, 187, 188, 189 and 190 show measured and restored correlation functions (top panels) and the corresponding source images (bottom panels). Results are shown for positively charged pions for $0 <$ centrality < 30 and several k_T selections. As was the case for negatively charged pions, these source images show patterns which are characteristic of the short- and long-range contributions to the source image.

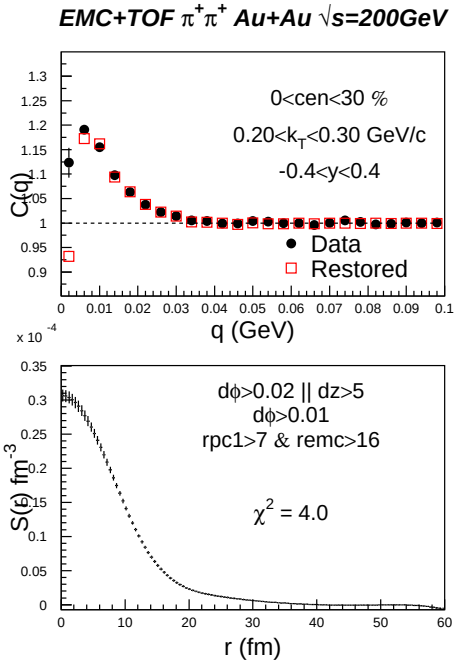

FIG. 183: *Experimental and restored correlation functions (top panel), and source image (bottom panel) for positively charged pion pairs detected in the combined acceptance of the EMC and TOF. Results are shown for* $0 <$ *centrality* < 30 *and* $0.2 < k_T < 0.3$ *GeV/c.*

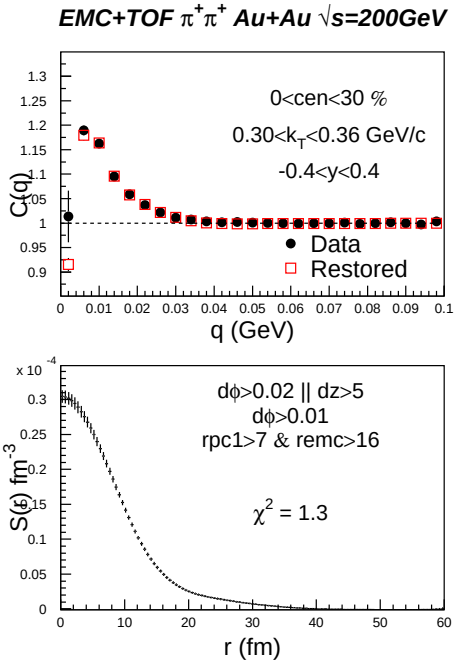

FIG. 184: *Experimental and restored correlation functions (top panel), and source image (bottom panel) for positively charged pion pairs detected in the combined acceptance of the EMC and TOF. Results are shown for* $0 <$ *centrality* < 30 *and* $0.3 < k_T < 0.36$ *GeV/c.*

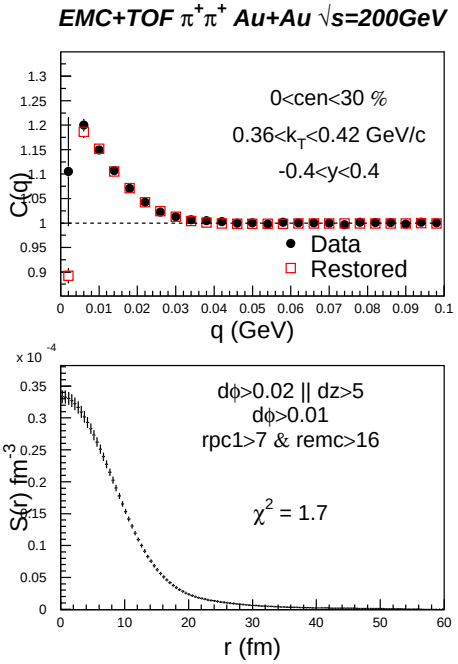

FIG. 185: *Experimental and restored correlation functions (top panel), and source image (bottom panel) for positively charged pion pairs detected in the combined acceptance of the EMC and TOF. Results are shown for* $0 <$ *centrality* < 30 *and* $0.36 < k_T < 0.42$ *GeV/c.*

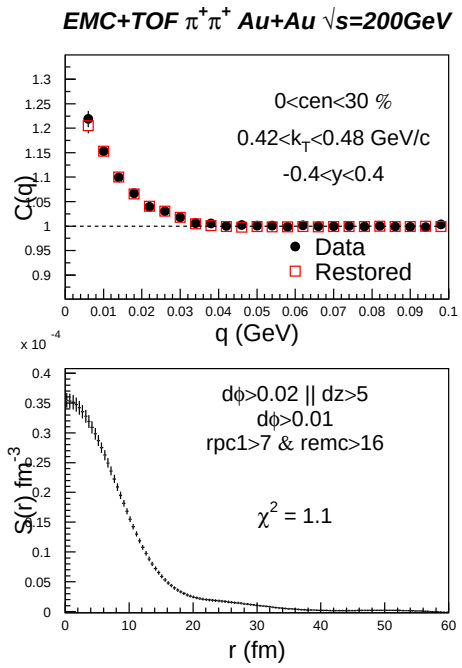

FIG. 186: *Experimental and restored correlation functions (top panel), and source image (bottom panel) for positively charged pion pairs detected in the combined acceptance of the EMC and TOF. Results are shown for* $0 <$ *centrality* < 30 *and* $0.42 < k_T < 0.48$ *GeV/c.*

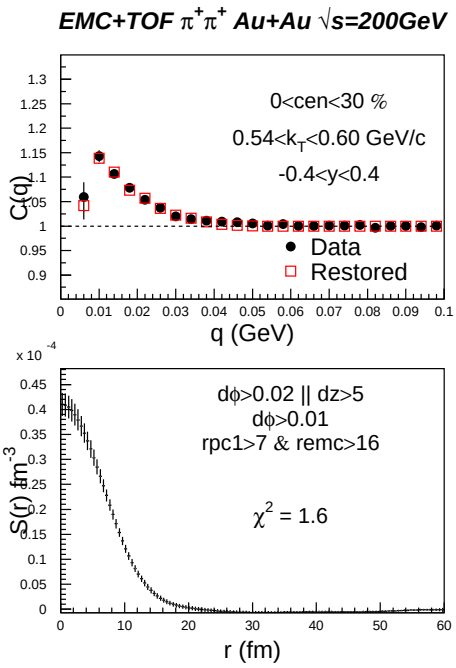

FIG. 188: *Experimental and restored correlation functions (top panel), and source image (bottom panel) for positively charged pion pairs detected in the combined acceptance of the EMC and TOF. Results are shown for* $0 <$ *centrality* < 30 *and* $0.54 < k_T < 0.60$ *GeV/c.*

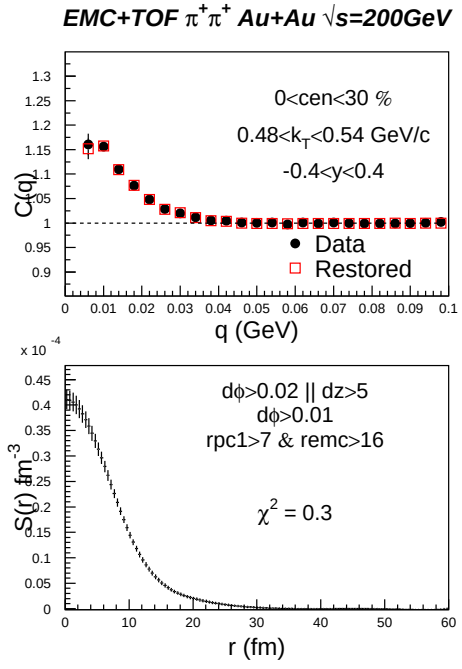

FIG. 187: *Experimental and restored correlation functions (top panel), and source image (bottom panel) for positively charged pion pairs detected in the combined acceptance of the EMC and TOF. Results are shown for* $0 <$ *centrality* < 30 *and* $0.48 < k_T < 0.54$ *GeV/c.*

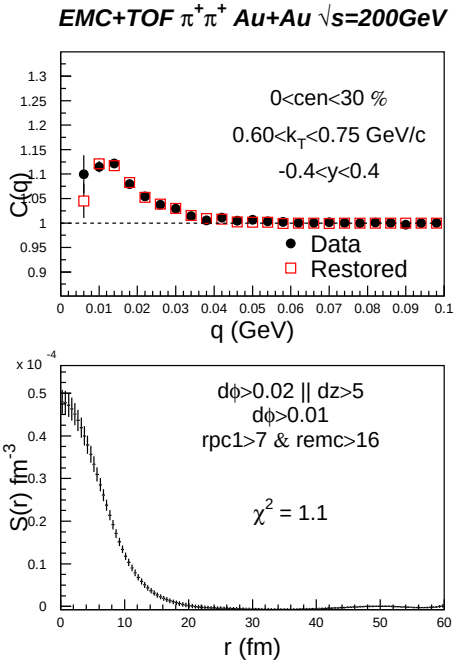

FIG. 189: *Experimental and restored correlation functions (top panel), and source image (bottom panel) for positively charged pion pairs detected in the combined acceptance of the EMC and TOF. Results are shown for* $0 <$ *centrality* < 30 *and* $0.60 < k_T < 0.75$ *GeV/c.*

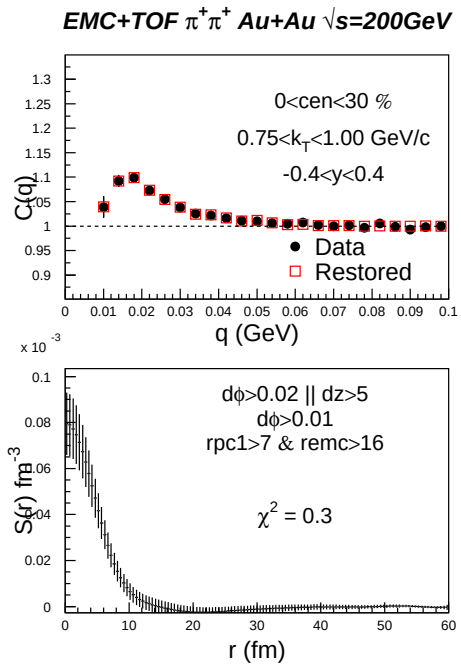

FIG. 190: *Experimental and restored correlation functions (top panel), and source image (bottom panel) for positively charged pion pairs detected in the combined acceptance of the EMC and TOF. Results are shown for* $0 <$ *centrality* < 30 *and* $0.75 < k_T < 1.0$ *GeV/c.*

7.2. Extraction of source image parameters

In the previous subsections it was shown that the source images for both negative and positively charged pions exhibit patterns which are characteristic of short- and long-range contributions to the source image. In order to quantify these contributions, the source images were fit with the following fit function:

$$S(r) = \frac{\lambda_{Gaus} e^{-\frac{r^2}{4R^2_{Gaus}}}}{\left(2\sqrt{\pi}R_{gaus}\right)^3} + \frac{\lambda_{\rm exp}}{N(\beta, R_{\rm exp})} e^{-\sqrt{\frac{r^2+\beta^2}{R_{\rm exp}}}},$$

$$N(\beta, R_{\rm exp}) = 4\pi\beta^3 \left(K_0(z) + \frac{2K_1(z)}{z^2}\right),$$

$$\beta = 2\frac{R^2_{Gaus}}{R_{\rm exp}},\ z = \frac{\beta}{R_{\rm exp}}.$$

Here, R_{Gaus} and λ_{Gaus} are the invariant radius and the fraction of particle pairs which contribute to short-range source. R_{exp} and λ_{exp} are the invariant radius and the fraction of particle pairs which contribute to the long-range source. K_0 and K_1 are Bessel functions.

7.2.1. Source image parameters for $\pi^+\pi^+$

Figs. 191, 192, 193, 194, 195, 196, 197 and 198 show $\pi^+\pi^+$ source images obtained for several k_T cuts and $0 <$ centrality < 30. In each figure, the long-range (exp) and short-range (Gauss) contributions to the source image which result from the fit are shown. They indicate significant contributions from both sources at low k_T. However, as $k_T$is increased, contributions from the long-range source become increasingly *unimportant* .

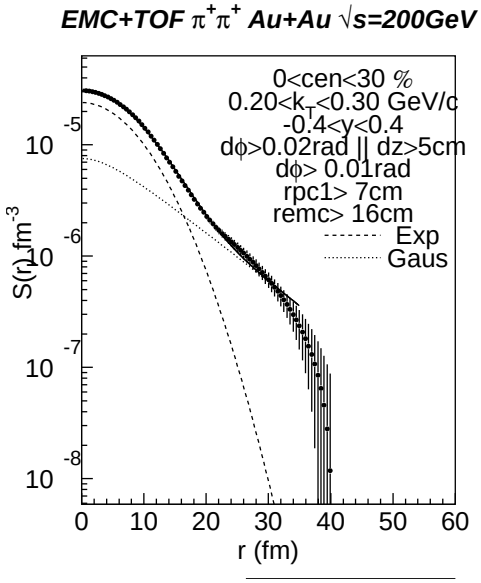

FIG. 191: *Source image for positively charged pion pairs detected in the combined acceptance of the EMC and TOF. The short- (Gauss) and long-range (exp) contributions to the source image are as indicated. Results are shown for* $0 <$ *centrality* < 30 *and* $0.2 < k_T < 0.3$ *GeV/c.*

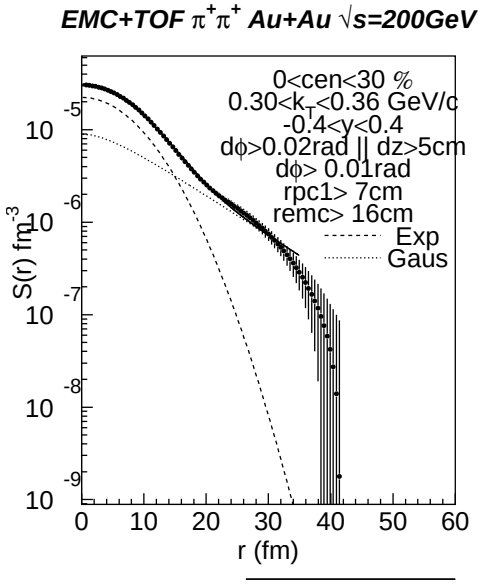

FIG. 192: *Source image for positively charged pion pairs detected in the combined acceptance of the EMC and TOF. The short- (Gauss) and long-range (exp) contributions to the source image are as indicated. Results are shown for* $0 <$ *centrality* < 30 *and* $0.3 < k_T < 0.36$ *GeV/c.*

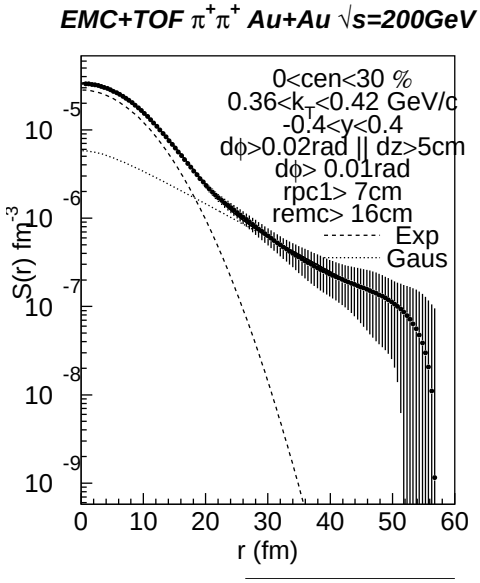

FIG. 193: *Source image for positively charged pion pairs detected in the combined acceptance of the EMC and TOF. The short- (Gauss) and long-range (exp) contributions to the source image are as indicated. Results are shown for* $0 <$ *centrality* < 30 *and* $0.36 < k_T < 0.42$ *GeV/c.*

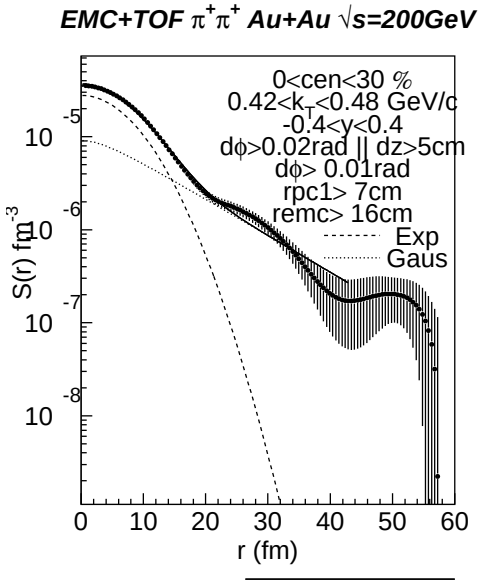

FIG. 194: *Source image for positively charged pion pairs detected in the combined acceptance of the EMC and TOF. The short- (Gauss) and long-range (exp) contributions to the source image are as indicated. Results are shown for* $0 <$ *centrality* < 30 *and* $0.42 < k_T < 0.48$ *GeV/c.*

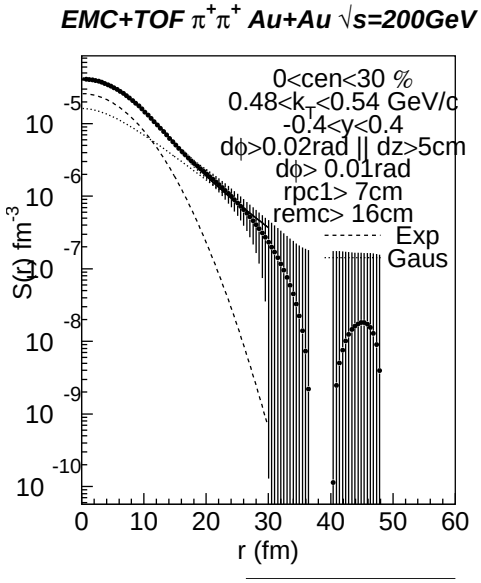

FIG. 195: *Source image for positively charged pion pairs detected in the combined acceptance of the EMC and TOF. The short- (Gauss) and long-range (exp) contributions to the source image are as indicated. Results are shown for* $0 <$ *centrality* < 30 *and* $0.48 < k_T < 0.54$ *GeV/c.*

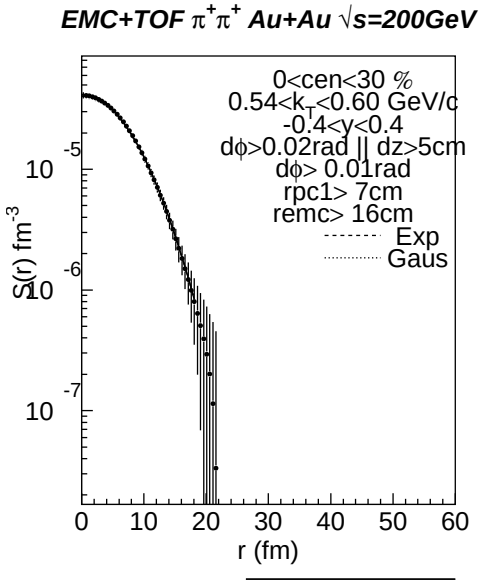

FIG. 196: *Source image for positively charged pion pairs detected in the combined acceptance of the EMC and TOF. The short- (Gauss) and long-range (exp) contributions to the source image are as indicated. Results are shown for* $0 <$ *centrality* < 30 *and* $0.54 < k_T < 0.60$ *GeV/c.*

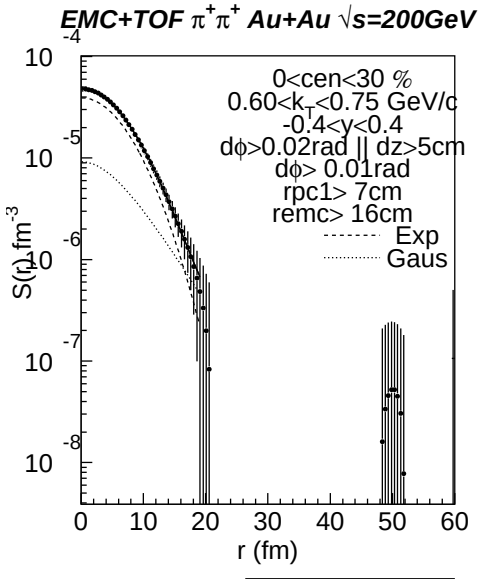

FIG. 197: *Source image for positively charged pion pairs detected in the combined acceptance of the EMC and TOF. The short- (Gauss) and long-range (exp) contributions to the source image are as indicated. Results are shown for* $0 <$ *centrality* < 30 *and* $0.60 < k_T < 0.75$ *GeV/c.*

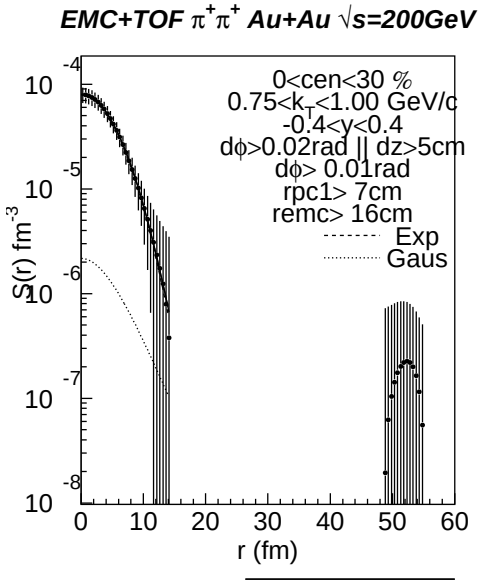

FIG. 198: *Source image for positively charged pion pairs detected in the combined acceptance of the EMC and TOF. The short- (Gauss) and long-range (exp) contributions to the source image are as indicated. Results are shown for* $0 <$ *centrality* < 30 *and* $0.75 < k_T < 1.0$ *GeV/c.*

7.2.2. Source image parameters for $\pi^-\pi^-$

Figs. 199, 200, 201, 202, 203, 204, 205 and 206 show $\pi^-\pi^-$ source images obtained for several k_T cuts and $0 <$ centrality < 30. In these figures, the long-range (exp) and short-range (Gauss) contributions to the source image which result from the fits are also shown. As was the case for positive pions, these source images indicate significant long- and short-range contributions at low k_T. The long-range source become increasingly *unimportant* as k_T is increased..

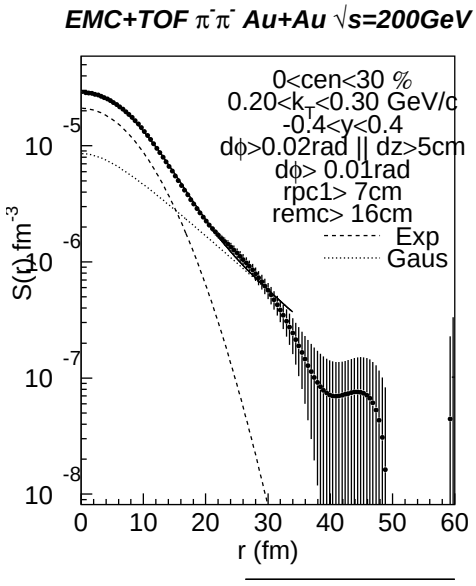

FIG. 199: *Source image for negatively charged pion pairs detected in the combined acceptance of the EMC and TOF. The short- (Gauss) and long-range (exp) contributions to the source image are as indicated. Results are shown for* $0 <$ *centrality* < 30 *and* $0.2 < k_T < 0.3$ *GeV/c.*

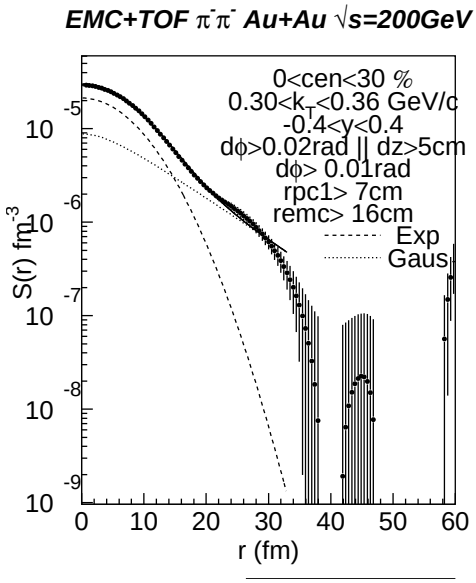

FIG. 200: *Source image for negatively charged pion pairs detected in the combined acceptance of the EMC and TOF. The short- (Gauss) and long-range (exp) contributions to the source image are as indicated. Results are shown for* $0 <$ *centrality* < 30 *and* $0.3 < k_T < 0.36$ *GeV/c.*

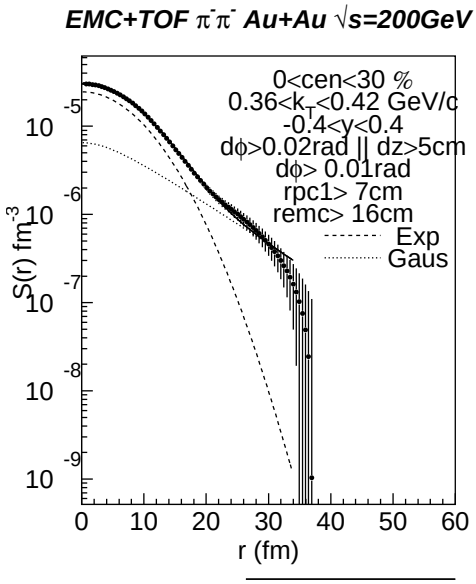

FIG. 201: *Source image for negatively charged pion pairs detected in the combined acceptance of the EMC and TOF. The short- (Gauss) and long-range (exp) contributions to the source image are as indicated. Results are shown for* $0 <$ *centrality* < 30 *and* $0.36 < k_T < 0.42$ *GeV/c.*

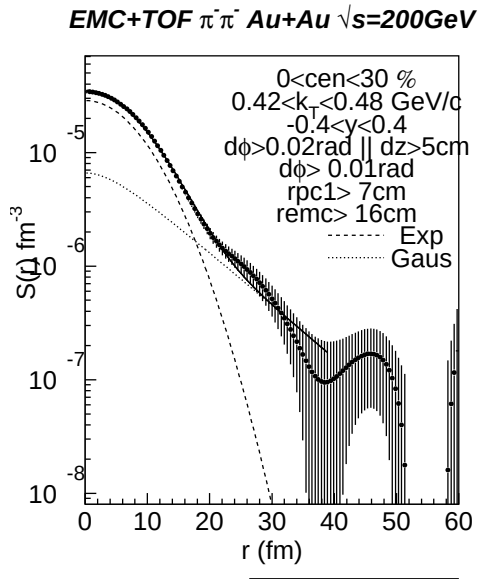

FIG. 202: *Source image for negatively charged pion pairs detected in the combined acceptance of the EMC and TOF. The short- (Gauss) and long-range (exp) contributions to the source image are as indicated. Results are shown for* $0 <$ *centrality* < 30 *and* $0.42 < k_T < 0.48$ *GeV/c.*

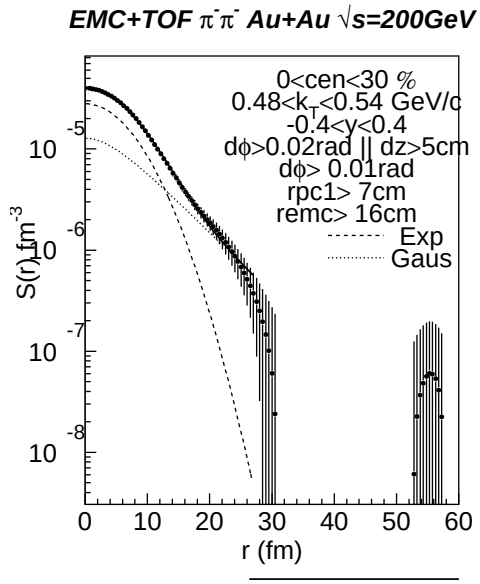

FIG. 203: *Source image for negatively charged pion pairs detected in the combined acceptance of the EMC and TOF. The short- (Gauss) and long-range (exp) contributions to the source image are as indicated. Results are shown for* $0 <$ *centrality* < 30 *and* $0.48 < k_T < 0.54$ *GeV/c.*

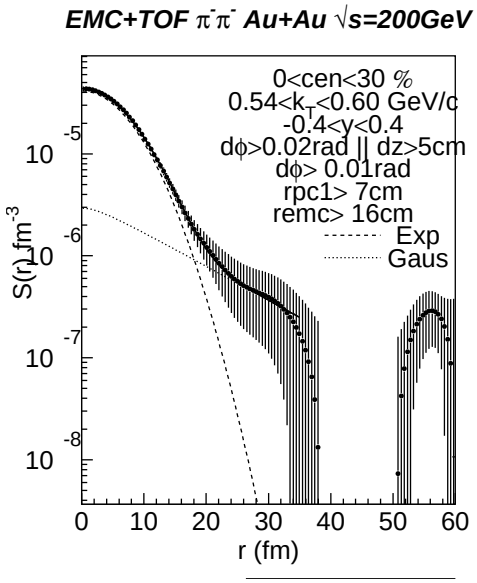

FIG. 204: *Source image for negatively charged pion pairs detected in the combined acceptance of the EMC and TOF. The short- (Gauss) and long-range (exp) contributions to the source image are as indicated. Results are shown for* $0 <$ *centrality* < 30 *and* $0.54 < k_T < 0.60$ *GeV/c.*

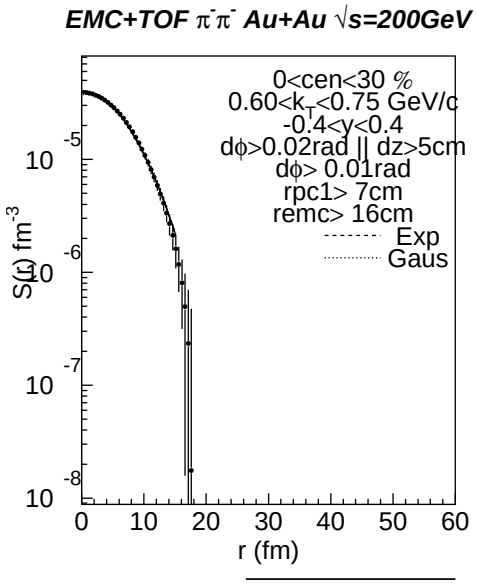

FIG. 205: *Source image for negatively charged pion pairs detected in the combined acceptance of the EMC and TOF. The short- (Gauss) and long-range (exp) contributions to the source image are as indicated. Results are shown for* $0 <$ *centrality* < 30 *and* $0.60 < k_T < 0.75$ *GeV/c.*

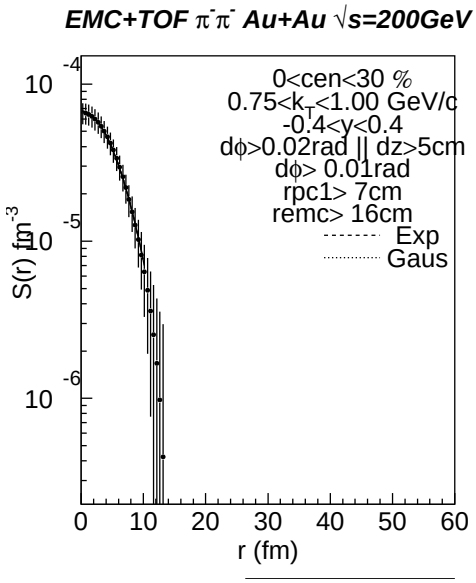

FIG. 206: *Source image for negatively charged pion pairs detected in the combined acceptance of the EMC and TOF. The short- (Gauss) and long-range (exp) contributions to the source image are as indicated. Results are shown for* $0 < centrality < 30$ *and* $0.75 < k_T < 1.0$ *GeV/c.*

7.3. m_T dependence of source image parameters for $\pi^-\pi^-$ and $\pi^+\pi^+$

7.3.1. $0 < Centrality < 30\%$

Figures 207, 208, 209 and 210 give a summary of the m_T dependence of the source parameters obtained via the fits to the source images presented earlier. Source parameters are compared for both positive and negative pions for the selection $0 <$ centrality < 30. They indicate rather good agreement between the source parameters for positive and negative pions. Fig. 207 indicate R_{Gauss} values of ~ 5.5 fm at low m_T for the short-range source. As m_T is increased, the radii for this source decreases to ~ 3 fm for $m_T \sim 0.85$ GeV. Fig. 208 shows much larger ($\sim 2X$) radii R_{exp}, for the long-range source. In addition, one can observe that the m_T dependence of this source is different from that for the short-range source. Here, it should be noted that there is very little if any contribution from the long-range source for $m_T \gtrsim 0.5$ GeV (see below). This being the case, R_{exp} values for $m_T \gtrsim 0.5$ GeV should be ignored.

Figs. 209 and 210 show the pair fractions for the short- (λ_{Gauss}) and long-range (λ_{exp}) sources respectively. Fig. 210 shows a relatively flat m_T dependence albeit with large error bars. More importantly, this figure shows that the fraction of pairs which contribute to the long-range source for $m_T \gtrsim 0.5$ GeV, is essentially zero. The m_T dependence of λ_{Gauss} points to an initial increase followed by a precipitous decrease.

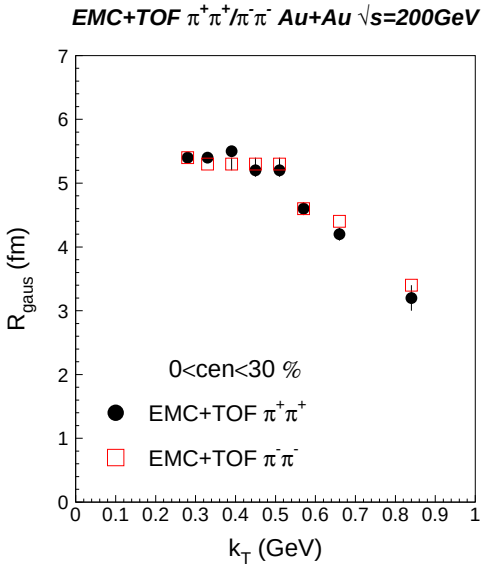

FIG. 207: *Short-range source radii R_{Gauss} vs m_T.*

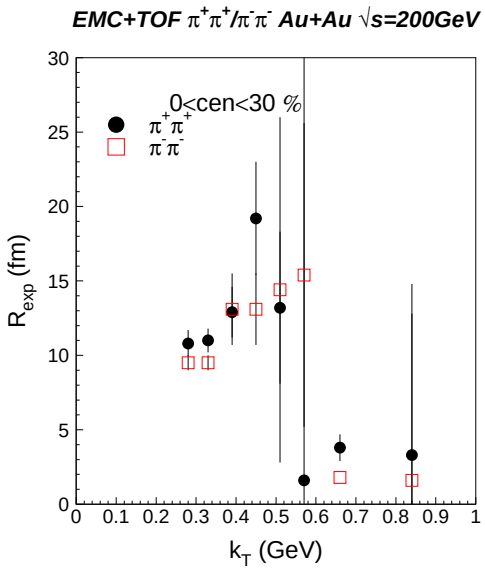

FIG. 208: *Long-range source radii R_{exp} vs m_T.*

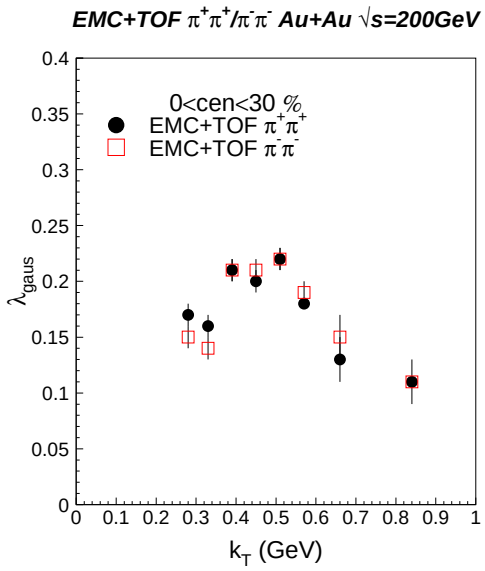

FIG. 209: *Short-range pair fraction λ_{Gauss} vs m_T.*

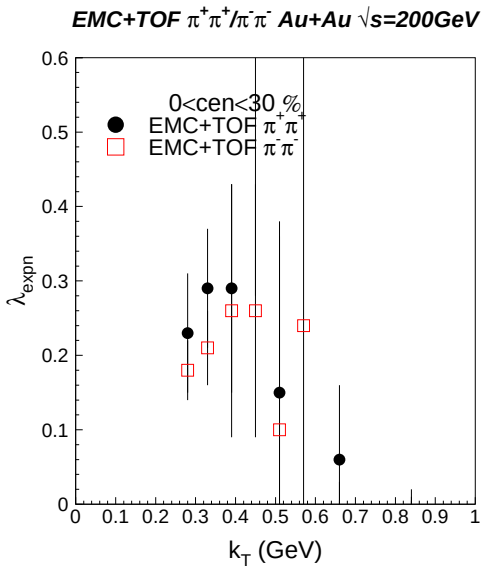

FIG. 210: *Long-range pair fraction λ_{exp} vs m_T.*

7.4. Centrality dependence of source image parameters for $\pi^-\pi^-$ and $\pi^+\pi^+$

7.4.1. Centrality dependence of short-range source

Figure 211, shows the centrality dependence of R_{Gauss} and λ_{Gauss}. The left and right panels show results for selections of $0.2 < k_T < 0.50$ and $0.5 < k_T < 1.0$ GeV/c respectively. The invariant radius is shown in the top panels and the pair fractions are shown in the bottom panels. The results indicate very good agreement between source parameters extracted for positive and negative pions. Both R_{Gauss} and λ_{Gauss} indicate a strong dependence on centrality.

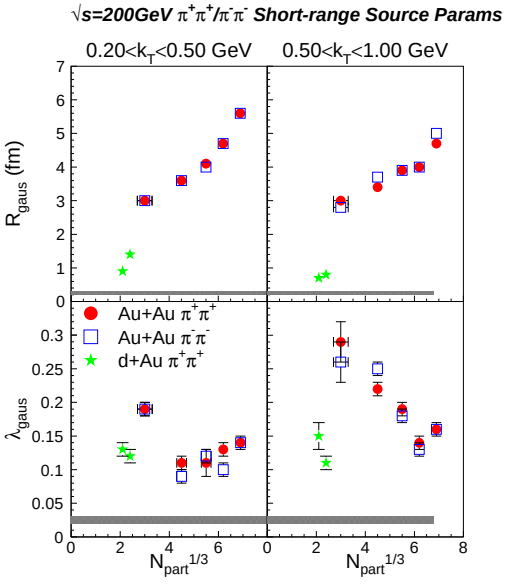

FIG. 211: *Short-range source parameters R_{Gauss}, λ_{Gauss} vs centrality. Results are shown for two separate k_T selections as indicated. The hatched marks indicate systematic errors for Au+Au. Systematic errors for d+Au are smaller.*

7.4.2. Centrality dependence of Long-range source

Figure 212 compares R_{inv} and λ values for the long- and short range sources for the selection $0.2 < k_T < 0.5$. The top panels show the centrality dependence of R_{Gauss} and R_{exp}. The bottom panels show results for λ_{Gauss} and λ_{exp}. The comparison indicates much larger R_{inv} values for the long-range source. However, this source also has a relatively strong dependence on centrality. The bottom right hand panel also points to the fact that the pair fractions associated with the long-range source are comparable or larger than the ones associated with the short-range s source.

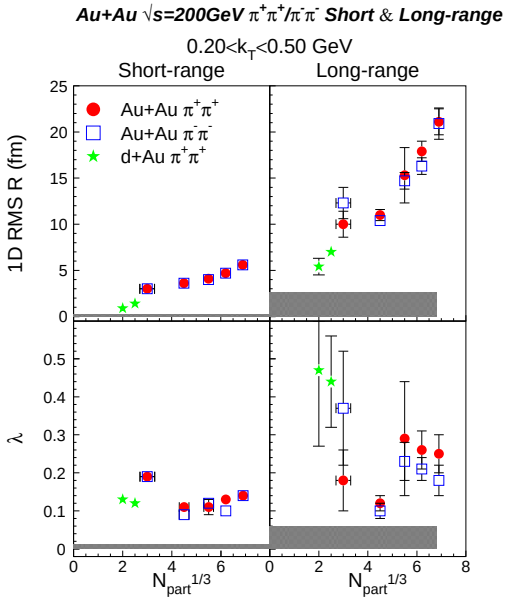

FIG. 212: *Comparison of short- and long-range source parameters for several centrality selections. Results are shown for the selection $0.2 < k_T < 0.$ GeV. The hatched marks indicate systematic errors for Au+Au. Systematic errors for d+Au are smaller.*

7.5. m_T dependence of source image parameters for $\pi^-\pi^-$ and $\pi^+\pi^+$

7.5.1. m_T dependence of the short-range source

Figure 213, shows the m_T dependence of R_{Gauss} and λ_{Gauss}. The left and right panels show results for selections of $0 < Centrality < 30\%$ and $30 < Centrality < 90\%$ respectively. The invariant radius is shown in the top panels and the pair fractions are shown in the bottom panels. The results indicate very good agreement between source parameters extracted for positive and negative pions. Both R_{Gauss} and λ_{Gauss} show a dependence on centrality.

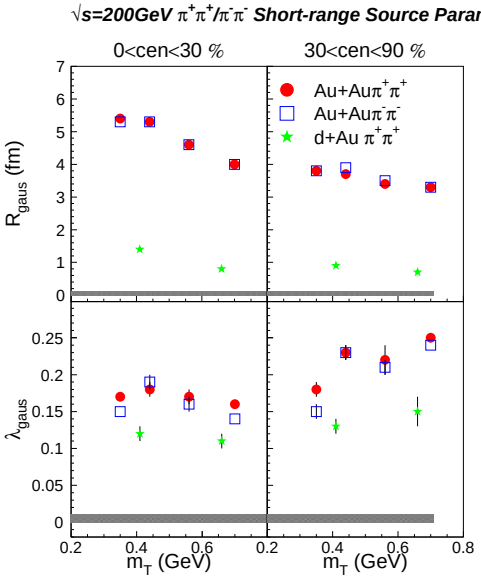

FIG. 213: *Short-range source parameters R_{Gauss}, λ_{Gauss} vs m_T. Results are shown for two separate centrality selections as indicated. The hatched marks indicate systematic errors for Au+Au. Systematic errors for d+Au are smaller.*

7.5.2. m_T dependence of the Long-range source

Figure 214 compares R_{inv} and λ values for the long- and short range sources for the selection $0 < Centrality < 30\%$. The top panels show the centrality dependence of R_{Gauss} and R_{exp}. The bottom panels show results for λ_{Gauss} and λ_{exp}. The comparison indicates much larger R_{inv} values for the long-range source. This source shows a weak m_T dependence, in contrast to the dependence shown by the short-range source. The bottom panels of the figure indicate similar pair fractions for the long- and short-range sources.

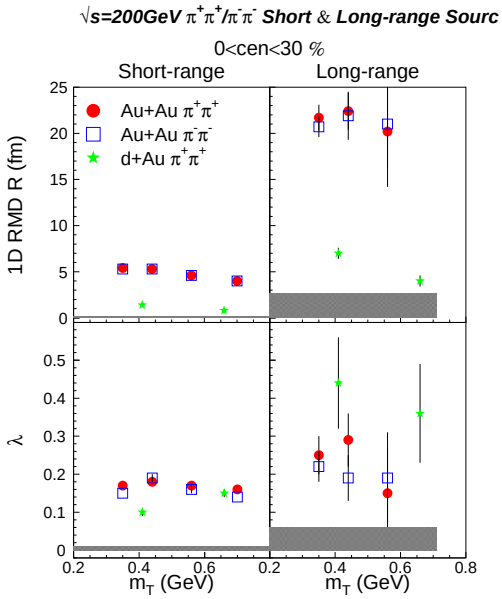

FIG. 214: *Comparison of short- and long-range source parameters for several m_T selections. Results are shown for the selection $0 < Centrality < 30\%$. The hatched marks indicate systematic errors for Au+Au. Systematic errors for d+Au are smaller.*

7.6. Influence of pair-cuts on the source functions

In Sec. 6 extensive comparisons were made between correlation functions obtained via systematic variation of the pair cuts used in our analysis. In this section we investigate the influence of similar pair-cut variations on the source images and the associated source parameters extracted from these images. We note here again that the cut variations used for these investigations have been significantly influenced by PWG discussions and PWG convener requests.

In brief, we find that "reasonable" systematic variation of the pair-cuts do not result in any significant change in the extracted source images and the associated source parameters. This is of course compatible with the observation that similar cuts did not result in any significant change in the generated correlation functions (see Sec. 6).

7.6.1. $\Delta\Phi_{DC}$ variation for $\Delta zed > 5cm$

Figs. 215, 216, 217, 218, 219, 220, 221 and 222 show $\pi^+\pi^+$ source images obtained for several k_T cuts and $0 <$ centrality < 30. The focus here is to show and compare the resulting source functions and source parameters when the $\Delta\phi_{DC}$ cut is increased from 0.01 to 0.02 rad for $\Delta zed >$ 5cm. For purposes of clarity, the long-range (exp) and short-range (Gauss) contributions to the source images are also shown. A quick comparison of these images with those presented in 7.1 (for standard cuts) indicate very little, if any, change in the source images obtained with this cut variation. Thus, it can be concluded that a more reasonable (smaller) variation of this cut would not result in a significantly different source images.

Figures 259, 260, 261 and 262 summarizes the comparison for the source parameters obtained with standard cuts versus that obtained with the cut variation described above. The good agreement between the results indicate that the cut variation does not lead to any significant change in the extracted source images.

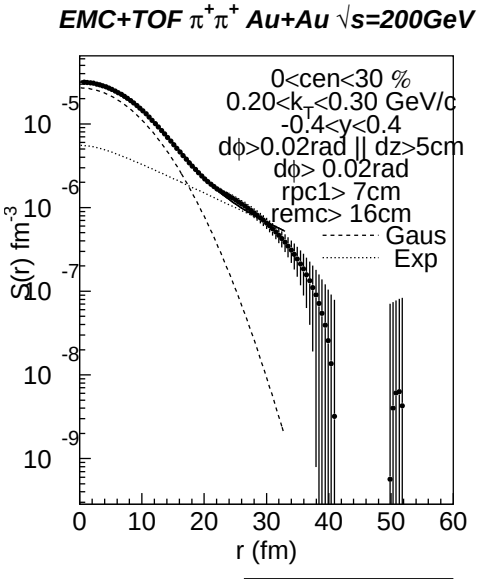

FIG. 215: *Source image for positively charged pion pairs detected in the combined acceptance of the EMC and TOF. The $\Delta\phi_{DC}$ cut is increased from 0.01 to 0.02 rad for $\Delta zed > 5cm$. The short- (Gauss) and long-range (exp) contributions to the source image are as indicated. Results are shown for $0 <$ centrality < 30 and $0.2 < k_T < 0.3$ GeV/c.*

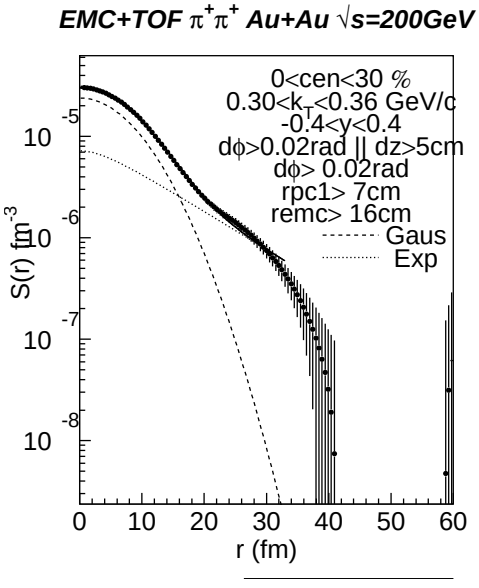

FIG. 216: *Source image for positively charged pion pairs detected in the combined acceptance of the EMC and TOF. The $\Delta\phi_{DC}$ cut is increased from 0.01 to 0.02 rad for $\Delta zed > 5cm$. The short- (Gauss) and long-range (exp) contributions to the source image are as indicated. Results are shown for $0 <$ centrality < 30 and $0.3 < k_T < 0.36$ GeV/c.*

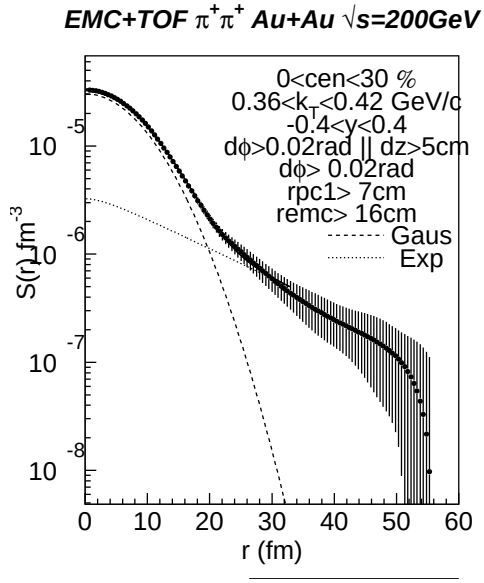

FIG. 217: *Source image for positively charged pion pairs detected in the combined acceptance of the EMC and TOF. The $\Delta\phi_{DC}$ cut is increased from 0.01 to 0.02 rad for $\Delta zed > 5cm$. The short- (Gauss) and long-range (exp) contributions to the source image are as indicated. Results are shown for $0 <$ centrality < 30 and $0.36 < k_T < 0.42$ GeV/c.*

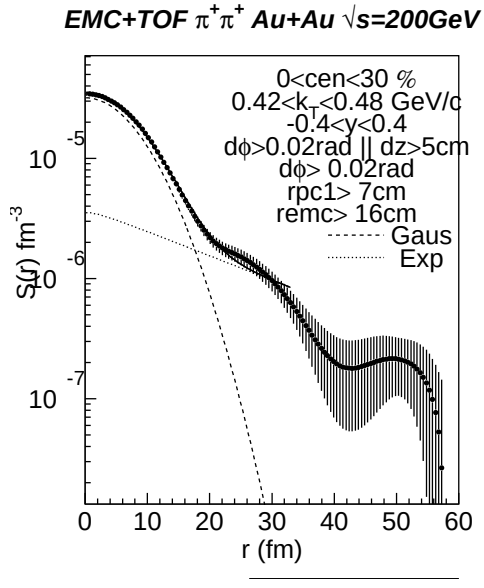

FIG. 218: *Source image for positively charged pion pairs detected in the combined acceptance of the EMC and TOF. The $\Delta\phi_{DC}$ cut is increased from 0.01 to 0.02 rad for $\Delta zed > 5cm$. The short- (Gauss) and long-range (exp) contributions to the source image are as indicated. Results are shown for $0 <$ centrality < 30 and $0.42 < k_T < 0.48$ GeV/c.*

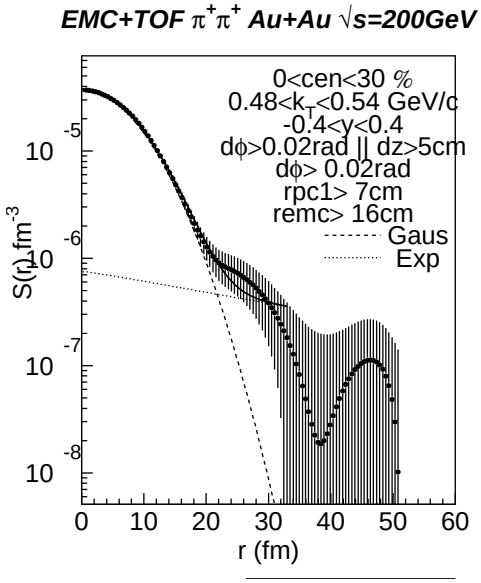

FIG. 219: *Source image for positively charged pion pairs detected in the combined acceptance of the EMC and TOF. The $\Delta\phi_{DC}$ cut is increased from 0.01 to 0.02 rad for $\Delta zed > 5cm$. The short- (Gauss) and long-range (exp) contributions to the source image are as indicated. Results are shown for $0 <$ centrality < 30 and $0.48 < k_T < 0.54$ GeV/c.*

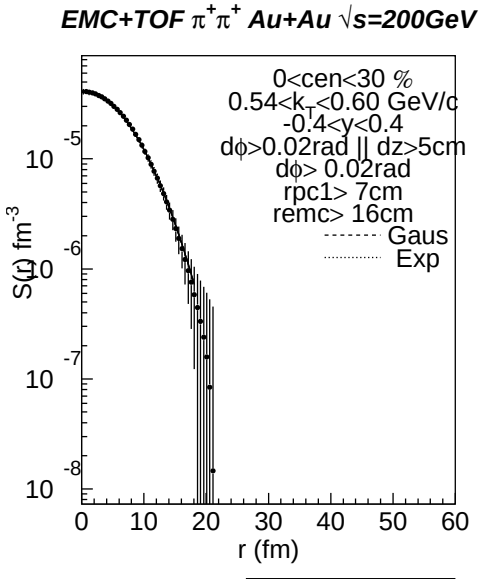

FIG. 220: *Source image for positively charged pion pairs detected in the combined acceptance of the EMC and TOF. The $\Delta\phi_{DC}$ cut is increased from 0.01 to 0.02 rad for $\Delta zed > 5cm$. The short- (Gauss) and long-range (exp) contributions to the source image are as indicated. Results are shown for $0 <$ centrality < 30 and $0.54 < k_T < 0.60$ GeV/c.*

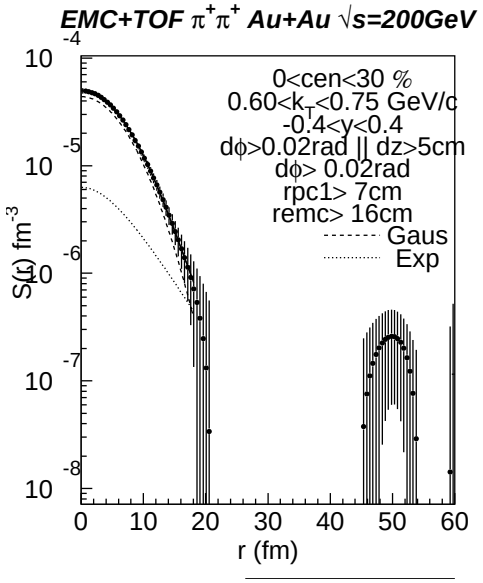

FIG. 221: *Source image for positively charged pion pairs detected in the combined acceptance of the EMC and TOF. The $\Delta\phi_{DC}$ cut is increased from 0.01 to 0.02 rad for $\Delta zed > 5cm$. The short- (Gauss) and long-range (exp) contributions to the source image are as indicated. Results are shown for $0 <$ centrality < 30 and $0.60 < k_T < 0.75$ GeV/c.*

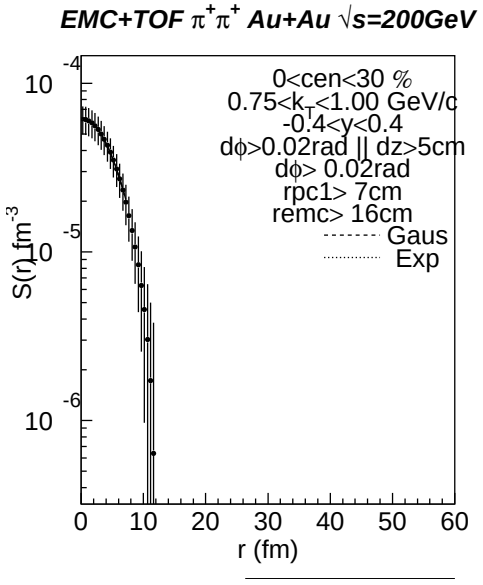

FIG. 222: *Source image for positively charged pion pairs detected in the combined acceptance of the EMC and TOF. The $\Delta\phi_{DC}$ cut is increased from 0.01 to 0.02 rad for $\Delta zed > 5cm$. The short- (Gauss) and long-range (exp) contributions to the source image are as indicated. Results are shown for $0 <$ centrality < 30 and $0.75 < k_T < 1.0$ GeV/c.*

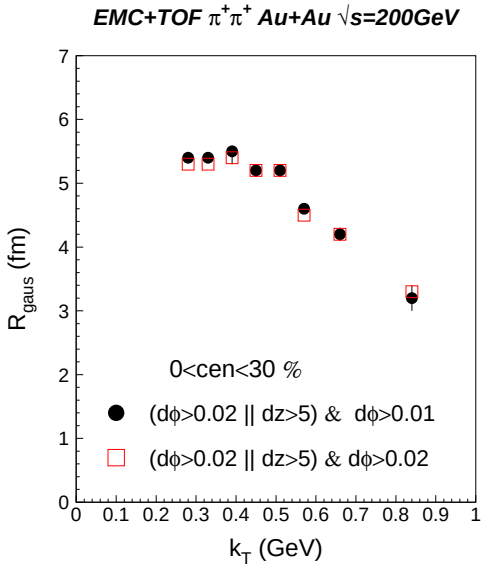

FIG. 223: *Short-range source radii R_{Gauss} vs m_T. Results are compared for standard cuts and a cut variation in which $\Delta\phi_{DC}$ cut is increased from 0.01 to 0.02 rad for $\Delta zed > 5cm$.*

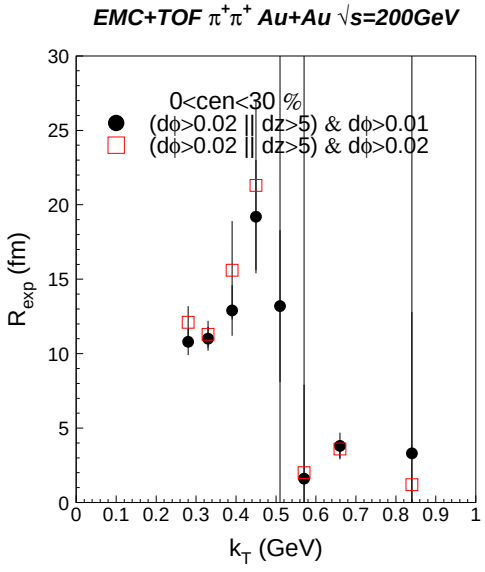

FIG. 224: *Long-range source radii R_{exp} vs m_T. Results are compared for standard cuts and a cut variation in which $\Delta\phi_{DC}$ cut is increased from 0.01 to 0.02 rad for $\Delta zed > 5cm$.*

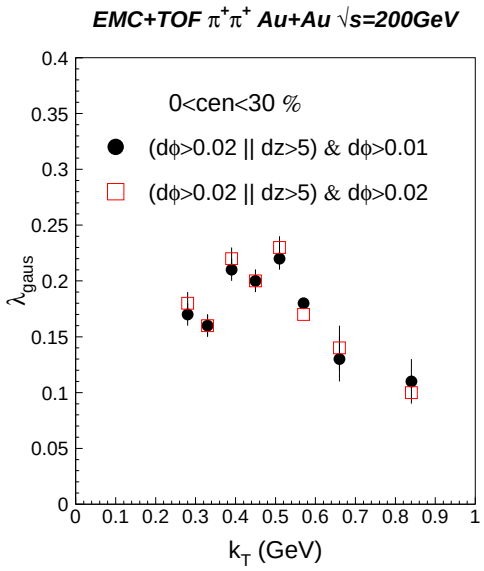

FIG. 225: *Short-range pair fraction λ_{Gauss} vs m_T. Results are compared for standard cuts and a cut variation in which $\Delta\phi_{DC}$ cut is increased from 0.01 to 0.02 rad for $\Delta zed > 5cm$.*

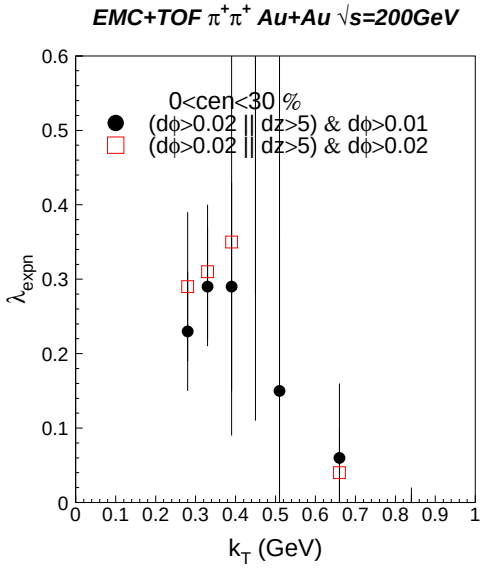

FIG. 226: *Long-range pair fraction λ_{exp} vs m_T. Results are compared for standard cuts and a cut variation in which $\Delta\phi_{DC}$ cut is increased from 0.01 to 0.02 rad for $\Delta zed > 5cm$.*

7.6.2. $\Delta\Phi_{DC}$ variation for $\Delta zed < 5cm$

Figs. 227, 228, 229, 230, 231, 232, 233 and 234 show $\pi^+\pi^+$ source images obtained for several k_T cuts and $0 <$ centrality < 30. The focus in this case is to show and compare the resulting source functions and source parameters when the $\Delta\phi_{DC}$ cut is increased from 0.02 to 0.03 rad for $\Delta zed <$ 5cm. For purposes of clarity, the long-range (exp) and short-range (Gauss) contributions to the source images are also shown. Here again, a quick comparison of these images with those presented in 7.1 (for standard cuts) indicate very little, if any, change in the source images obtained with this cut variation. Thus, it can be concluded that a more reasonable (smaller) variation of this cut would not result in significantly different source images.

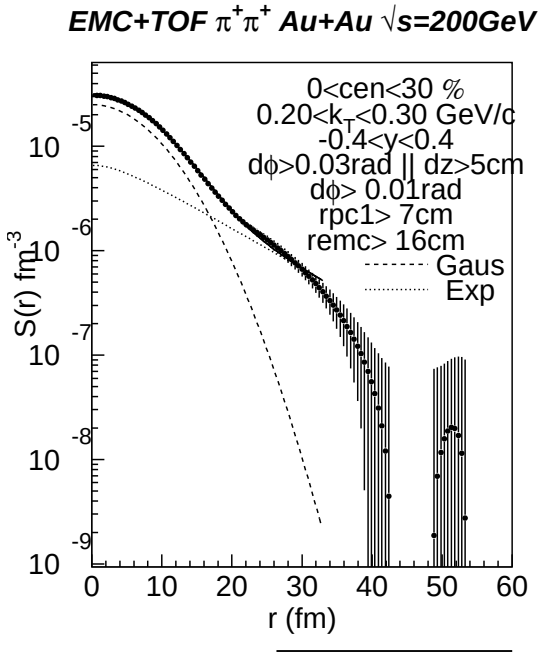

FIG. 227: *Source image for positively charged pion pairs detected in the combined acceptance of the EMC and TOF. The $\Delta\phi_{DC}$ cut is increased from 0.02 to 0.03 rad for $\Delta zed <$ 5cm. The short- (Gauss) and long-range (exp) contributions to the source image are as indicated. Results are shown for $0 <$ centrality < 30 and $0.2 < k_T < 0.3$ GeV/c.*

Figures 259, 260, 261 and 262 summarizes the comparison for the source parameters obtained with standard cuts versus that obtained with the cut variation described above. The good agreement between the results indicate that the cut variation does not lead to any significant change in the extracted source images.

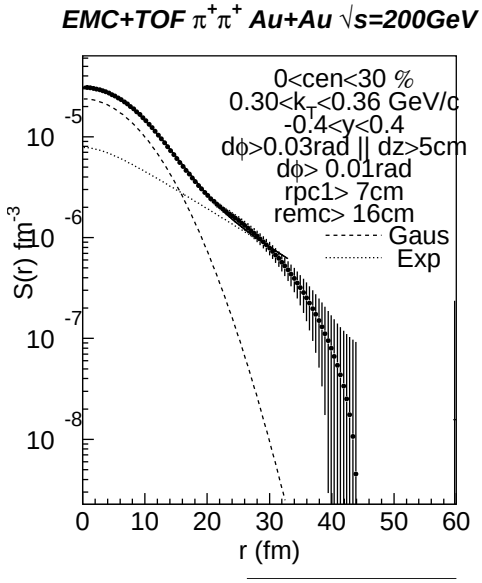

FIG. 228: *Source image for positively charged pion pairs detected in the combined acceptance of the EMC and TOF. The $\Delta\phi_{DC}$ cut is increased from 0.02 to 0.03 rad for $\Delta zed <$ 5cm. The short- (Gauss) and long-range (exp) contributions to the source image are as indicated. Results are shown for $0 <$ centrality < 30 and $0.3 < k_T < 0.36$ GeV/c.*

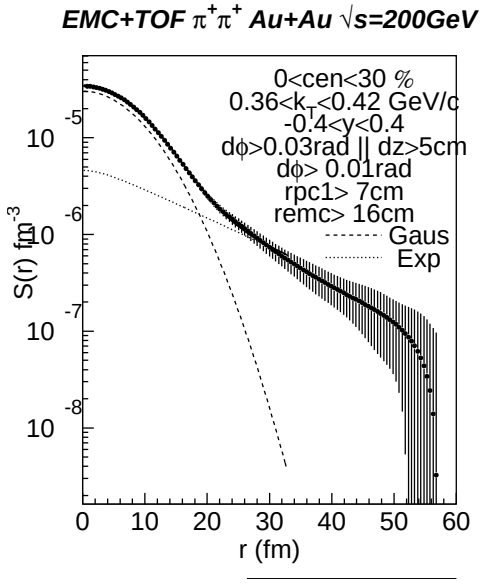

FIG. 229: *Source image for positively charged pion pairs detected in the combined acceptance of the EMC and TOF. The $\Delta\phi_{DC}$ cut is increased from 0.02 to 0.03 rad for $\Delta zed <$ 5cm. The short- (Gauss) and long-range (exp) contributions to the source image are as indicated. Results are shown for $0 <$ centrality < 30 and $0.36 < k_T < 0.42$ GeV/c.*

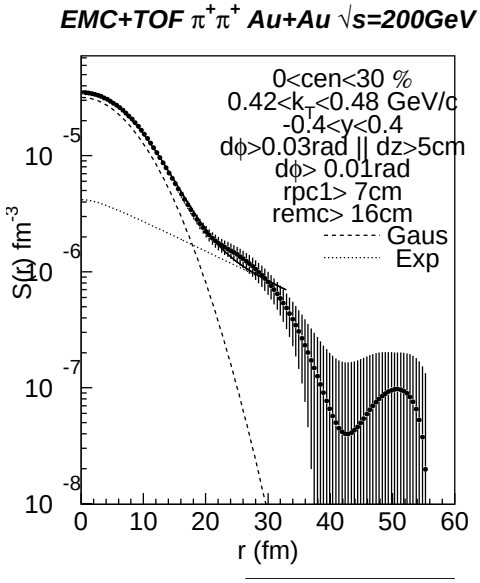

FIG. 230: *Source image for positively charged pion pairs detected in the combined acceptance of the EMC and TOF. The $\Delta\phi_{DC}$ cut is increased from 0.02 to 0.03 rad for $\Delta zed < 5cm$. The short- (Gauss) and long-range (exp) contributions to the source image are as indicated. Results are shown for $0 <$ centrality < 30 and $0.42 < k_T < 0.48$ GeV/c.*

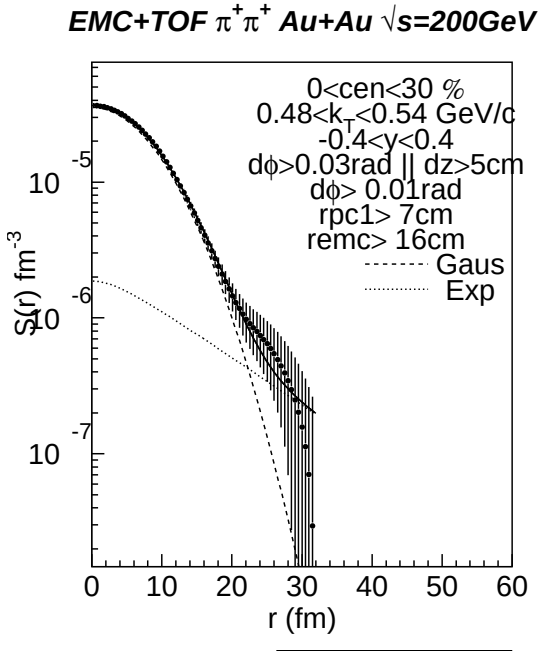

FIG. 231: *Source image for positively charged pion pairs detected in the combined acceptance of the EMC and TOF. The $\Delta\phi_{DC}$ cut is increased from 0.02 to 0.03 rad for $\Delta zed < 5cm$. The short- (Gauss) and long-range (exp) contributions to the source image are as indicated. Results are shown for $0 <$ centrality < 30 and $0.48 < k_T < 0.54$ GeV/c.*

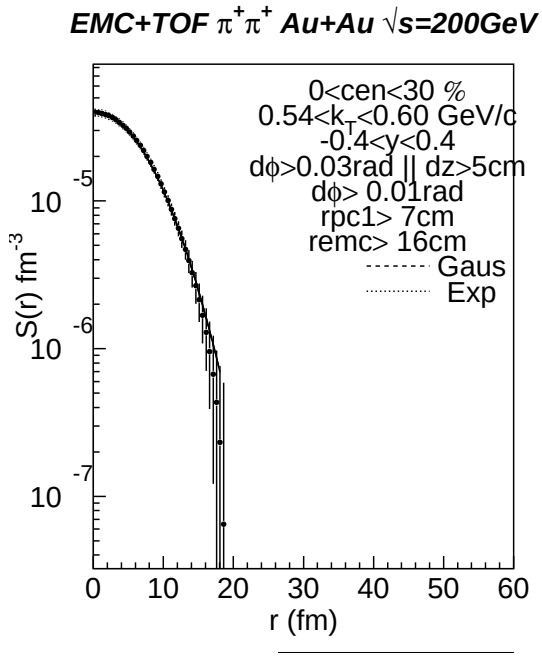

FIG. 232: *Source image for positively charged pion pairs detected in the combined acceptance of the EMC and TOF. The $\Delta\phi_{DC}$ cut is increased from 0.02 to 0.03 rad for $\Delta zed < 5cm$. The short- (Gauss) and long-range (exp) contributions to the source image are as indicated. Results are shown for $0 <$ centrality < 30 and $0.54 < k_T < 0.60$ GeV/c.*

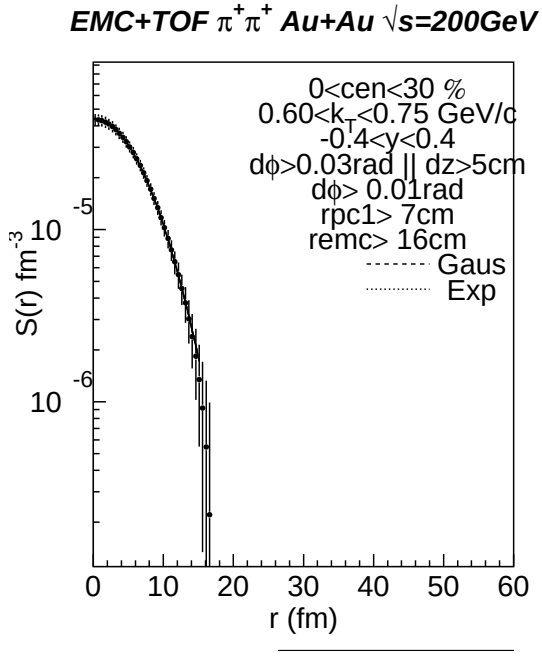

FIG. 233: *Source image for positively charged pion pairs detected in the combined acceptance of the EMC and TOF. The $\Delta\phi_{DC}$ cut is increased from 0.02 to 0.03 rad for $\Delta zed < 5cm$. The short- (Gauss) and long-range (exp) contributions to the source image are as indicated. Results are shown for $0 <$ centrality < 30 and $0.60 < k_T < 0.75$ GeV/c.*

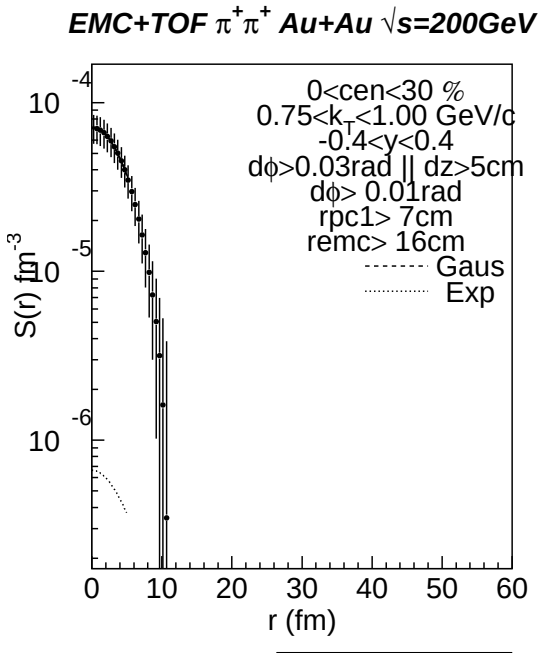

FIG. 234: *Source image for positively charged pion pairs detected in the combined acceptance of the EMC and TOF. The $\Delta\phi_{DC}$ cut is increased from 0.02 to 0.03 rad for $\Delta zed < 5cm$. The short- (Gauss) and long-range (exp) contributions to the source image are as indicated. Results are shown for $0 <$ centrality < 30 and $0.75 < k_T < 1.0$ GeV/c.*

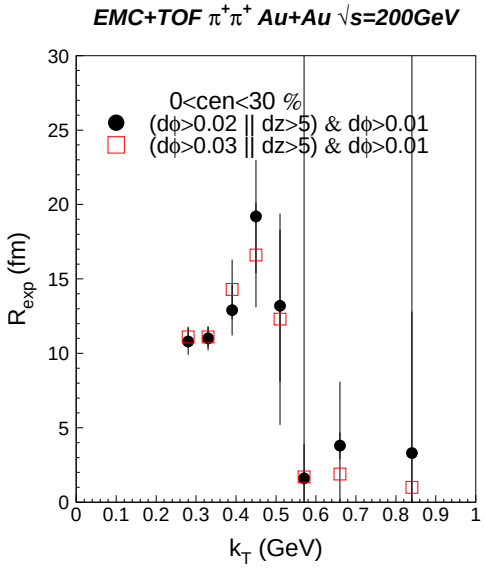

FIG. 236: *Long-range source radii R_{exp} vs m_T. Results are compared for standard cuts and a cut variation in which $\Delta\phi_{DC}$ cut is increased from 0.02 to 0.03 rad for $\Delta zed < 5cm$.*

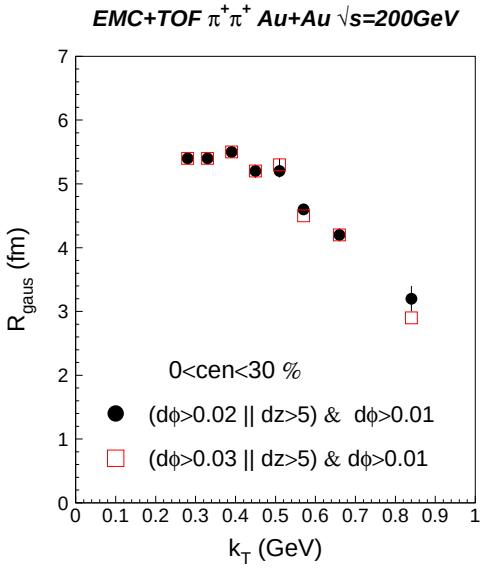

FIG. 235: *Short-range source radii R_{Gauss} vs m_T. Results are compared for standard cuts and a cut variation in which $\Delta\phi_{DC}$ cut is increased from 0.02 to 0.03 rad for $\Delta zed < 5cm$.*

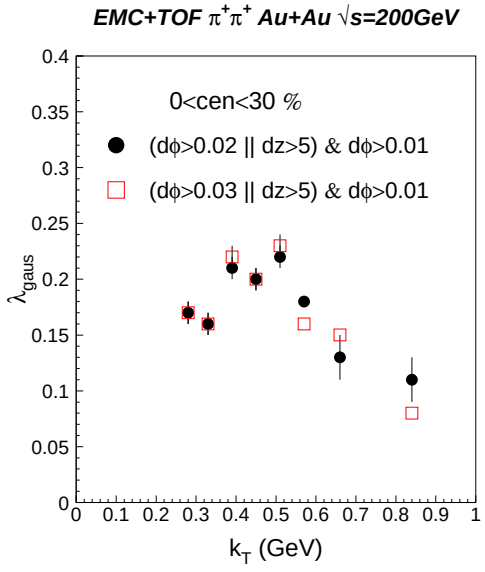

FIG. 237: *Short-range pair fraction λ_{Gauss} vs m_T. Results are compared for standard cuts and a cut variation in which $\Delta\phi_{DC}$ cut is increased from 0.02 to 0.03 rad for $\Delta zed < 5cm$.*

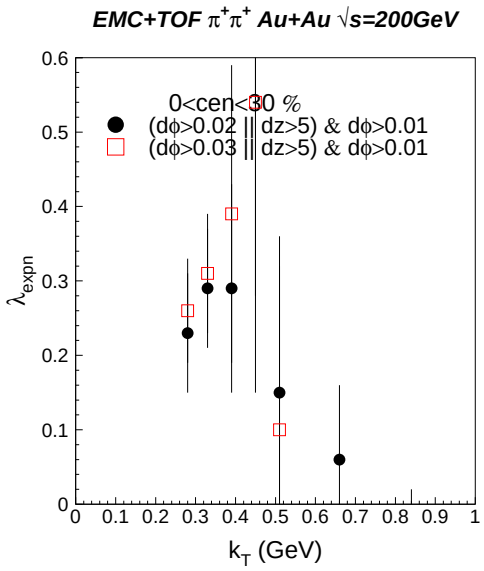

FIG. 238: *Long-range pair fraction λ_{exp} vs m_T. Results are compared for standard cuts and a cut variation in which $\Delta\phi_{DC}$ cut is increased from 0.02 to 0.03 rad for $\Delta zed < 5cm$.*

7.6.3. $\Delta\Phi_{DC}$ variation for $\Delta zed < 1cm$

Figs. 239, 240, 241, 242, 243, 244, 245 and 246 show $\pi^+\pi^+$ source images obtained for several k_T cuts and $0 <$ centrality < 30. The focus in this case is to show and compare the resulting source functions and source parameters when the $\Delta\phi_{DC}$ cut is increased from 0.02 to 0.06 rad for $\Delta zed <$ 1cm. For purposes of clarity, the long-range (exp) and short-range (Gauss) contributions to the source images are also shown. A quick comparison of these images with those presented in 7.1 (for standard cuts) indicate very little change in the source images obtained with this cut variation.

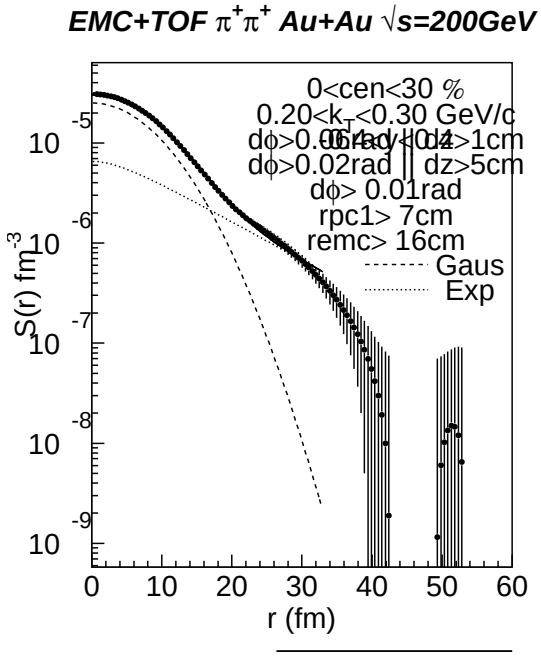

FIG. 239: *Source image for positively charged pion pairs detected in the combined acceptance of the EMC and TOF. The $\Delta\phi_{DC}$ cut is increased from 0.02 to 0.06 rad for $\Delta zed <$ 1cm. The short- (Gauss) and long-range (exp) contributions to the source image are as indicated. Results are shown for $0 <$ centrality < 30 and $0.2 < k_T < 0.3$ GeV/c.*

Figures 259, 260, 261 and 262 summarizes the comparison for the source parameters obtained with standard cuts versus that obtained with the cut variation described above. The good agreement between the results indicate that the cut variation does not lead to any significant change in the extracted source images.

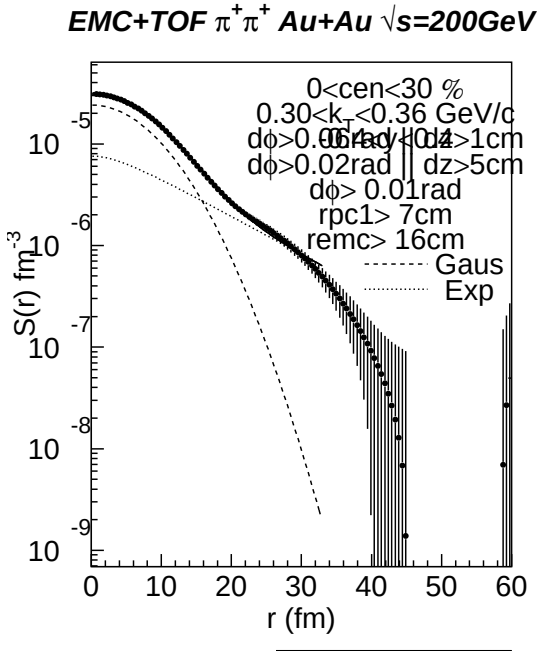

FIG. 240: *Source image for positively charged pion pairs detected in the combined acceptance of the EMC and TOF. The $\Delta\phi_{DC}$ cut is increased from 0.02 to 0.06 rad for $\Delta zed <$ 1cm. The short- (Gauss) and long-range (exp) contributions to the source image are as indicated. Results are shown for $0 <$ centrality < 30 and $0.3 < k_T < 0.36$ GeV/c.*

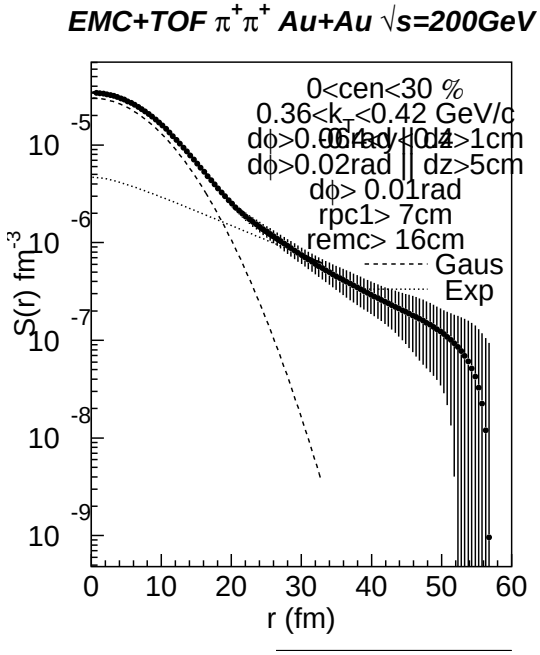

FIG. 241: *Source image for positively charged pion pairs detected in the combined acceptance of the EMC and TOF. The $\Delta\phi_{DC}$ cut is increased from 0.02 to 0.06 rad for $\Delta zed <$ 1cm. The short- (Gauss) and long-range (exp) contributions to the source image are as indicated. Results are shown for $0 <$ centrality < 30 and $0.36 < k_T < 0.42$ GeV/c.*

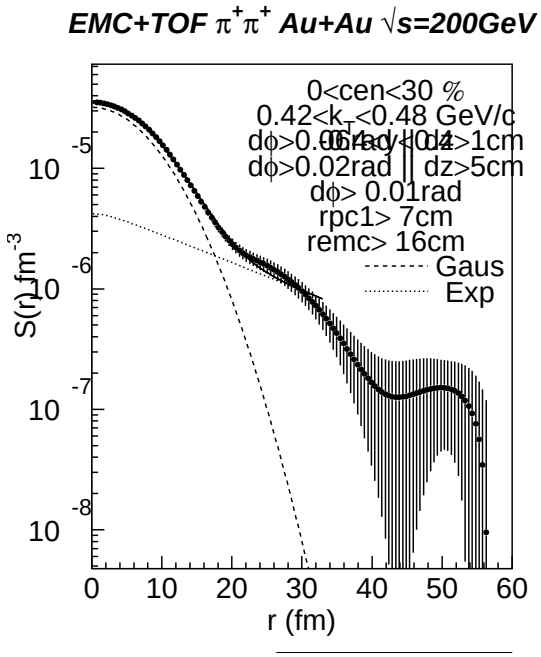

FIG. 242: *Source image for positively charged pion pairs detected in the combined acceptance of the EMC and TOF. The $\Delta\phi_{DC}$ cut is increased from 0.02 to 0.06 rad for $\Delta zed < 1cm$. The short- (Gauss) and long-range (exp) contributions to the source image are as indicated. Results are shown for $0 <$ centrality < 30 and $0.42 < k_T < 0.48$ GeV/c.*

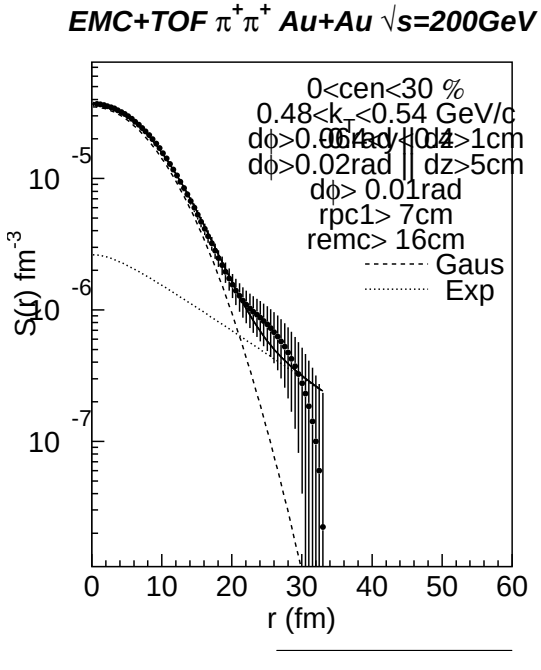

FIG. 243: *Source image for positively charged pion pairs detected in the combined acceptance of the EMC and TOF. The $\Delta\phi_{DC}$ cut is increased from 0.02 to 0.06 rad for $\Delta zed < 1cm$. The short- (Gauss) and long-range (exp) contributions to the source image are as indicated. Results are shown for $0 <$ centrality < 30 and $0.48 < k_T < 0.54$ GeV/c.*

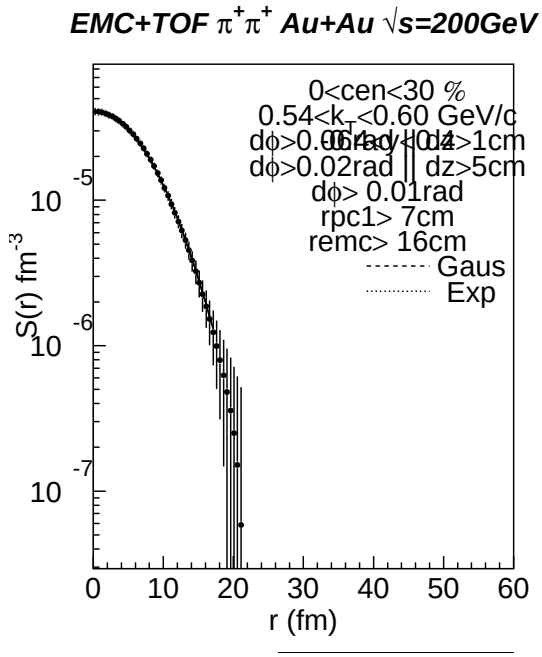

FIG. 244: *Source image for positively charged pion pairs detected in the combined acceptance of the EMC and TOF. The $\Delta\phi_{DC}$ cut is increased from 0.02 to 0.06 rad for $\Delta zed < 1cm$. The short- (Gauss) and long-range (exp) contributions to the source image are as indicated. Results are shown for $0 <$ centrality < 30 and $0.54 < k_T < 0.60$ GeV/c.*

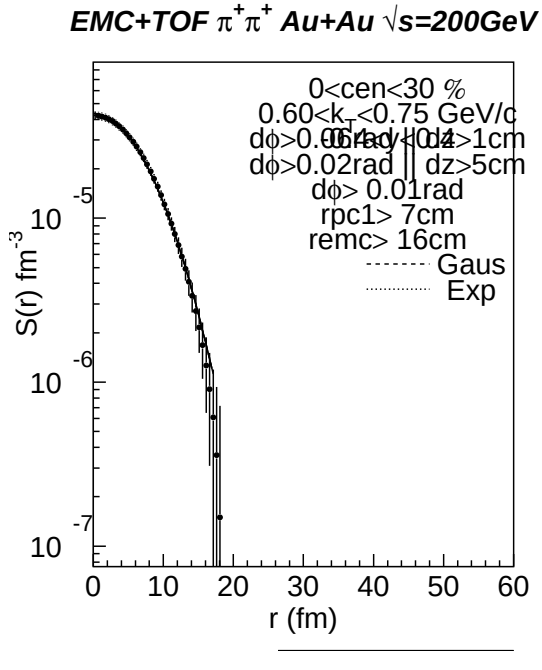

FIG. 245: *Source image for positively charged pion pairs detected in the combined acceptance of the EMC and TOF. The $\Delta\phi_{DC}$ cut is increased from 0.02 to 0.06 rad for $\Delta zed < 1cm$. The short- (Gauss) and long-range (exp) contributions to the source image are as indicated. Results are shown for $0 <$ centrality < 30 and $0.60 < k_T < 0.75$ GeV/c.*

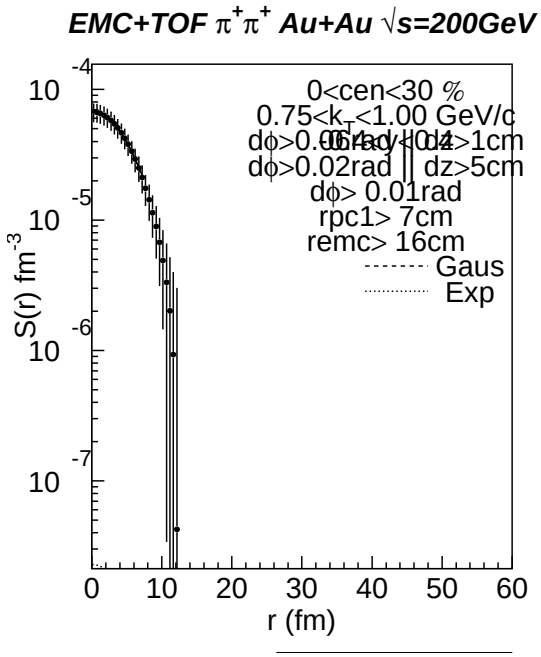

FIG. 246: *Source image for positively charged pion pairs detected in the combined acceptance of the EMC and TOF. The $\Delta\phi_{DC}$ cut is increased from 0.02 to 0.06 rad for $\Delta zed < 1cm$. The short- (Gauss) and long-range (exp) contributions to the source image are as indicated. Results are shown for $0 <$ centrality < 30 and $0.75 < k_T < 1.0$ GeV/c.*

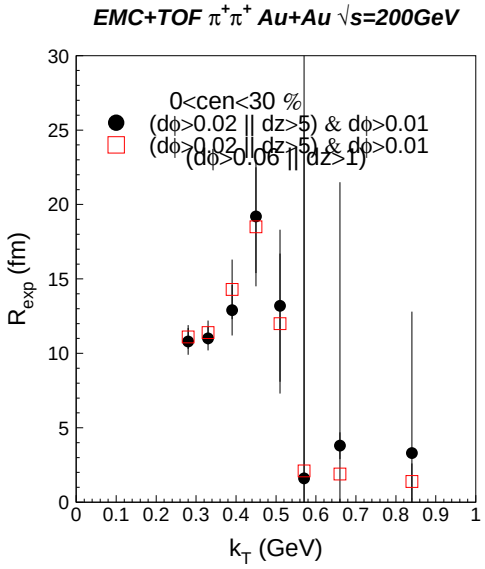

FIG. 248: *Long-range source radii R_{exp} vs m_T. Results are compared for standard cuts and a cut variation in which $\Delta\phi_{DC}$ cut is increased from 0.01 to 0.06 rad for $\Delta zed < 1cm$.*

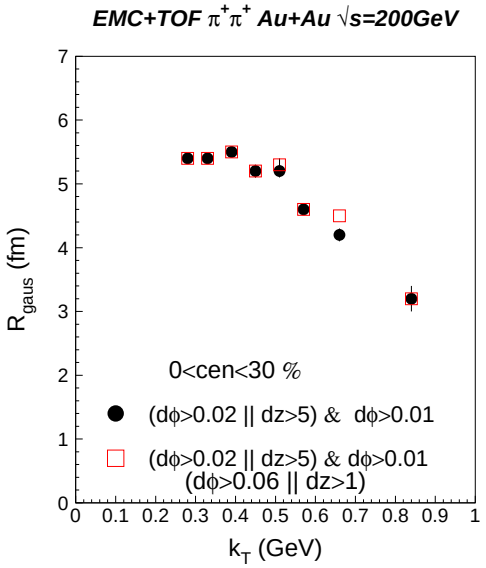

FIG. 247: *Short-range source radii R_{Gauss} vs m_T. Results are compared for standard cuts and a cut variation in which $\Delta\phi_{DC}$ cut is increased from 0.01 to 0.06 rad for $\Delta zed < 1cm$.*

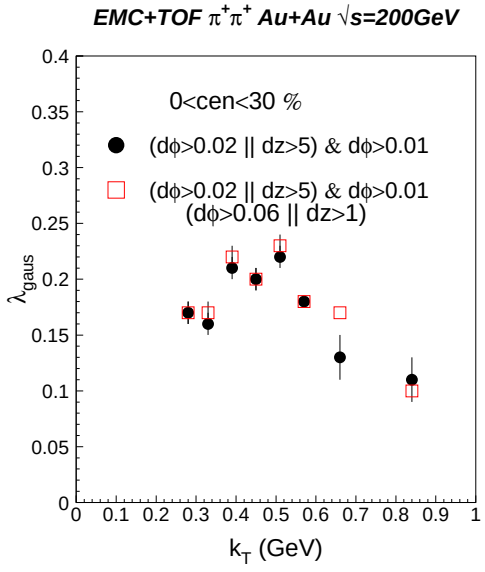

FIG. 249: *Short-range pair fraction λ_{Gauss} vs m_T. Results are compared for standard cuts and a cut variation in which $\Delta\phi_{DC}$ cut is increased from 0.01 to 0.06 rad for $\Delta zed < 1cm$.*

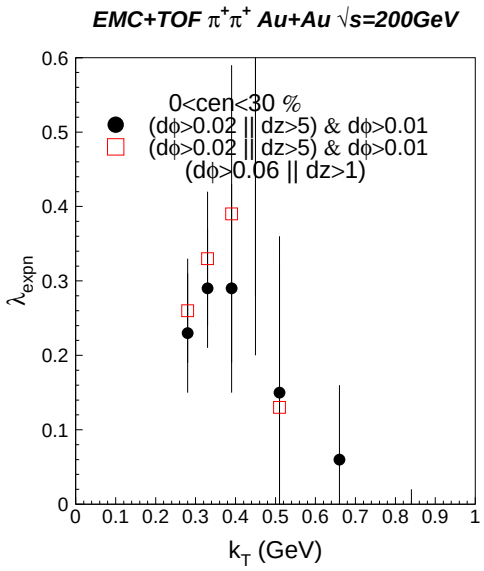

FIG. 250: *Long-range pair fraction λ_{exp} vs m_T. Results are compared for standard cuts and a cut variation in which $\Delta\phi_{DC}$ cut is increased from 0.01 to 0.06 rad for $\Delta zed < 1cm$.*

7.6.4. Simultaneous $\Delta\Phi_{DC}$ variations for $\Delta zed < 5cm$ and $\Delta zed > 5cm$

Figs. 251, 252, 253, 254, 255, 256, 257 and 258 show $\pi^+\pi^+$ source images obtained for several k_T cuts and $0 <$ centrality < 30. The focus in this case is to show and compare the resulting source functions and source parameters when the $\Delta\phi_{DC}$ cut is simultaneously increased from (a) 0.02 to 0.03 rad for $\Delta zed <$ 5cm and (b) 0.02 to 0.03 rad for $\Delta zed >$ 5cm. The long-range (exp) and short-range (Gauss) contributions to the source images are shown in each figure. A comparison of these images with those presented in 7.1 (for standard cuts) indicate relatively little change.

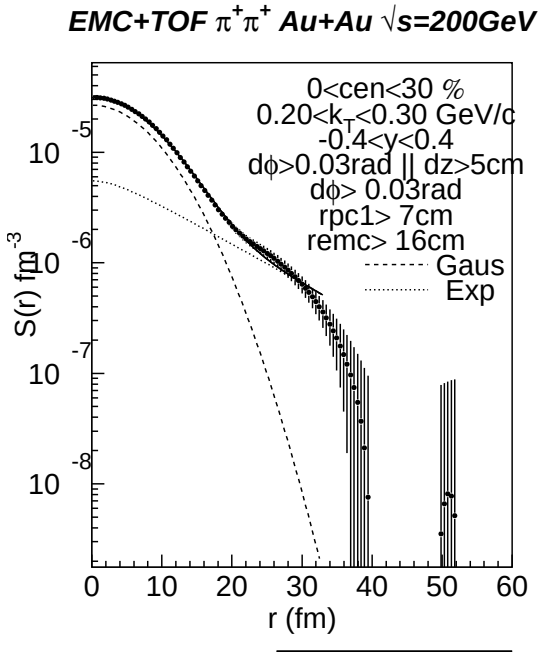

FIG. 251: *Source image for positively charged pion pairs detected in the combined acceptance of the EMC and TOF. The $\Delta\phi_{DC}$ cut is simultaneously increased from (a) 0.02 to 0.03 rad for $\Delta zed <$ 5cm and (b) 0.02 to 0.03 rad for $\Delta zed >$ 5cm. The short- (Gauss) and long-range (exp) contributions to the source image are as indicated. Results are shown for $0 <$ centrality < 30 and $0.2 < k_T < 0.3$ GeV/c.*

Figures 259, 260, 261 and 262 summarizes the comparison for the source parameters obtained with standard cuts versus that obtained with the cut variation described above. The good agreement between the results indicate that the cut variation does not lead to any significant change in the extracted source images.

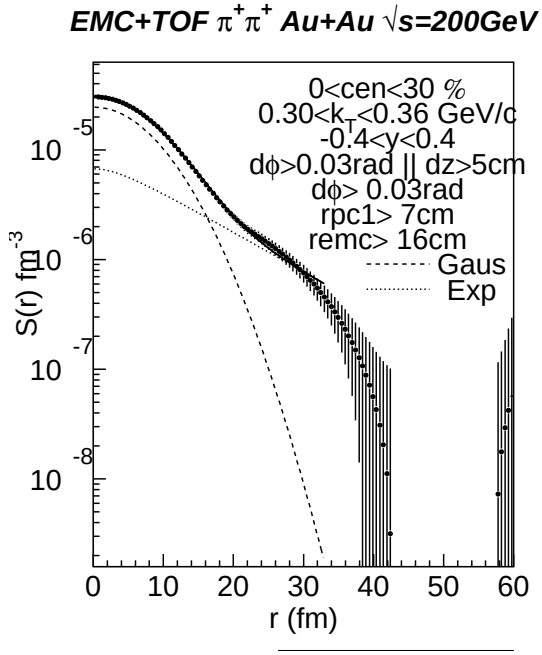

FIG. 252: *Source image for positively charged pion pairs detected in the combined acceptance of the EMC and TOF. The $\Delta\phi_{DC}$ cut is simultaneously increased from (a) 0.02 to 0.03 rad for $\Delta zed <$ 5cm and (b) 0.02 to 0.03 rad for $\Delta zed >$ 5cm. The short- (Gauss) and long-range (exp) contributions to the source image are as indicated. Results are shown for $0 <$ centrality < 30 and $0.3 < k_T < 0.36$ GeV/c.*

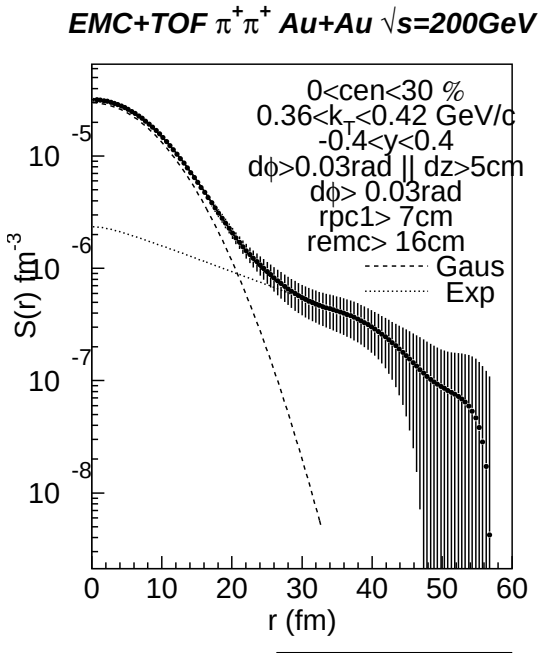

FIG. 253: *Source image for positively charged pion pairs detected in the combined acceptance of the EMC and TOF. The $\Delta\phi_{DC}$ cut is simultaneously increased from (a) 0.02 to 0.03 rad for $\Delta zed < 5cm$ and (b) 0.02 to 0.03 rad for $\Delta zed > 5cm$. The short- (Gauss) and long-range (exp) contributions to the source image are as indicated. Results are shown for $0 <$ centrality < 30 and $0.36 < k_T < 0.42$ GeV/c.*

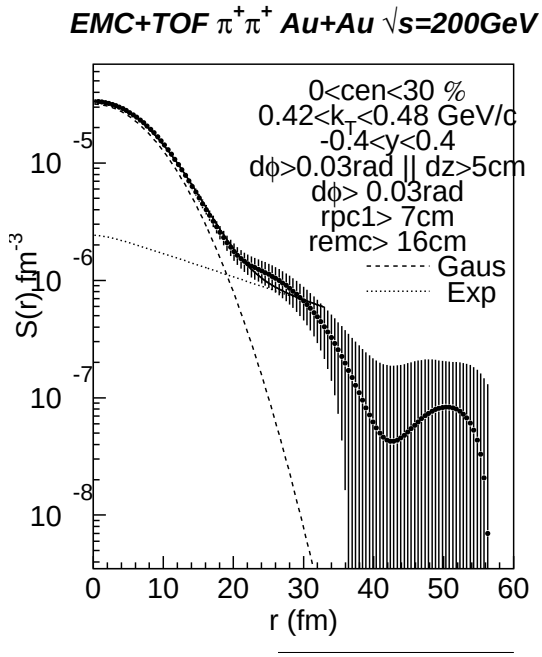

FIG. 254: *Source image for positively charged pion pairs detected in the combined acceptance of the EMC and TOF. The $\Delta\phi_{DC}$ cut is simultaneously increased from (a) 0.02 to 0.03 rad for $\Delta zed < 5cm$ and (b) 0.02 to 0.03 rad for $\Delta zed > 5cm$. The short- (Gauss) and long-range (exp) contributions to the source image are as indicated. Results are shown for $0 <$ centrality < 30 and $0.42 < k_T < 0.48$ GeV/c.*

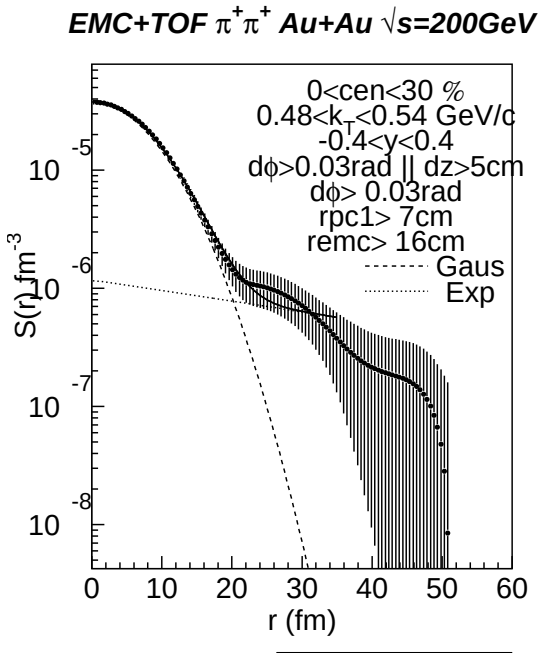

FIG. 255: *Source image for positively charged pion pairs detected in the combined acceptance of the EMC and TOF. The $\Delta\phi_{DC}$ cut is simultaneously increased from (a) 0.02 to 0.03 rad for $\Delta zed < 5cm$ and (b) 0.02 to 0.03 rad for $\Delta zed > 5cm$. The short- (Gauss) and long-range (exp) contributions to the source image are as indicated. Results are shown for $0 < centrality < 30$ and $0.48 < k_T < 0.54$ GeV/c.*

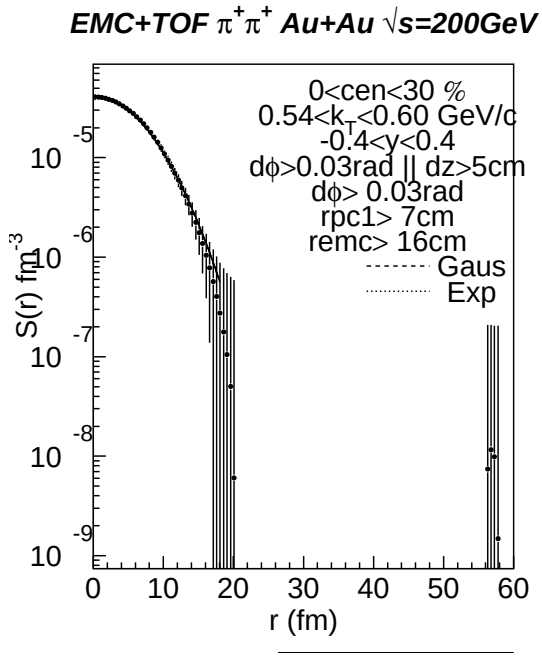

FIG. 256: *Source image for positively charged pion pairs detected in the combined acceptance of the EMC and TOF. The $\Delta\phi_{DC}$ cut is simultaneously increased from (a) 0.02 to 0.03 rad for $\Delta zed < 5cm$ and (b) 0.02 to 0.03 rad for $\Delta zed > 5cm$. The short- (Gauss) and long-range (exp) contributions to the source image are as indicated. Results are shown for $0 < centrality < 30$ and $0.54 < k_T < 0.60$ GeV/c.*

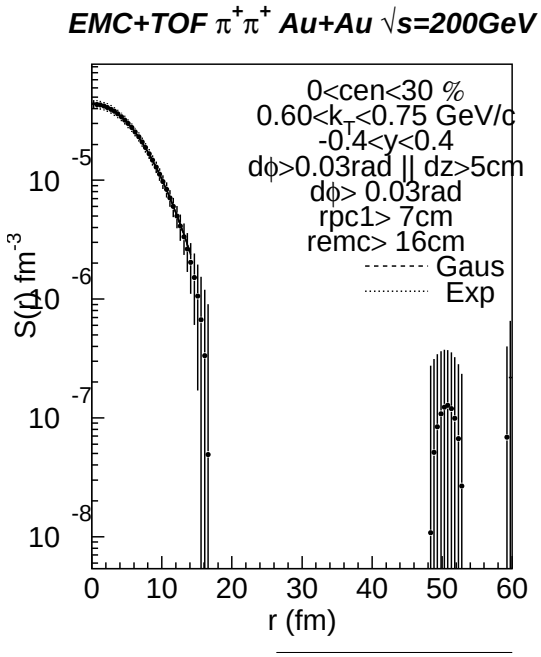

FIG. 257: *Source image for positively charged pion pairs detected in the combined acceptance of the EMC and TOF. The $\Delta\phi_{DC}$ cut is simultaneously increased from (a) 0.02 to 0.03 rad for $\Delta zed < 5cm$ and (b) 0.02 to 0.03 rad for $\Delta zed > 5cm$. The short- (Gauss) and long-range (exp) contributions to the source image are as indicated. Results are shown for $0 <$ centrality < 30 and $0.60 < k_T < 0.75$ GeV/c.*

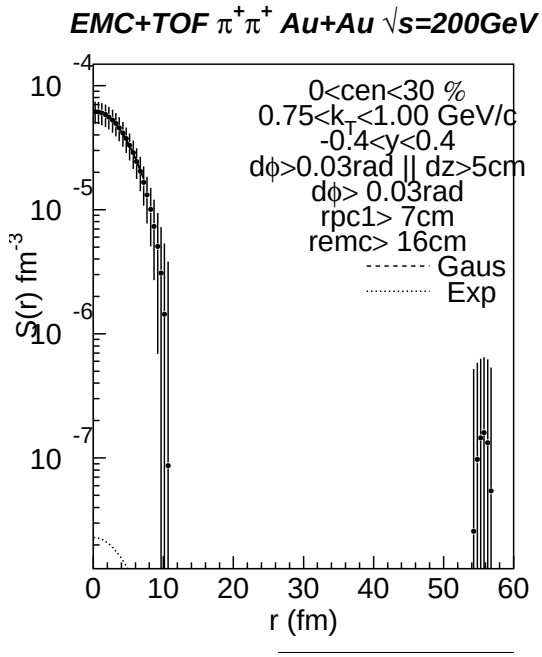

FIG. 258: *Source image for positively charged pion pairs detected in the combined acceptance of the EMC and TOF. The $\Delta\phi_{DC}$ cut is simultaneously increased from (a) 0.02 to 0.03 rad for $\Delta zed < 5cm$ and (b) 0.02 to 0.03 rad for $\Delta zed > 5cm$. The short- (Gauss) and long-range (exp) contributions to the source image are as indicated. Results are shown for $0 <$ centrality < 30 and $0.75 < k_T < 1.0$ GeV/c.*

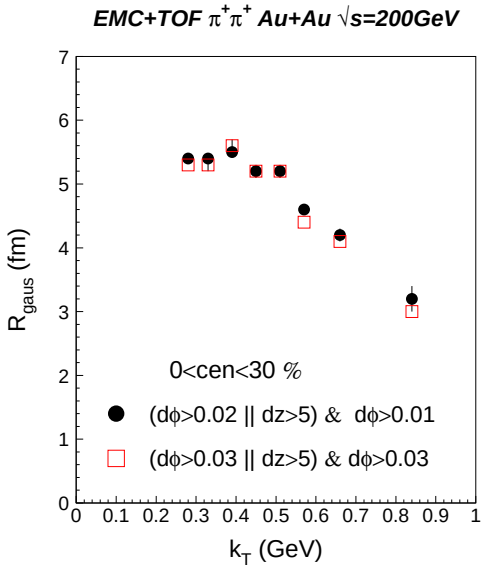

FIG. 259: *Short-range source radii R_{Gauss} vs m_T. Results are compared for standard cuts and a cut variation in which $\Delta\phi_{DC}$ is simultaneously increased from (a) 0.02 to 0.03 rad for $\Delta zed < 5cm$ and (b) 0.02 to 0.03 rad for $\Delta zed > 5cm$.*

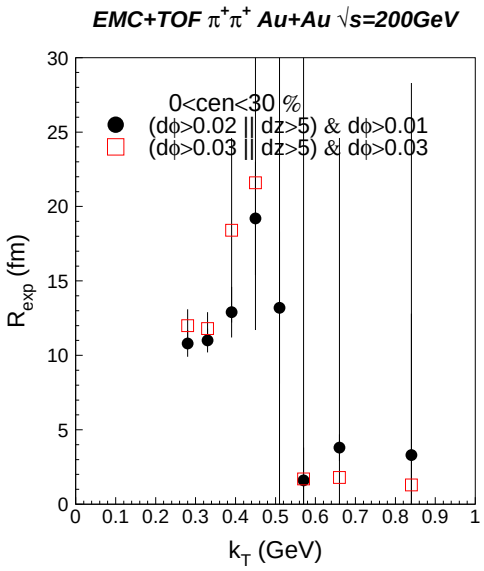

FIG. 260: *Long-range source radii R_{exp} vs m_T. Results are compared for standard cuts and a cut variation in which $\Delta\phi_{DC}$ is simultaneously increased from (a) 0.02 to 0.03 rad for $\Delta zed < 5cm$ and (b) 0.02 to 0.03 rad for $\Delta zed > 5cm$.*

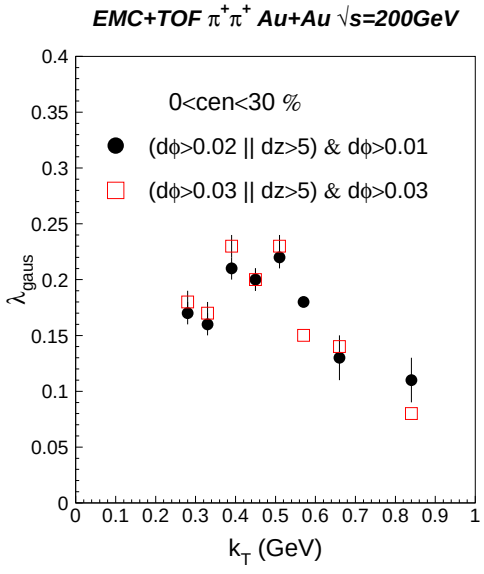

FIG. 261: *Short-range pair fraction λ_{Gauss} vs m_T. Results are compared for standard cuts and a cut variation in which $\Delta\phi_{DC}$ is simultaneously increased from (a) 0.02 to 0.03 rad for $\Delta zed < 5cm$ and (b) 0.02 to 0.03 rad for $\Delta zed > 5cm$.*

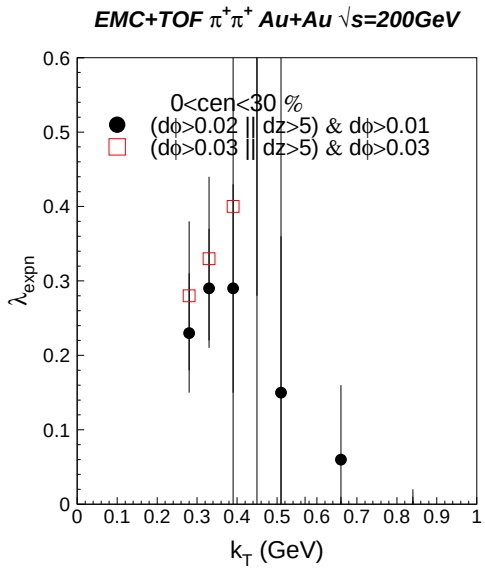

FIG. 262: *Long-range pair fraction λ_{exp} vs m_T. Results are compared for standard cuts and a cut variation in which $\Delta\phi_{DC}$ is simultaneously increased from (a) 0.02 to 0.03 rad for $\Delta zed < 5cm$ and (b) 0.02 to 0.03 rad for $\Delta zed > 5cm$.*

7.7. A Quick Test of the Influence of Momentum Resolution

An important question is whether or not the momentum resolution has significant impact on the generated correlation functions and hence the extracted source images. There are several approaches that can be used to address this question. For example, one can carry out momentum resolution corrections to correlation function. Another quick approach is to smear the momentum of measured tracks with realistic resolution factors (such as the measured value) and study the effect of this smearing on the measured correlation function. The latter approach does not account for the effect of momentum resolution but it can provide valuable insight on the sensitivity of the correlation functions to an $\sim 100\%$ decrease in the momentum resolution.

Figs. 263, 264, 265, 266, 267, 268, 269 and 270 compare correlation functions with and without momentum smearing. The filled and open points show results with and without a 1.0% momentum smearing for positively charged pions obtained for several k_T cuts and a centrality selection of 0-30%. The comparison shows that a 1% momentum smearing does not lead to any significant change in the correlation functions outside of the statistical error bars. We therefore conclude that corrections to the correlation functions which take account of the measured momentum resolution (1.0%) would not lead to any change in the correlation functions and hence the source images.

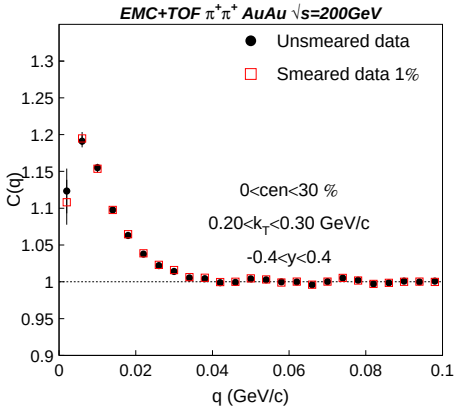

FIG. 263: *Comparison of experimental correlation functions with and without a 1% smearing of the momentum of the measured tracks. Results are shown for* $0 < centrality < 30$ *and* $0.2 < k_T < 0.3$ *GeV/c.*

Figures 271, 272, 273 and 274 summarizes the comparison for the source parameters obtained with and without momentum smearing. The good agreement between the results indicate that a momentum resolution of 1% does not have a strong influence on the extracted source images.

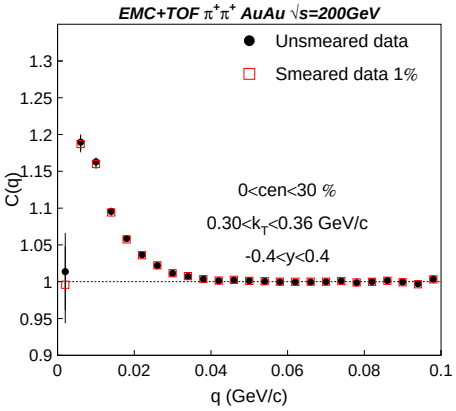

FIG. 264: *Comparison of experimental correlation functions with and without a 1% smearing of the momentum of the measured tracks. Results are shown for* $0 < centrality < 30$ *and* $0.3 < k_T < 0.36$ *GeV/c.*

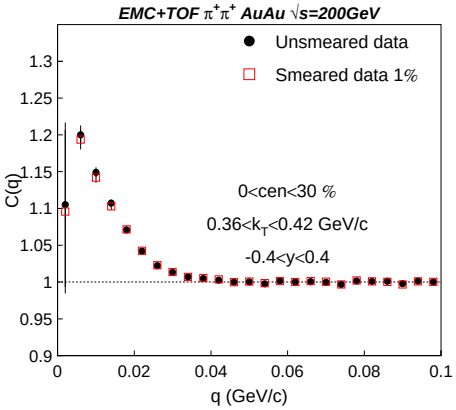

FIG. 265: *Comparison of experimental correlation functions with and without a 1% smearing of the momentum of the measured tracks. Results are shown for* $0 < centrality < 30$ *and* $0.36 < k_T < 0.42$ *GeV/c.*

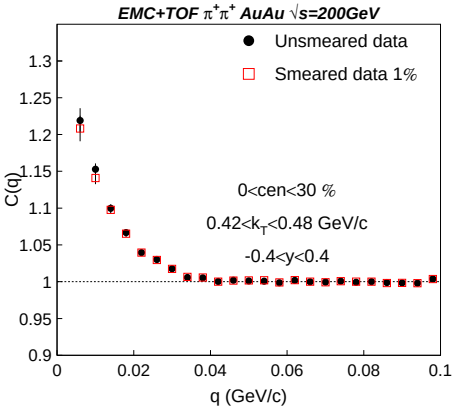

FIG. 266: *Comparison of experimental correlation functions with and without a 1% smearing of the momentum of the measured tracks. Results are shown for* $0 <$ *centrality* < 30 *and* $0.42 < k_T < 0.48$ *GeV/c.*

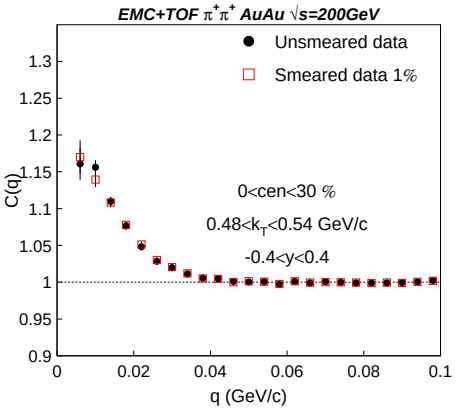

FIG. 267: *Comparison of experimental correlation functions with and without a 1% smearing of the momentum of the measured tracks. Results are shown for* $0 <$ *centrality* < 30 *and* $0.48 < k_T < 0.54$ *GeV/c.*

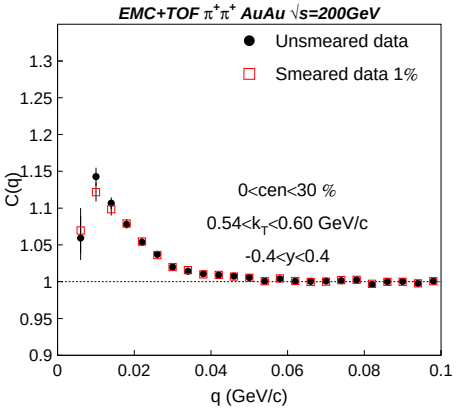

FIG. 268: *Comparison of experimental correlation functions with and without a 1% smearing of the momentum of the measured tracks. Results are shown for* $0 <$ *centrality* < 30 *and* $0.54 < k_T < 0.60$ *GeV/c.*

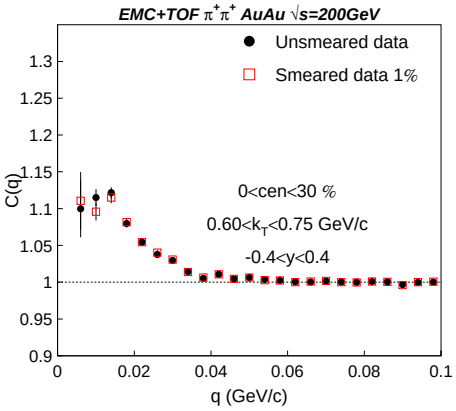

FIG. 269: *Comparison of experimental correlation functions with and without a 1% smearing of the momentum of the measured tracks. Results are shown for* $0 <$ *centrality* < 30 *and* $0.60 < k_T < 0.75$ *GeV/c.*

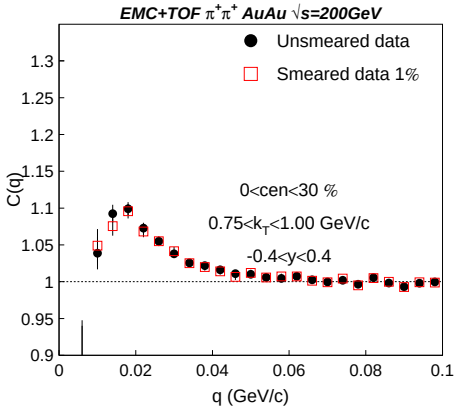

FIG. 270: *Comparison of experimental correlation functions with and without a 1% smearing of the momentum of the measured tracks. Results are shown for* $0 <$ *centrality* < 30 *and* $0.75 < k_T < 1.0$ *GeV/c.*

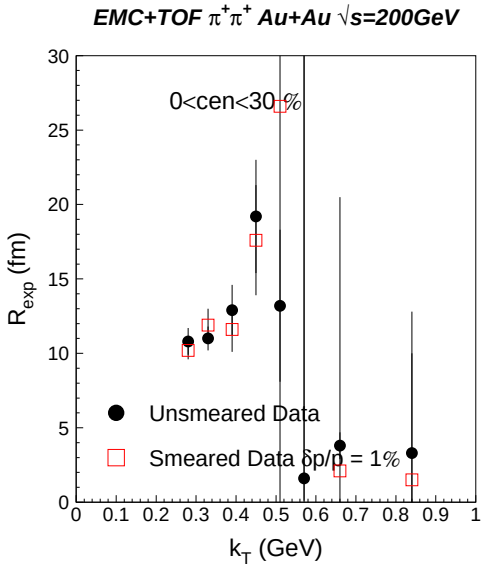

FIG. 272: *Long-range source radii* R_{exp} *vs* k_T*. Results are compared for standard cuts with and without a 1% momentum smearing.*

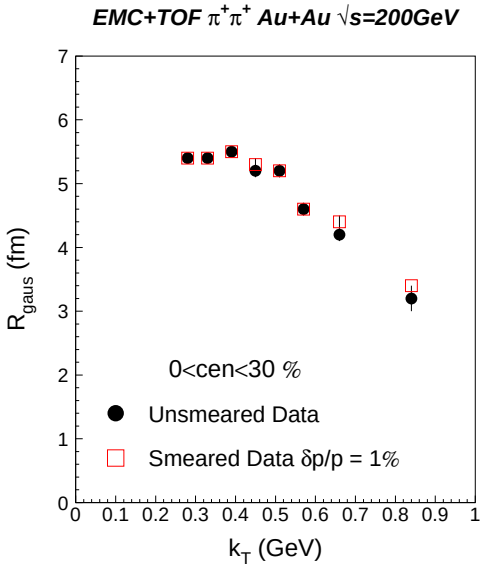

FIG. 271: *Short-range source radii* R_{Gauss} *vs* k_T*. Results are compared for standard cuts with and without a 1% momentum smearing.*

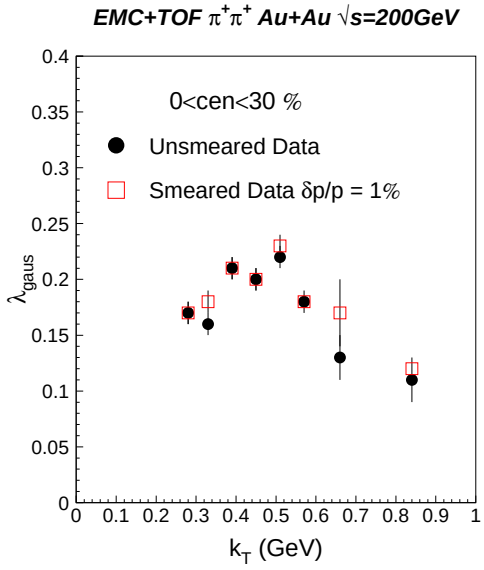

FIG. 273: *Short-range pair fraction* λ_{Gauss} *vs* k_T*. Results are compared for standard cuts with and without a 1% momentum smearing.*

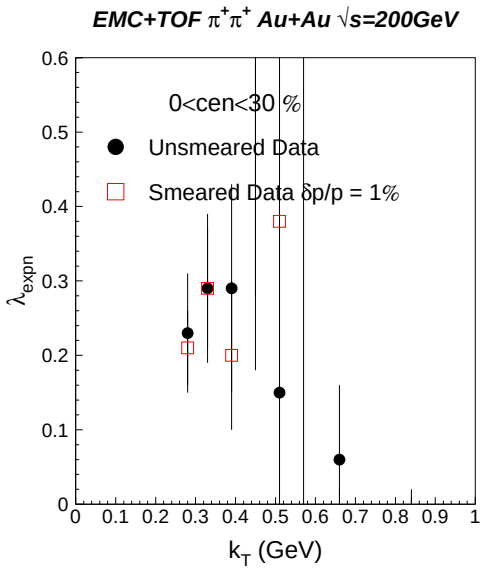

FIG. 274: *Long-range pair fraction λ_{exp} vs k_T. Results are compared for standard cuts with and without a 1% momentum smearing.*

7.8. A Brief Note About Systematic Errors

One of the important virtues of an analysis which involves correlation functions is that they lead to relatively small systematic errors. This of course depends on whether or not the correlation function analysis is properly executed, (ie. careful study and choice of cuts etc.). A proper analysis typically leads to systematic errors which are less than or equal to statistical errors. Such an error can be *estimated* by varying cuts and repeating the entire analysis. Here it is important to point out that such an estimate can be influenced by fluctuations resulting from a change in statistics with cut variations, especially if the systematic variations are inside the statistical error bars.

In what follows, we outline a procedure for systematic error estimates which result from cut variations.

Correlation functions were generated (for several k_T and centrality selections) and imaged for several track-pair cuts as listed below. We refer to each of these as a trial:

- Trial-1 = $(dphi > 0.02 || dz > 5 + dphi > 0.01$
- Trial-2 = $(dphi > 0.06 || dz > 1 + dphi > 0.02 || dz > 5 + dphi > 0.01$
- Trial-3 = $(dphi > 0.02 || dz > 5 + dphi > 0.01$ momentum smeared
- Trial-4 = $(dphi > 0.02 || dz > 5 + dphi > 0.02$
- Trial-5 = $(dphi > 0.03 || dz > 5 + dphi > 0.01$
- Trial-6 = $(dphi > 0.03 || dz > 5 + dphi > 0.03$
- Trial-7 = $(dphi > 0.04 || dz > 5 + dphi > 0.02$

Representative examples of the results obtained from each of these trials are shown in Figs. 275 - 278. They show the variation of R_{Gauss}, R_{exp}, λ_{Gauss} and λ_{exp} as a function of trial respectively. The maximum variation of these parameters over the range of trials is used as an estimate of the systematic error associated with cut variations. This estimate does not take account of possible correlated errors due to the fitting procedure. However, we estimate that such errors would lead to a smaller systematic error estimate in several cases. This is of course not an important issue since by enlarge, the systematic errors obtained are much less than the statistical errors.

A recent preliminary request can be found at:

https://www.phenix.bnl.gov/WWW/p/draft/rlacey/Imaging/DraftNote/Prelim$_R$*equest.ppt*

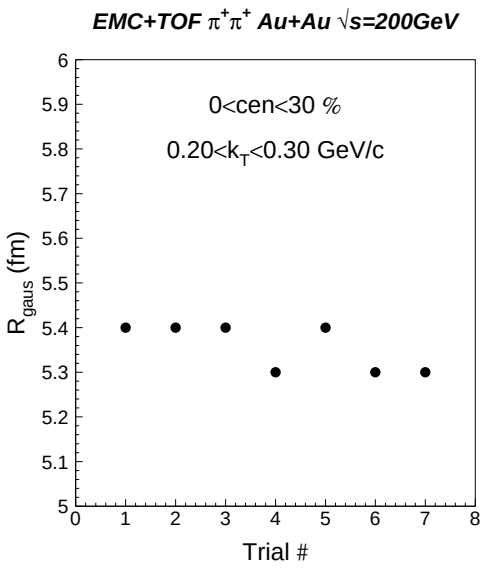

FIG. 275: *Short-range source parameters R_{Gauss} vs. trial number. Results are shown for the selection $0.2k_T < 0.3$ GeV/c and centrality 0-30%.*

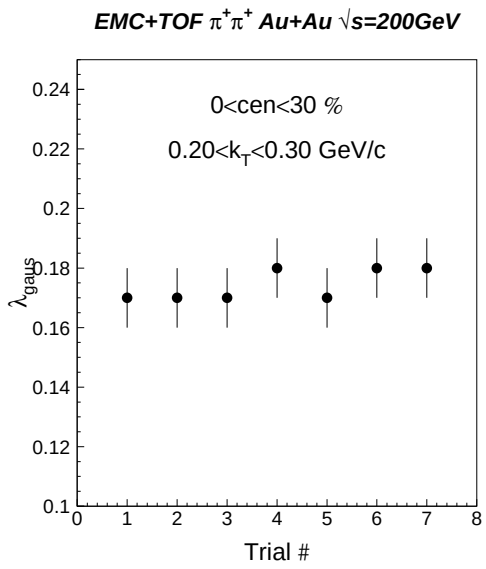

FIG. 277: *Short-range pair fraction λ_{Gauss} vs. trial number. Results are shown for the selection $0.2k_T < 0.3$ GeV/c and centrality 0-30%.*

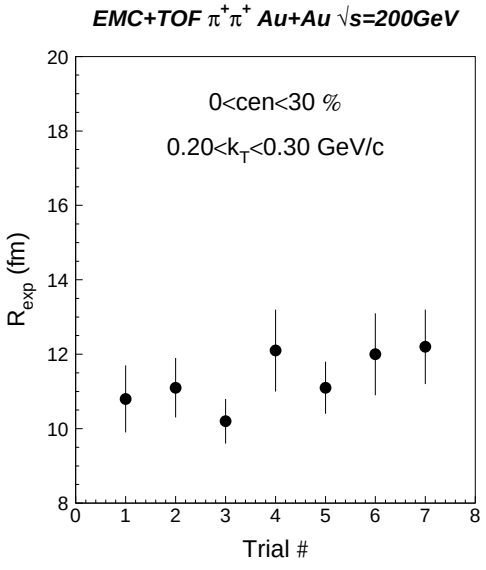

FIG. 276: *Long-range source parameters R_{exp} vs. trial number. Results are shown for the selection $0.2k_T < 0.3$ GeV/c and centrality 0-30%.*

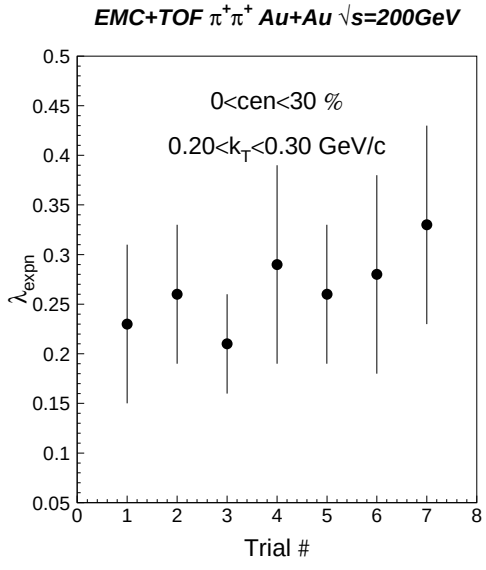

FIG. 278: *Long-range pair fraction λ_{exp} vs. trial number. Results are shown for the selection $0.2k_T < 0.3$ GeV/c and centrality 0-30%.*

[1] U. Heinz and B. V. Jacak, "Two-Particle Correlations in Relativistic Heavy-Ion Collisions", Annu. Rev. Nucl. Part. Sci., (**49**), 1999, p. 529-579

[2] D. A. Brown, P. Danielewicz, "Imaging Of Sources In Heavy-Ion Reactions", Phys. Lett. **B 398**:252-258 (1997).

[3] D. A. Brown, P. Danielewicz, "Optimized Discretization Of Sources Imaged In Heavy-Ion Reactions", Phys. Rev. **C 57**:2474-2483 (1998).

[4] D. A. Brown, P. Danielewicz, "Observing Non-Gaussian Sources in Heavy-Ion Reactions", Phys. Rev. **C 64**: 014902 (2001).

[5] D. A. Brown, P. Danielewicz, HBT-progs Version 1.0, *http://www-phys.llnl.gov/Research/source_imaging/HBTprogs.html*

[6] Akitomo Enokizono, PPG021: Charged pion HBT analysis of Au+Au at $\sqrt{s_{NN}}$ = 200 GeV , Phenix Analysis notes AN 246, AN 213.

[7] S.E. Koonin, Phys. Lett. **B70**, 43 (1977); S. Pratt, T. Csörgő and T. Zimányi, Phys. Rev. C **42**, 2646 (1990).

[8] S.Y. Panitkin et al., (E895 Collaboration), "Model Independent Source Imaging using two pion correlations in 2-GeV/A TO 8-GeV/A Au + Au Collisions", Phys.Rev.Lett.**87**:112304,2001

[9] G. Verde et al., "Probing transport theories via two proton source imaging", Phys.Rev.C **67** :034606,2003

[10] P. Chung et al., (E895 Collaboration), "Comparison of Source Images for protons, π^-'s and Λ's in 6 AGeV Au+Au collisions", Phys.Rev.Lett. 91 (2003) 162301

[11] B. Jacak QA webpage *http://www.phenix.bnl.gov/phenix/ WWW/p/draft/jacak/qa/*

[12] A. Taranenko et al., "Hadron Identification in EMC (PbSc)", *https://www.phenix.bnl.gov/phenix/WWW/p/draft /arkadij/lambdanote1/emctof.ps*

[13] T. Chujo, A. Kiyomichi, T. Sakaguchi, J. Velkovska, "Identified Charged Hadron Spectra and Particle Ratios at $\sqrt{s}$=200 GeV, Phenix Analysis Notes for PPG015/026: AN 148, AN 187

[14] T. Chujo, "Run selection for Run2 PID Analysis II", https://www.phenix.bnl.gov/WWW/p/draft/chujo/ HWGana/highpt_acc/goodruns.htm

[15] T. Chujo, CVS:offline/analysis/HWGana/AuAu

[16] A. Taranenko et al., Phenix Analysis Note AN 281

[17] A. Taranenko, "Hadron Identification in EMC (PbSc) for dAu run", analysis note in preparation